Molecular Regulation of Adipogenesis in Secondary Lymphoedema: a Common Complication of Cancer Therapies

Yinan Yuan

ORCID 0000-0001-9087-7532

Submitted in total fulfilment of the requirements for the degree of Doctor of Philosophy

October 2018

Faculty of Medicine, Dentistry and Health Sciences,
Sir Peter MacCallum Cancer Centre, Department of Oncology,
The University of Melbourne
Victoria, Australia

Abstract

Secondary lymphoedema is a common, chronic disease caused by inadequate drainage of interstitial tissue fluid from a limb due to damaged lymphatic vessels. It may develop after radiation therapy or cancer surgery involving lymph node dissection, in particularly for breast cancer, as well as a variety of other conditions. The resulting accumulation of interstitial fluid promotes pathological changes including oedema, expansion of fat and dermal fibrosis, which contribute to extensive chronic tissue swelling, typically in the upper or lower limbs. There is no curative treatment or molecular-based therapy for secondary lymphoedema, and current treatments for this condition have limited efficacy so it is an important unmet clinical need in medicine with an estimated 300,000 patients in Australia. A pharmacological intervention to restrict or reduce expansion of fat tissue and associated tissue swelling would be highly beneficial for patients however, the molecular mechanisms driving the development of fat in secondary lymphoedema are unknown. Here, a surgical mouse tail model of secondary lymphoedema is employed to investigate molecular pathways that drive expansion of fat tissue in this condition, and to explore a potential pharmacological approach for restricting this process.

The mouse model of secondary lymphoedema employed exhibited key pathophysiological features of clinical secondary lymphoedema such as tissue swelling, subcutaneous oedema, dermal fibrosis and excess formation of fat. With the expansion of fat occurring during the early phase of lymphoedema, and elevated levels of fat persisting in the chronic phase, this mouse lymphoedema model was well suited for studying molecular mechanisms driving the initial expansion of fat as well as the persistence of excess fat tissue in the chronic setting. Whole-genome microarray analysis was used to study the mouse lymphoedema model which revealed that mRNA for insulin-like growth factor binding protein 5 (IGFBP5), an inhibitor of the insulin-like growth factor 1 receptor (IGF1R) adipogenic signalling pathway, was down-regulated in the model compared to controls. Further analyses by immunohistochemistry revealed the presence of IGF1 and IGF1R on adipocytes in the model and

in a clinical sample of secondary lymphoedema, and activated IGF1R in the clinical sample. Moreover, the levels of IGF1 (an activating ligand for IGF1R) associated with adipocytes, were elevated in the mouse lymphoedema model. Thus, the IGF1R signalling axis could be active and promote expansion of fat tissue in secondary lymphoedema. Importantly, pharmacological targeting of this pathway in the mouse lymphoedema model with linsitinib, a small molecule tyrosine kinase inhibitor of IGF1R, led to significant reductions in tissue swelling and fat expansion which was associated with decreases in both the number and size of adipocytes. Furthermore, linsitinib also restricted the degree of dermal fibrosis in the mouse lymphoedema model.

The work presented in this thesis demonstrated the role of the IGF1R signalling pathway in promoting adipogenesis in a mouse model of secondary lymphoedema. Hence, pharmacologically targeting IGF1R might be a viable therapeutic approach for restricting expansion of fat and tissue swelling in secondary lymphoedema patients.

Declaration

I declare that

i) this thesis comprises only my original work towards the Doctor of Philosophy except where indicated in the Preface;

ii) due acknowledgement has been made in the text to all other material used; and

iii) this thesis is fewer than the maximum word limit in length, exclusive of tables, maps bibliographies and appendices.

Yinan Yuan

October 2018

Preface

This thesis comprises my original work with the exception to the following:
The work outlined in Sections 3.2.1 and 3.2.2 in Chapter 3 was based on a surgical mouse tail model of secondary lymphoedema generated by Dr. Sidney Levy (Peter MacCallum Cancer Centre). Figure 3.2A&B were obtained from the Ph. D thesis of Dr. Sidney Levy. A whole-genome microarray analysis outlined in Section 3.3 was performed by Yong Qiang Yeo, a former Honours student in our laboratory. Figure 3.4 was originally produced in the Honours thesis of Mr. Yong Qiang Yeo, and was modified in this thesis.

Custom-made algorithms using MetaMorph® Microscopy Automation and Image Analysis Software, for the purposes of quantification of fat tissue and dermal fibrosis, were created by Mr. Cameron Nowell, Microscopy Manager, Ludwig Institute for Cancer Research, Parkville, VIC, Australia.

Custom-made algorithms using Microsoft Excel, for the purposes of analysis of data generated by the MetaMorph® software algorithms described above, were created by Mr. Jimmy Zeng, Windows Programmer, Web Developer and IT Support Manager, Ludwig Institute for Cancer Research, Parkville, VIC, Australia.

Sectioning of mouse tail tissues obtained from animal experiments, for the purpose of subsequent immunohistochemical and histological analyses, was performed by Mrs Basha Przybylowski and Mrs Dhanya Menon from Centre for Advanced Histology and Microscopy (CAHM), Peter MacCallum Cancer Centre.

No third-party editorial assistance was provided in preparation of this thesis.

All chapters consist of unpublished material not submitted for publication at the time of thesis submission.

This thesis was funded by an Australian Postgraduate Scholarship ($25K/annum) for 3.5 years. The final year was funded from the budget of the Tumour Angiogenesis and Microenvironment Programme, Peter MacCallum Cancer Centre.

Acknowledgement

Completion of this doctoral thesis was not possible without the support of numerous people at Peter Mac. First and foremost I would like to thank my supervisor Professor Marc Achen for choosing me as one of his Ph.D. students. I cannot find enough words with which to express my feeling of thanks for his dedicated supervision, invaluable suggestions and constant support that went a long way to the successful completion of my work. I appreciated his guidance in research and the writing of this thesis, and all his contributions of time and ideas to make my Ph.D. experience motivating and encouraging. I also thank my other supervisor Professor Steven Stacker. I greatly appreciated that Marc and Steven provided me with funding that made the last year of my Ph.D. studies possible. I would also like to thank my mentor Professor Rick Pearson for providing knowledge and advice on aspects of my scientific work.

My special appreciation goes to Dr. Sidney Levy, who willingly provided me with training in the surgery to generate the animal model of secondary lymphoedema during his busy time as a clinician. Learning the surgery was indeed one the most precious, exciting and challenging experiences during my Ph.D. Without his support it would not have been possible to conduct much of the research described in this thesis. I am also grateful to Dr. David Speakman for his provision of a precious sample of human secondary lymphoedema which was difficult to obtain.

I am grateful for the time I spent with colleagues in my laboratory. To Michael, James, Valeria and Fei - we worked so hard and encouraged each other to go through the tough times of Ph.D. To Sally and Sarah, I totally enjoyed working and taking with you, and thanks for all your kind support when I was having difficult times during my Ph.D. To Adam, thanks for your help and advice on my CV when I was looking for a post-doctoral position. I also want to thank David and Elena from the Pathology Department for their valuable guidance and help with immunohistochemistry. I would also like to acknowledge my close colleague, Dr. Sophie Paquet-Fifield, who gave me the support that I needed during the first year of my Ph.D.

I also want to pay respect to the influential people outside of my science life. My parents gave me unconditional love and support both spiritually and financially from China and New Zealand. To my wonderful loving wife, Anna Yuan, I would like to thank you for becoming a part of my family during the second year of my Ph.D., and ever since, for always being there to share this journey with me until the completion of this work.

Lastly, I would like to acknowledge my grandparents, Jitsuko Haga and Weixiang Yuan, who passed away before the completion of this thesis due to illnesses. I know you are both seeing me from heaven, and I hope that I have made you feel proud of me as your grandson.

List of Publications

Sato, T., Paquet-Fifield, S., Harris, N. C., Roufail, S., Turner, D. J., Yuan, Y., Zhang, Y. F., Fox, S. F., Hibbs, M. L., Wiklinson-Berka, J. L., Williams, R. A., Stacker, S. A., Sly, P. D., Achen, M. G. (2016). VEGF-D promotes pulmonary oedema in hyperoxic acute lung injury. *Journal of Pathology*, 239(2), 152-161.

Table of Contents

Chapter 2

Materials and Methods

Chapter 3

Identification of Molecular Signalling Mechanisms Driving Formation of Fat Tissue in Mouse Model of Secondary Lymphoedema

Chapter 4

Pharmacologically Targeting Formation of Fat Tissue in the Mouse Model of Secondary Lymphoedema

List of Tables and Figures

Chapter 1 Literature Review

Chapter 2 Materials and Methods

Chapter 3 Identification of Molecular Signalling Mechanisms Driving Formation of Fat Tissue in Mouse Model of Secondary Lymphoedema

Chapter 4 Pharmacologically Targeting Formation of Fat Tissue in the Mouse Model of Secondary Lymphoedema

List of Abbreviations

ABC	Avidin-biotin complex
ANOVA	Analysis of variance
BAT	Brown adipose tissue
BMI	Body mass index
BMP	Bone morphogenic protein 4
C/EBPα	CCAAT/enhancer binding protein-alpha
CAHM	Centre for Advanced Histology and Microscopy
CDNA	Complementary DNA
CDT	Complete decongestive therapy
CPX1	Carboxypeptidase X1
DMSO	Dimethyl Sulphoxide
EDTA	Ethylenediamine tetraacetic acid
FBS	Fetal bovine serum
FFPE	Formalin-fixed paraffin-embedded
FGF	Fibroblast growth factor
FOXC2	Forkhead box C2
GAS6	Growth arrest-specific gene 6
H&E	Haematoxylin and eosin
H_2O_2	Hydrogen peroxide
HFD	High-fat diet
HGF	Hepatocyte growth factor
IGF1	Insulin-like growth factor 1
IGF1R	Insulin-like growth factor 1 receptor
IGFBP5	Insulin-like growth factor binding protein 5
iNOS	Induced nitric oxide synthase
IR	Insulin receptor
LECs	Lymphatic endothelial cells
LP-ICG	liposomal indocyanine green
LIVE1	Lymphatic vessel endothelial hyaluronan receptor 1
mAbs	Monoclonal antibodies
MAPK	Mitogen-activated protein kinase
MCE	Mitotic clonal expansion
MSCs	Mesenchymal stem cells
NP-40	Nonidet P-40

NSAIDs	Non-steroidal anti-inflammatory drugs
OBB	Odyssey® Blocking Buffer
OPN	Osteopontin
PBS	Phosphate-buffered saline
PECAM1	Platelet and endothelial cell adhesion molecule 1
PI3K	Phosphoinositol-3-kinase
p-IGF1R	Phosphorylated IGF1R
$PPAR_{\Upsilon}$	Peroxisome proliferator-activated receptor gamma
PREF1	Preadipocyte factor 1
PROX1	Prospero homeobox 1
RA	Retinoid acid
RPMI	Roswell Park Memorial Institute
SDS-PAGE	Sodium dodecyl sulfate polyacrylamide gel electrophoresis
SVF	Stromal vascular fraction
TAM	Tyro3/Axl/Mertk
TBS	Tris-buffered saline
TBST	TBS/0.1% Tween 20
TEP	Trypsin, ethylenediamine tetraacetic acid and phenol red
TGFβ	Transforming growth factor β
TGFβR1/2	TGFβ receptor-type 1 and type 2
TIFF	Tagged Image File Format
TIPs	Tension-induced/inhibited proteins
TNB	Tris - NaCl blocking buffer
TNFα	Tissue necrosis factor alpha
TNT	Tris-NaCl-Tween
TSA	Tyramide Signal Amplification
TSP1	Thrombosponding 1
VEGFR3	Vascular endothelial growth factor 3
VEGFs	Vascular endothelial growth factors
WAT	White adipose tissue

Chapter 1
Literature Review

1.1 Introduction

Secondary lymphoedema is a chronic disease characterised by the accumulation of interstitial fluid within tissues due to damaged lymphatic vessels, leading to swelling and dysfunction of limbs [1]. It can be caused by disruption or obstruction of lymphatic vessels due to surgery (e.g. lymphadenectomy) and/or radiotherapy during, for example, breast cancer treatment. It can be highly debilitating both physically and psychologically for patients due to reduced quality of life associated with limb discomfort, anxiety, depression, sexual dysfunction and social isolation [2]. Unfortunately, current treatment choices for lymphoedema are limited to conventional therapies such as massage, manual lymph drainage, remedial exercise and compression bandaging [3]. These treatments not only have limited efficacy in controlling the disease, but they fail to address the cause. Hence, this condition represents an important unmet clinical need in medicine.

It is well known that the pathological features of lymphoedema include oedema, inflammation, dermal fibrosis and formation of fat tissue [4, 5]. Of these, a key driver of tissue swelling in lymphoedema is the expansion of fat tissue [6] which may be promoted by components of fluid that accumulate in the affected limb. Although the pathophysiological aspects of lymphoedema are well understood, the underlying molecular mechanisms that drive the development of fat tissue remain elusive. Therefore, a better understanding of the molecular mechanisms promoting adipogenesis in lymphoedema is necessary for development of therapeutic strategies targeting formation of fat tissue for restricting the development of, or treating, secondary lymphoedema.

1.2 General aspects of secondary lymphoedema

Lymphedema is a slow but progressive condition characterised by impairment of lymph

flow from tissues to the blood circulation due to disrupted lymphatic vasculature, with subsequent accumulation of interstitial fluid which ultimately leads to chronic swelling of a limb (Figure 1.1). Secondary lymphoedema is etiologically distinct from primary lymphoedema, or hereditary lymphoedema which is a rare disease caused by intrinsic abnormalities of lymphatic function due to defects in genes that are involved in the growth and development of normal lymphatic vasculature [7]. The causes of secondary lymphoedema include trauma, infections and inflammation, but the disruption of the lymphatic vasculature due to surgical interventions (e.g. lymphadenectomy) and/or radiotherapy for breast cancer is most common in the developed world [8-11]. The condition, however, can occur not only in breast cancer patients, but can develop in patients with any cancer types which require lymph node dissection or radiotherapy treatment, such as head and neck, genitourinary and gynaecological cancers and melanoma [12].

It is estimated that approximately 300,000 Australians have cancer-related lymphoedema; up to 20 percent of Australian cancer survivors have secondary lymphoedema, and more than 8,000 new cases arise each year [13, 14]. In addition, the incidence of secondary lymphoedema varies considerably depending on the aggression of breast cancer surgery, from as low as 13% in women undergoing breast conservation with sentinel lymphadenectomy without chemotherapy to as high as approximately 60% in women who undergo breast conservation and chemotherapy with axillary lymphadenectomy or radiotherapy [15].

Patients with surgically disrupted lymphatic vessels have a reduced capability to transport lymph, which can lead to lymph stasis. Chronic lymph stasis fosters the accumulation of lymph fluid and oedema rich in protein and cellular metabolites, which is often followed by a change in tissue composition characterised by increased adipose deposits and dermal fibrosis, thus leading to profound swelling of a limb. As secondary lymphoedema is a condition caused by a lymphatic obstruction, the next section will cover our basic knowledge about the lymphatic system, which is then followed by, most pertinent to this review, its relationship with the development of fat tissue in secondary lymphoedema.

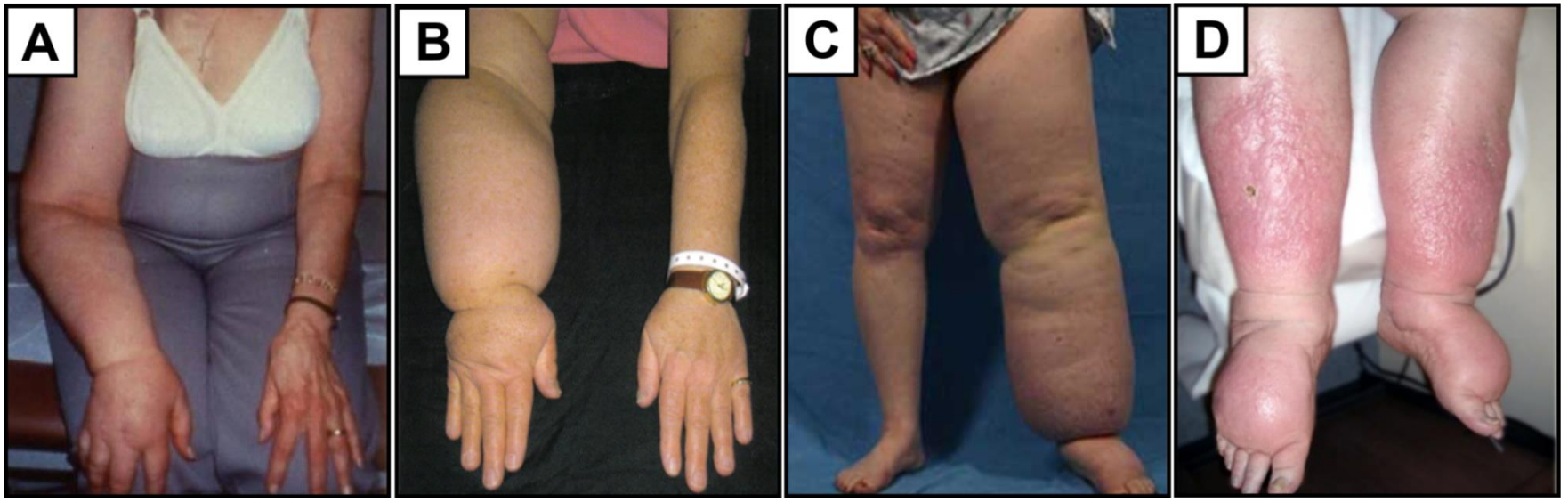

Figure 1.1 Clinical representation of secondary lymphoedema. (A) and (B) Upper limb secondary lymphoedema resulting from mastectomy. (C) Lower limb secondary lymphoedema following radiotherapy and lymphadenectomy for Hodgkin's lymphoma. (D) Bilateral lower limb secondary lymphoedema with associated skin and tissue changes. The sources of these images are as follows: (A) J. Zuther. "The Role of Complete Decongestive Therapy in Breast Cancer Treatment Related Lymphedema", Lymphedema blog, March 2012. http://www.lymphedemablog.com/2012/03/23/the-role-of-complete-decongestive-therapy-in-breast-cancer-related-lymphedema/. Accessed June 2016. (B) Women's Health and Education Centre. "Breast Cancer Surgical Treatment Complications & Lymphedema", August 2011. http://www.womenshealthsection.com/content/gyno/gyno005.php3. Accessed June 2016. (C) MacLellan. R.A and Greene. A.K., 2010. BMJ Best Practice Lymphoedema. BMJ Publishing Group. November 2015. (D) "Lymphoedema & Laser therapy". http://www.lympholaser.com.au/lymphoedema_p_s.html. Accessed July 2016.

1.3 Lymphatic system – overview

Humans have two specialised vascular systems for effective circulation: the blood vasculature which is responsible for delivering oxygen and nutrients around the body while carrying away waste products for detoxification and replenishment, and the lymphatic vasculature which runs in parallel with the blood vasculature, and plays various crucial roles, including the regulation of interstitial fluid homeostasis, immune surveillance, and lipid absorption [16, 17]. The following sections cover current knowledge on organ-specific lymphatic system in the human body.

1.3.1 Dermal lymphatic system

The dermal lymphatic system is a highly structured network consisting of distinct types of vessels. Interstitial fluid is absorbed at the epidermis of the skin by highly permeable initial lymphatics which have a discontinuous basement membrane and lack lymphatic-associated smooth muscle cells [18]. The initial lymphatics are composed of a monolayer of lymphatic endothelial cells (LECs) which are supported by short anchoring filaments that keep the vessels from collapsing due to increased interstitial fluid pressure [19]. The fluid is then absorbed and transported via deeper lymphatic pre-collectors to subcutaneous lymphatic collectors. The lymphatic pre-collectors have an uneven distribution of one-way valves which prevents the backflow of the fluid. They also have a discontinuous basement membrane and are occasionally covered with a layer of smooth muscle cells which enable them to have dual functions: absorption and transport of lymph [20]. The larger lymphatic collectors are distinct from initial lymphatics and pre-collectors in that they have a complete basement membrane and are fully covered by smooth muscle cells. The collectors also have intraluminal valves which are more regularly distributed than in pre-colelctors. Multiple lymphatic collectors converge to form lymphatic trunks (e.g. jugular, subclavian, bronchomediastinal, lumber and intestinal lymph trunks), which drain lymph into lymphatic ducts that transport lymph into the venous circulation [21].

The lymph in the lymphatic collectors also enters lymph nodes. Lymph nodes are secondary lymphoid organs which are important in the initiation and regulation of the adaptive immune response[22]. Afferent lymphatic vessels deliver lymph carrying antigens from the collectors to the subcapsular sinus in the nodes where they are recognised by immune cells, such as B and T cells [23]. Lymph carried by the afferent lymphatic vessels is then filtered through the medullary sinus, and ultimately exists via efferent lymphatic vessels to drain either into another node or to a lymphatic duct [23].

The thoracic duct is the body's largest lymphatic duct which originates from the cisterna chyli and passes through the diaphragm from the abdomen into the thorax. The thoracic duct drains lymph from the lower-half and upper-left quadrant of the body, including both the lower limbs, the abdomen, left thorax, upper-left limb, left head and neck and right-lower back, before transporting it into the bloodstream via the left internal jugular and left subclavian veins. The lymph from the remaining parts of the body, such as the right head and neck, upper-right limb, right thorax and upper-right back, is drained by the right lymphatic duct into the bloodstream via the right internal jugular and right subclavian veins [21].

1.3.2 Intestinal lymphatic system

The intestinal lymphatic system plays an important role in the uptake and transport of nutrients, dietary fat and lipid soluble vitamins and drugs [24]. Each small intestinal villus contains a single lymphatic vessel at the centre, called a lacteal. Intestinal lacteals transport dietary lipids as large (200-1,000 nm in diameter) triglyceride-loaded particles or chylomicrons, as well as other interstitial fluid components, such as hormones and immune cells, from villi to the sub-mucosal and mesenteric lymph collectors [23]. Intestinal lymph is transported to the mesenteric lymph nodes and to the thoracic duct from cisternal chyli, and ultimately released into the bloodstream via the left internal jugular and left subclavian veins [21].

1.3.3 Brain lymphatic system

It has long been considered that the central nervous system lacks lymphatic vasculature. It was not until recently however, that the existence of a lymphatic network was confirmed in the meningeal compartments in mice[25]. These lymphatic vessels are found lining the dural sinuses between the layers of dura mater, the most external layer of the meninges which drains blood from both the internal and external veins of the brain into the internal jugular veins [25]. The function of the dural lymphatics is to drain cerebrospinal fluid and interstitial fluid of the brain into the deep cervical lymph nodes, both for the transport of immune cells and for the clearance of macromolecules [25, 26]. A mouse study demonstrated that the dural lymphatics are involved in the clearance of neurotoxic misfolded proteins and peptides, such as tau proteins, from the brain [27]. This suggests that the brain lymphatic system could be a potential therapeutic target for Alzheimer's disease which is caused by accumulation of tau in the brain. Moreover, the glymphatic system has been recently discovered as a potential waste clearance system in the brain. This system utilises perivascular channels composed of astroglial cells to promote elimination of neurotoxic proteins from the brain interstitial fluid, such as amyloid β, to the cerebrospinal fluid which drains into the peripheral lymphatic system [28, 29]. Further research is required to better understand the functions and roles of the human brain lymphatic system in neurodegenerative diseases.

1.3.4 Ocular lymphatic system

Schlemm's canal is a specialised endothelium-lined vessel that encircles the margin of the cornea of the eyes. Schlemm's canal drains aqueous humor which is produced by the ciliary epithelium, and provides nutrients to the cornea and lens via the episcleral veins [30]. Glaucoma is caused by increased intraocular pressure due to impaired Schlemm's canal and impeded aqueous humor drainage [31]. Interestingly, molecular studies have demonstrated that the endothelial cells of Schlemm's canal express both blood and lymphatic endothelium markers, such as vascular endothelial growth factor receptor 3 (VEGFR3), prospero homeobox protein 1

(PROX1), platelet and endothelial cell adhesion molecule 1 (PECAM1) and forkhead box C2 (FOXC2) [30, 32, 33]. However, Schlemm's canal endothelial cells lack expression of other lymphatic endothelial markers, such as lymphatic vessel endothelial hyaluronan receptor 1 (LYVE1) and podoplanin, which prevents these endothelial cells being considered as "true" lymphatic vessels [33].

1.3.5 Pulmonary lymphatic system

Pulmonary lymphatic vessels are found in the visceral pleura, the serous membrane that covers the surface of each lung, as well as in the interlobular and intralobular septa in the vicinity of blood vessels. Smaller lymphatics may be present in interalveolar septa, and occasionally independent of blood vessels [34]. The functions of pulmonary lymphatic vessels include maintenance of interstitial fluid homeostasis for effective gas exchange in alveoli [35]. Notably, pulmonary lymphatics are present before birth, and an animal study using mice has demonstrated that the lymphatic vessels facilitate the clearance of lung interstitial fluid in the fetus, thereby allowing the developing lungs to prepare for inflation at birth [36]. Pulmonary lymphatic vessels are also important in regulating inflammatory and immune responses, transporting antigen-presenting dendritic cells to draining lymph nodes in and near the lungs (e.g. hilar, bronchial and mediastinal lymph nodes) where the adaptive immune responses are triggered [37].

1.3.6 Hepatic lymphatic system

The liver plays a critical role in lymphatic fluid production as 25-50% of lymph passing through the thoracic duct is produced in the liver [38]. The liver has sinusoidal capillaries which are distinct from blood capillaries in that they are devoid of basement membranes and consist of one layer of liver sinusoidal endothelial cells. Hepatic lymph originates from plasma components filtered through the liver sinusoidal endothelial cells into the interstitial space between the sinusoidal endothelial cells and hepatocytes, known as the space of Disse [39]. The majority of lymph in the periportal space of Disse seeps into the space of Mall, a space between the stroma

of the portal tract (consisting of a portal venule, hepatic arteriole, bile ducts and lymphatic vessels) and the outermost hepatocytes, and drains into lymphatic vessels in the portal tract. The hepatic lymphatic vessels in the portal tract converge to form collecting lymphatics, which drain the lymph into lymph nodes at the hepatic hilum [38]. The efferent vessels from these lymph nodes connect to celiac lymph nodes, which drain the lymph into the cisterna chyli and thoracic duct before transporting it to the blood circulation [38]. The rest of lymph in the space of Disse flows through the space around the hepatic central vein or underneath the hepatic capsule, which ultimately drains into mediastinal lymph nodes [38].

1.3.7 Renal lymphatic system

Renal lymphatic vessels are found around the renal artery in the cortex of the kidney (i.e. interlobular and intralobular lymphatics). There are also lymphatic vessels within the renal capsule and subcapsular cortical region [40, 41]. Although no lymphatic vessels have been found in the medullary region in normal human kidneys, an old autopsy study reported that they were present in cancer settings [42]. Ishikawa et al. also found lymphatic vessels sporadically present in close proximity to the juxtaglomerular apparatus [43], where renin is produced and acts in a paracrine fashion [44]. This explains relatively high levels of renin in renal lymph, which is not present in lymph from other organs [45].

The main function of the renal lymphatics is to regulate oncotic pressure necessary for tubular reabsorption, by controlling the volume, pressure and albumin concentration in the interstitial fluid [41]. Renal lymphatics also play an important role in immune cell trafficking as they can transport lymph from the kidney to various distant lymph nodes and eventually connect to the origin of the thoracic duct via the cisterna chyli [41].

1.3.8 Cardiac lymphatic system

The mammalian cardiac lymphatic vasculature is present in all layers of the heart; the

subepicardium, the myocardium and the subendocardium. Lymph is drained from the subendocardial plexus to the myocardial plexus and then to the subepicardial plexus. Once the lymph is in the subepicardial plexus, it flows unidirectionally through lymphatic collectors extending from the base of the heart to the pulmonary artery, and drains into the mediastinal lymph nodes before entering the thoracic duct [46].

The cardiac lymphatic system plays an important role in the maintenance of myocardial interstitial fluid and immune cell homeostasis. An imbalance between cardiac lymphatic drainage and myocardial blood microvascular permeability results in myocardial oedema which can lead to cardiac dysfunction [47]. Importantly, increased lymphatic vessel growth by lymphangiogenesis in the heart has been demonstrated in experimental models of myocardial infarction and ischemia [48, 49]. These studies showed that augmentation of endogenous cardiac lymphangiogenesis with VEGFC treatment reduced inflammation, oedema and fibrosis, and overall improved cardiac function in mice. Joaquim et al. claimed that the improved cardiac function was due to an increased drainage of immune cells (e.g. pro-inflammatory macrophages) from the injury site to the mediastinal lymph nodes [48].

Overall, recent discoveries in organ-specific lymphatic systems have significantly deepened our understanding of lymphatic biology. In this thesis, the focus will be on the dermal lymphatic system given its relevance to secondary lymphoedema.

1.4 Fat tissue in secondary lymphoedema

1.4.1 Lymphatic system and fat tissue

There is a close relationship between the lymphatic system and fat tissue, given that anatomically subcutaneous fat tissue lies in close proximity to the lymphatic vasculature in the dermis (Figure 1.2) [50]. Lymphatic collectors and mesenteric lymph nodes are surrounded by visceral or subcutaneous fat tissue, and dietary lipids are transported as chylomicrons through

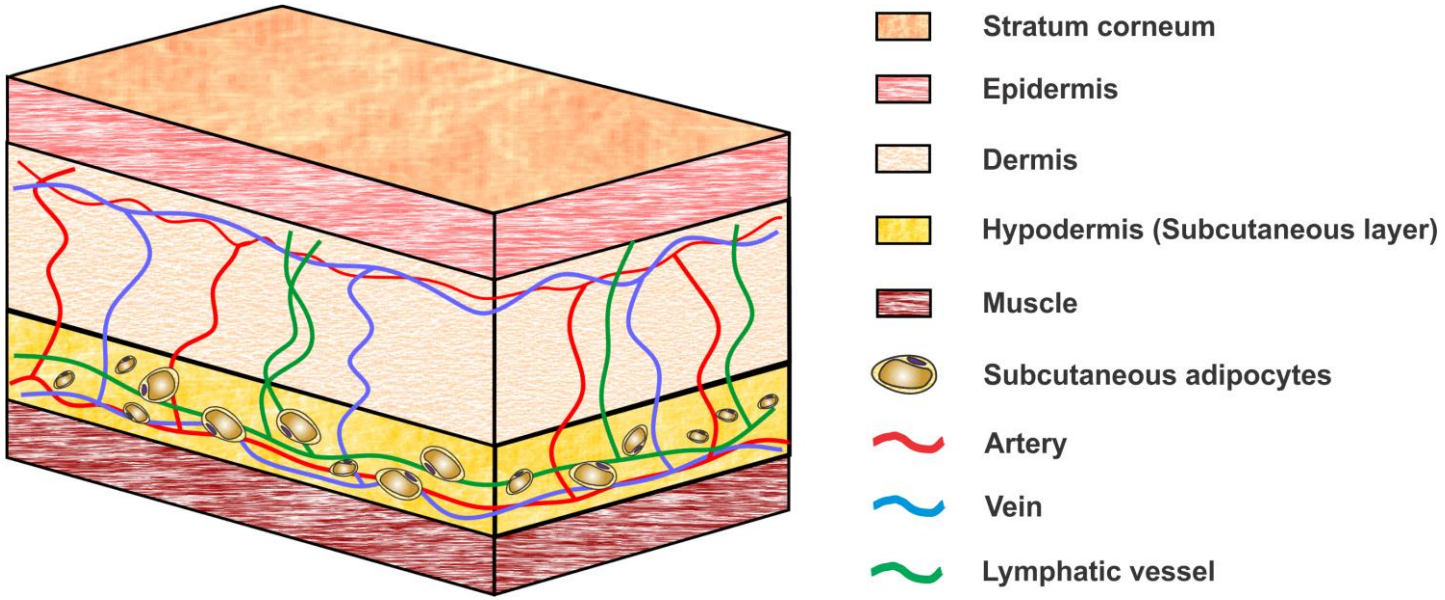

Figure 1.2 Schematic representation of human skin layers. Human skin is mainly composed of three layers; epidermis, dermis and hypodermis (subcutaneous layer). The stratum corneum is the outermost layer of the epidermis. Blood vessels and lymphatic vessels are found in the dermis and subcutaneous layer, and run in parallel to each other. The dermal lymphatic vessels lie close to subcutaneous fat tissue. Other dermal components, such as hair follicles, sweat glands and nerves, are excluded for simplicity.

lacteals to the bloodstream [24]. Fat tissue surrounding lymph nodes, the central system for immune surveillance, is itself involved in inducing local, transient immune responses [51-53]. A study showed that there was an increased rate of lipolysis by the adipocytes adjacent to lymph nodes upon immune stimulation in mice, compared to adipocytes more distantly located from the nodes [52]. Also, free fatty acids released by lipolysis were shown to induce proliferation of lymphocytes *in vitro* [51]. Furthermore, addition of lymphatic fluid to culture media enhanced lipogenesis compared with culture media supplemented only with serum [54]. Interestingly, fat tissue tends to accumulate adjacent to lymphatic structures. For example, an *in vivo* study demonstrated that chronic immune stimulation of lymph nodes in rats led to formation of additional mature adipocytes by increasing both the size (hypertrophy) and the number (hyperplasia) of adipocytes surrounding the stimulated nodes [55]. These findings correlate well with clinical reports showing that accumulation of subcutaneous fat tissue occurs proximal to affected lymphatic vessels in patients with lymphoedema [56, 57].

There is however, limited data on the exact component(s) of the interstitial fluid that induces the formation of fat tissue in lymphoedema. This has been studied in mice deficient for the transcription factor PROX1 which is crucial for LEC differentiation and patterning – these mice exhibit abnormal lymphatic vessels and develop lymphoedema [30]. A lipidomic profiling of lymph collected from both Prox1 heterozygous and wild-type mice showed no significant differences in the composition of free fatty acids between the two groups, although some free fatty acids (e.g. oleic acid, α-linoleic acid, palmitoleic acid and palmitic acid) in the lymph from the both study groups induced hypertrophy of adipocytes and promoted adipogenesis in 3T3-L1 mouse preadipocytes [58]. Further, a recent substantial lipidomic analysis in humans showed that the majority of lipid molecules including phosphatidylcholines, phosphatidylethanolamines, cholesterol esters as well as fatty acids were present in a highly similar abundance in lymphoedematous and non-lymphoedematous individuals, suggesting that adipocytes in lymphoedematous tissues may be essentially the same as adipocytes in normal tissues in terms of lipid content [59]. On the other hand, other studies showed that levels of specific pro-

inflammatory fatty acids, such as arachidonic acid and ceramides, increased up to 1.4-fold in lymphoedema as compared to non-lymphoedematous controls [60, 61]. These findings raise the possibility that accumulation of fat tissue in lymphoedema may be induced by abnormal exposure of adipocytes to leaking lymph containing free fatty acids with a capacity to enhance adipogenesis.

1.4.2 Clinical evidence of development of fat tissue in patients with secondary lymphoedema

Lymphatic vessels serve as a critical conduit for immune cell trafficking and interstitial fluid transport. Normally, fluid leaking out of blood vessels is collected by lymphatic vessels and transported back to the blood circulation. However, in secondary lymphoedema arising from surgical lymph node ablation in breast cancer patients, the normal lymphatic drainage may be impaired due to damaged lymphatic collectors and smaller lymphatics, which leads to accumulation of interstitial fluid and eventually the formation of fat tissue in affected regions. In fact, the concept suggesting the relationship between an impaired lymphatic system and formation of fat tissue existed as early as the 19th century. Paul Unna, a German dermatologist, observed that fat accumulated as a result of the stagnation of tissue by lymphatic or venous interruption [62]. Schinger *et al*. reported that "the subcutaneous fat was strikingly abundant in all cases" in surgically excised skin and subcutaneous tissue from patients with secondary lymphoedema [63]. Further evidence comes from a case report which demonstrated that cutaneous lymphatic malformation resulted in secondary late-onset fat hypertrophy [56]. Traditionally, it has long been thought that the swelling of a lymphedematous arm is solely due to accumulated lymph fluid [64]. However, clinical studies by Brorson *et al.* have revealed that most of the increased soft tissue volume in lymphedematous arms comes from an increased volume of fat tissue [65]. For example, analyses by dual X-ray absorptiometry revealed that there was an average of 73% (range 43-111%) greater fat volume in a lymphedematous arm compared to a normal arm [65]. Of note, an average of 55% (range 32-81%) of the excess volume of the lymphoedematous arm was found to be due to accumulation of fat tissue. Further analyses in the aspirate derived from lymphoedematous arms also showed excess amount of fat tissue, with a reported range of 68% to 93% greater fat volume compared to normal arms (Figure 1.3) [6]. These clinical findings of increased volume of

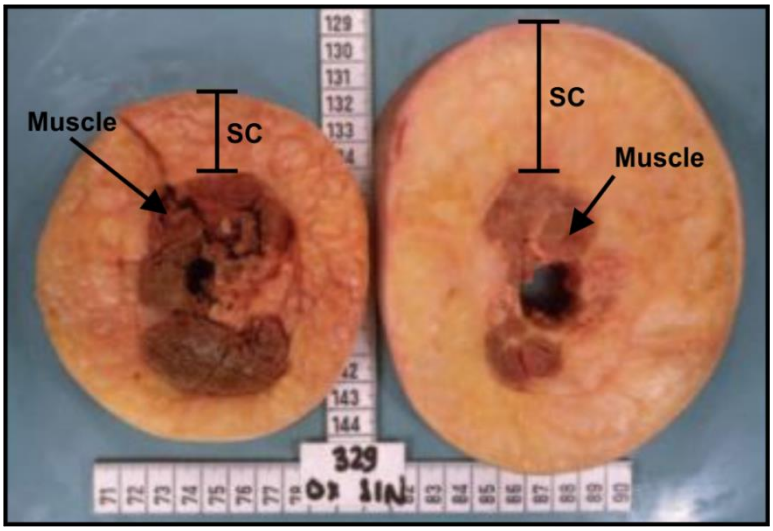

Figure 1.3 Comparison between cross-sections of lymphoedematous and normal arms. The lymphoedematous arm (right) has an increased thickness of the subcutaneous layer due to excess fat tissue in comparison to the normal non-lymphoedematous arm (left). SC denotes subcutaneous layer. The image is adapted from Brorson H. and Freccero C. 2008. Liposuction as a treatment for lymphoedema, pp.11-25. In: *Lymph/Lipoedema Treatment in its Different Approaches*. Jobst 1st Symposium 2008. Aberdeen, Scotland: Wounds UK.

fat tissue in lymphedematous limbs suggest that excess fat tissue significantly contributes to a marked increase in the arm volume following breast cancer surgery, thus emphasising the importance of developing therapeutic strategies targeting the expansion of fat tissue in secondary lymphoedema.

1.4.3 Evidence of development of fat tissue in animal models of lymphoedema

Evidence of increased formation of fat tissue in lymphoedema can be derived from studies using transgenic mouse models of primary lymphoedema. For example, activation of the vascular endothelial growth factor receptor 3(VEGFR3) tyrosine kinase, which is expressed specifically on LECs, is associated with the growth and maintenance of lymphatic vessels in normal adults [66]. Studies using a *Chy*-mouse model with a heterozygous inactivating *Vegfr3* mutation have shown an extensive swelling of limbs due to hypoplastic cutaneous lymphatic vessels and increased levels of subcutaneous fat tissue and collagen deposition in oedematous regions, which resembles clinical lymphoedema [67, 68]. Additionally, mice heterozygous for an inactivating *Prox1* mutation exhibited abnormal lymph leakage and accumulation, which in turn resulted in adult-onset obesity [69]. The increase in body weight in these mice was shown to be due to accumulation of subcutaneous and intra-abdominal fat, particularly around lymph nodes and in the mesentery rich in lymphoid tissue. These findings are further supported by the fact that leaky lymphatics promote obesity in *Prox1* heterozygous mice, and restoring PROX1 levels in these mice improves lymphatic function, which in turn leads to decreased body weight resulting from reduced levels of subcutaneous fat tissue [58]. Further evidence of increased formation of fat tissue due to impaired lymphatic vasculature was demonstrated in a mouse model of secondary lymphoedema in which lymphatic vessels in tails were surgically disrupted by a full circumferential incision. This study by Zampell *et al.* demonstrated that surgical ablation of lymphatics in the tail leads to lymph stasis, which in turn contributes to a significant increase in subcutaneous fat tissue as a result of both hypertrophy and hyperplasia of adipocytes [5]. These findings are consistent with those from a *Prox1* mutant mouse model [69]. In addition to the increased levels of subcutaneous fat tissue, the surgically ablated tails also exhibit other

pathophysiological features of clinical lymphoedema, such as dermal fibrosis and inflammation [5, 70]. Notably, the increased adipose deposits in the tails post-operatively were found to be associated with increased expression of genes involved in adipose differentiation, such as the genes for CCAAT/enhancer binding protein-alpha (C/EBPα), peroxisome proliferator-activated receptor gamma ($PPAR_{\Upsilon}$) and adiponectin, a peptide hormone secreted by adipocytes [71]. This finding is consistent with a gene expression study reporting that human lymphoedema-associated adipose-derived stem cells have increased expression of $PPAR_{\Upsilon}$ compared with those derived from non-lymphoedematous subcutaneous fat tissue, suggesting that lymphoedema may render these cells more sensitive to adipogenic stimuli [72].

It is important to note, however, that the above animal models of lymphoedema do not perfectly mimic the entire spectrum of chronic lymphoedema in humans. Firstly, studies were conducted for a short period of time (e.g. 6 to 10 weeks). Clinical lymphoedema, on the other hand, typically develops slowly. Although the timing of onset of symptoms is highly variable among patients, it usually develops within 2 to 3 years, but sometimes can develop decades after surgery [73, 74]. Secondly, lymphoedema in humans is a chronic disease which does not heal naturally, whereas these animal models exhibit a slow but gradual regression of swelling due to wound healing which would make it difficult to investigate the outcomes of any long-term therapies. Nevertheless, these animal models demonstrate that an impaired lymphatic system can lead to pathological phenotypes which closely correlate with clinical features of human lymphoedema, such as formation of fat tissue.

1.4.4 Obesity and lymphoedema

Numerous studies have shown that development of fat tissue and lymphoedema may have a reciprocal relationship. While impaired lymphatic function in lymphoedema is thought to promote accumulation of fat tissue, it is also evident that increased fat deposition contributes to lymphoedema. In fact, obesity is a strong predisposing factor for the development of secondary lymphoedema in breast cancer patients [75]. In an early study involving 1,007 breast cancer

patients, it was reported that 55% of patients weighing more than 90 kg had marked swelling in the arms following mastectomy, whereas only approximately 35% of patients weighing up to 70 kg had swelling [76]. The correlation between body mass index (BMI) and the development of upper limb lymphoedema has also been studied extensively. For example, a case study reported that individuals with a BMI greater than 30 kg/m^2 had almost three times the risk of developing post-operative arm lymphoedema compared with those with a BMI less than 25 kg/m^2 [77]. In another study, Werner *et al.* found that BMI was closely associated with the development of arm lymphoedema after radiotherapy, and that the 5-year incidence of lymphoedema in patients with a BMI greater than 29 kg/m^2 was three times higher than in patients with lower BMI (36% versus 12%, respectively) [78]. Consistently, a larger study involving 936 breast cancer patients reported that high body weight and BMI were strongly correlated with severity of lymphoedema following axillary lymph node dissection [73]. Greene *et al.* have shown that severe obesity combined with BMI greater than 59 kg/m^2 is significantly associated with development of lower limb lymphedema [79]. Also, the average BMI was found to be significantly greater in breast cancer patients with lymphedema compared to those without lymphedema (70.1 kg/m^2 versus 42.0 kg/m^2, respectively) [79]. Although these studies provide ample evidence that swelling of a limb in secondary lymphoedema increases with severity of obesity, the influence of BMI should be examined with caution. BMI may not necessarily be the most reliable indicator of obesity because it does not distinguish between fat and muscle, which may shift toned individuals into an overweight status, even though they have low fat levels.

Argrim *et al.* investigated the correlation between obesity and lymphatic drainage in fat tissue. It was reported that obese individuals had significantly lower fat tissue lymphatic flow indicating that obesity may impair the removal of macromolecules from the interstitial space [80]. The removal of macromolecules and fluid from the interstitial space requires interstitial fluid transport as well as lymphatic drainage [81]. An animal experiment demonstrated that axillary lymph node dissection in rat forelegs led to a marked swelling of the leg, reduced interstitial flow rate and impaired lymphatic drainage [82]. Moreover, Savetsky *et al.* showed that lymph node

uptake of technetium in the upper extremity was significantly reduced in mice with surgically-induced lymphoedema, and this phenomenon was even worse in obese mice as compared to lean mice [70]. Additionally, there is increasing evidence showing that high-fat diet (HFD)-induced obesity is a key determinant of predisposition to, or severity of, lymphoedema. For example, HFD-induced obesity led a fewer dermal lymphatics, impaired lymphatic vessel function and a greater accumulation of perilymphatic lipid in mice [83]. Further, increased adiposity has been shown to render mice more susceptible to an increased extent of surgically-induced lymphoedema [84]. It was also shown that apolipoprotein E-deficient mice, which spontaneously develop hypercholesterolemia and obesity, were more likely to develop tissue swelling, lymphatic leakiness and impaired lymphatic transport due to degeneration of lymphatic vessels compared to wild-type mice [85].

While recent studies provide novel insights into the effects of weight control on lymphatic function in obesity, whether exercise-induced weight loss is as effective as diet-induced weight loss for improving lymphatic function remains elusive. For example, Hespe *et al.* showed that impaired lymphatic function in obese mice may be reversed by aerobic exercise due to decreased levels of inflammation [86]. Indeed, this finding is supported by another study demonstrating that exercise resulted in a marked reduction in inflammatory responses without causing any significant weight loss [87]. In addition, Nitti et al. investigated the effect of weight loss on lymphatic function in diet-induced obese mice. It was demonstrated that weight loss through diet restriction reversed elevated levels of inflammatory cells (e.g. T cells and macrophages), and decreased perilymphatic expression of the inducible nitric oxide (iNOS), a negative regulator of the collecting lymphatic pumping function [88], thus leading to improved lymphatic function. These findings are consistent with the observation that inhibition of iNOS decreases inflammation and improves lymphatic function in obese mice [89], and the known role of inflammatory cytokines in impairing lymphatic vessel function [90, 91].

Further research is required to determine how the interplay between the development of

fat tissue, inflammation and lymphatic vessels plays a role in the development of secondary lymphoedema. Nevertheless, given the body of evidence showing the correlation between increased adiposity and impaired lymphatic function, obese individuals may be at higher risk for developing lymphoedema due to impaired lymphatic vessel function even before surgical cancer treatment.

1.5 Clinical strategies that modulate lymphoedema

To date, no curative treatments for lymphoedema are available, and control of lymphoedema symptoms by a variety of physiotherapeutic interventions has been the mainstay of treatment options. The goal of current therapy is directed towards symptomatic relief and reducing the excess volume of affected areas as much as possible. Treatment options can be classified into two categories, namely physical therapy and surgical therapy [92].

1.5.1 Physical therapy

Management of secondary lymphoedema is often approached through complete decongestive therapy (CDT), a form of physical therapy, which consists of four components: manual lymphatic drainage, compression bandaging, skin care and lymphatic exercise [93]. CDT is performed to decrease limb swelling and oedema, reduce dermal fibrosis and the risk of infections, increase interstitial fluid drainage from the congested areas, relieve patient discomfort and improve overall quality of life.

1.5.1.1 Manual lymphatic drainage and compressing bandaging

Manual lymphatic drainage is usually conducted by well-trained lymphoedema therapists, and is aimed to stimulate the lymphatic collectors to increase their pumping rate, thereby removing excess interstitial fluid or lymph from congested areas into unaffected regions where the fluid can be drained. Typically, manual lymphatic drainage is applied to tissues in which lymphatic vessels are still in a ‘reversible’ condition, rather than in more advanced stages of lymphoedema where lymphatics are dominated by fat tissue and smooth muscle hyperplasia [94, 95].

Compression bandaging also plays a critical role in reducing lymphoedema volume. It exerts its effect by narrowing superficial lymphatic vessels, thus increasing interstitial pressure and limiting blood capillary filtration, which leads to an increased rate of lymph flow [96-98]. However, inconsistent findings have been reported among studies of the therapeutic effects of manual lymphatic drainage and compression bandaging. A study investigating the effect of manual lymphatic drainage alone demonstrated that lymphoedema patients experienced significantly reduced excess limb volume and dermal thickness of the upper arm [99]. In addition, another manual lymphatic drainage-based early physiotherapy programme, which consisted of manual lymphatic drainage and massage of scar tissue combined with some shoulder exercises, showed that these physical approaches effectively reduced the occurrence of secondary lymphoedema in women after lymphadenectomy [100]. However, Badger *et al*. concluded in a different study, involving both manual lymphatic drainage and compressing bandaging, that the reduction in limb volume was attributed only to the compressing bandaging, and that manual lymphatic drainage provided no extra benefit in reducing tissue swelling at any point during the trial [101]. In contrast, other studies reported an extra positive benefit of manual lymphatic drainage, in addition to compressing bandaging, for reducing excess limb volume [102, 103]. Importantly, Vignes *et al*. reported that the use of manual lymphatic drainage alone increased the risk of failure to maintain reduced limb volume after CDT in lymphoedema patients, although the reasons underlying the increased risk are not known [104]. In conclusion, the benefits conferred by manual lymphatic drainage versus compressing bandaging remain somewhat unclear.

1.5.1.2 Skin care

Good hygiene is considered an essential element in the management of lymphoedema. Given that bacteria and fungi may enter through the dry and cracked skin common in lymphoedema patients, keeping skin moist is thought to be critical for reducing the chance of infection (e.g. cellulitis). Cellulitis is a relatively common complication in patients with lymphoedema. It arises from impaired immune surveillance and accumulation of protein-rich

fluid as a result of impedance to lymphatic flow and clearance. The resulting abnormal tissue microenvironment serves as a favourable niche for bacteria and fungi to grow [105].

1.5.1.3 Exercise

Obesity is a key risk factor for lymphoedema because it is thought to contribute to reduced lymphatic clearance, which leads to oedema, tissue swelling and a favourable tissue environment for bacterial growth [106]. Hence, appropriate exercises for reducing obesity are beneficial for patients with lymphoedema in terms of minimising the risk of tissue swelling and infection. Lymphoedema patients who conducted appropriate exercises were shown to have improved flexibility, increased strength, improved body composition, and improved lymphatic flow due to an increased musculoskeletal pumping system [79, 107]. A study demonstrated that secondary lymphoedema patients who carried out gentle arm exercise, combined with deep breathing, had significantly reduced arm volume and subjective symptoms compared to the control group that had no interventions, and the reduction in arm volume was maintained over a one-month period without any adverse effects [108]. In addition, two randomised prospective clinical trials showed that women with secondary lymphoedema who underwent weight-lifting programmes had a decreased incidence of lymphoedema onset after breast cancer surgery as compared to the control group [109, 110]. Moreover, it was demonstrated that a combination of aerobic exercise and resistance exercise significantly improved self-esteem, physical fitness and body composition in patients without exacerbating lymphoedema or causing serious adverse effects [111]. The quality of life and social physique anxiety among breast cancer survivors were also significantly improved by the combination of the aerobic and resistance exercise [112]. These studies were, however, limited by low adherence and recruitment rate, and a short intervention period. Therefore, additional research with larger study groups and a longer follow-up period is required to more accurately assess the potential beneficial effect of exercise on the development of secondary lymphoedema.

1.5.2 Surgical therapy

Surgical therapy is a treatment option available for patients unresponsive to conventional physiotherapy due to the severity of late-stage lymphoedema. Three major surgical approaches for treating lymphoedema are discussed below: liposuction, resection, and microsurgery.

1.5.2.1 Liposuction

Liposuction has been employed to treat lymphoedema with the intention of reducing limb volume by removing excess subcutaneous fat using aspiration cannulae through skin incisions [113]. This approach is based on clinical data demonstrating that there is more fat tissue in the arms of patients with post-operative lymphoedema compared with unaffected arms [6]. Brorson *et al.* demonstrated that treatment of secondary lymphoedema patients with liposuction resulted in a profound reduction of limb volume, due to removal of fat and reduction of tissue oedema, at 4 years follow-up [114]. However, the long-term nature of the reduced limb volume may have required continuous post-operative compression bandaging, given that a marked increase in arm volume was observed in patients who discontinued their compression bandaging post-liposuction [115]. In assessing the potential utility of liposuction for treating lymphoedema, it is important to note that this approach is associated with complications including nerve and vessel damage, infection, bleeding and cellulitis [116, 117].

1.5.2.2 Resection

Resection procedures (also known as excisional procedures) involve the surgical removal of redundant skin and excess subcutaneous fat tissue thus aiming to provide improved comfort and reduced infection [118], although they fail to directly address lymphatic dysfunction. Several studies reported a reduction of excess tissue volume in secondary lymphoedema patients by approximately 20% in response to resection procedures [119, 120]. The major disadvantage of this approach is its high degree of morbidity due to significant loss of blood, infection, hematoma, skin necrosis and loss of limb function [121]. Moreover, long-term post-operative physiotherapy may be necessary to sustain the reduced limb volume after resection procedures.

1.5.2.3 Microsurgery

Microsurgical techniques used to treat secondary lymphoedema are aimed at improving lymphatic function and thereby removing accumulated interstitial fluid. This is done by creating a channel or anastomosis between the lymphatic system and venous system. This method commonly involves the creation of an anastomosis between a lymphatic vessel and a vein (lymphatic-venous anastomosis) [122], but it can also be done between lymph nodes and veins (lymph node-vein anastomosis) [123], or between distal and proximal lymphatics [124]. A prospective clinical study showed that lymphatic-venous anastomosis in secondary lymphoedema patients resulted in a 42% reduction in upper limb volumes which was maintained in long-term follow-up [125]. In addition, case studies demonstrated that lymphatic-venous anastomosis in two patients, who had lower-limb lymphoedema for 3 or 5 years, improved lymphatic function as assessed by indocyanine green lymphography, although the studies were limited by the small number of cases and a short follow-up period [126]. These findings imply that the pathological changes which occur at a late-stage of lymphoedema might be reversible. The limitation of the technique is that it is difficult to assess the condition of lymphatic vessels, i.e. whether a vessel is suitable for lymphatic-venous anastomosis or not. Also, as for other types of surgery, lymphoedema patients may require life-long use of compression garments to prevent the recurrence of swelling. These limitations in surgical approaches underscore the importance of developing non-invasive therapeutic strategies aimed at reducing tissue swelling in secondary lymphoedema.

1.6 Current molecular targeted strategies that modulate lymphoedema in animal models

To date, existing treatment strategies for secondary lymphoedema largely rely on physiotherapeutic and surgical interventions with the intention to reduce oedema volume, and thus lack the ability to address the underlying molecular mechanisms that drive the formation of fat and tissue swelling. In recent years, however, with improvement of our understanding of molecular mechanisms of lymphatic development, there has been an increasing interest in promoting the growth of new lymphatic vessels (lymphangiogenesis) as a potential therapeutic

strategy for secondary lymphoedema. As shown in the Figure 1.4, lymphangiogenesis is regulated by several molecular signalling cascades, involving vascular endothelial growth factors (VEGFs) [127], hepatocyte growth factor (HGF) [128] and transforming growth factor β (TGFβ) [129]. TGFβ can also promote dermal fibrosis, which is another key pathological feature of clinical secondary lymphoedema [130]. Animal studies have also shown that non-steroidal anti-inflammatory drugs (NSAIDs) [131] and retinoic acid [132] may have beneficial effects in treating lymphoedema. Lastly, there is emerging evidence that immune cells, such as macrophages and regulatory T cells, can modulate lymphangiogenesis in animal models of lymphoedema.

1.6.1 VEGFC/VEGFD/VEGFR3 signalling axis

The VEGF family of secreted proteins and their cell surface receptors are involved in development and growth of the blood vascular and lymphatic systems. Lymphatic remodelling and lymphangiogenesis are principally regulated by two VEGF family members, VEGFC and VEGFD, which drive these processes by activating VEGFR3 expressed on LECs [133, 134]. These ligands can also activate VEGFR2 on LECs which can contribute to signalling for lymphatic remodelling [135]. VEGFR3 forms homodimers, as well as heterodimers with VEGFR2, upon binding of VEGFC and VEGFD, which leads to autophosphorylation of specific tyrosine residues in the intracellular catalytic portion of the receptors. This, in turn leads to activation of downstream signalling pathways, such as the phosphoinositol-3-kinase (PI3K)/Akt and mitogen-activated protein kinase (MAPK) pathways [135]. A study with homozygous VEGFC-deficient mice demonstrated a critical role for VEGFC in lymphatic development, and heterozygous mice developed lymphoedema [136]. In addition, ectopic expression of soluble VEGFR3 in the skin, which inhibited VEGFC and VEGFD signalling in this tissue, blocked fetal lymphangiogenesis in the skin and induced regression of pre-existing lymphatic vessels, leading normal lymphatic development.

The strategy of promoting lymphangiogenesis to achieve improved outcomes in

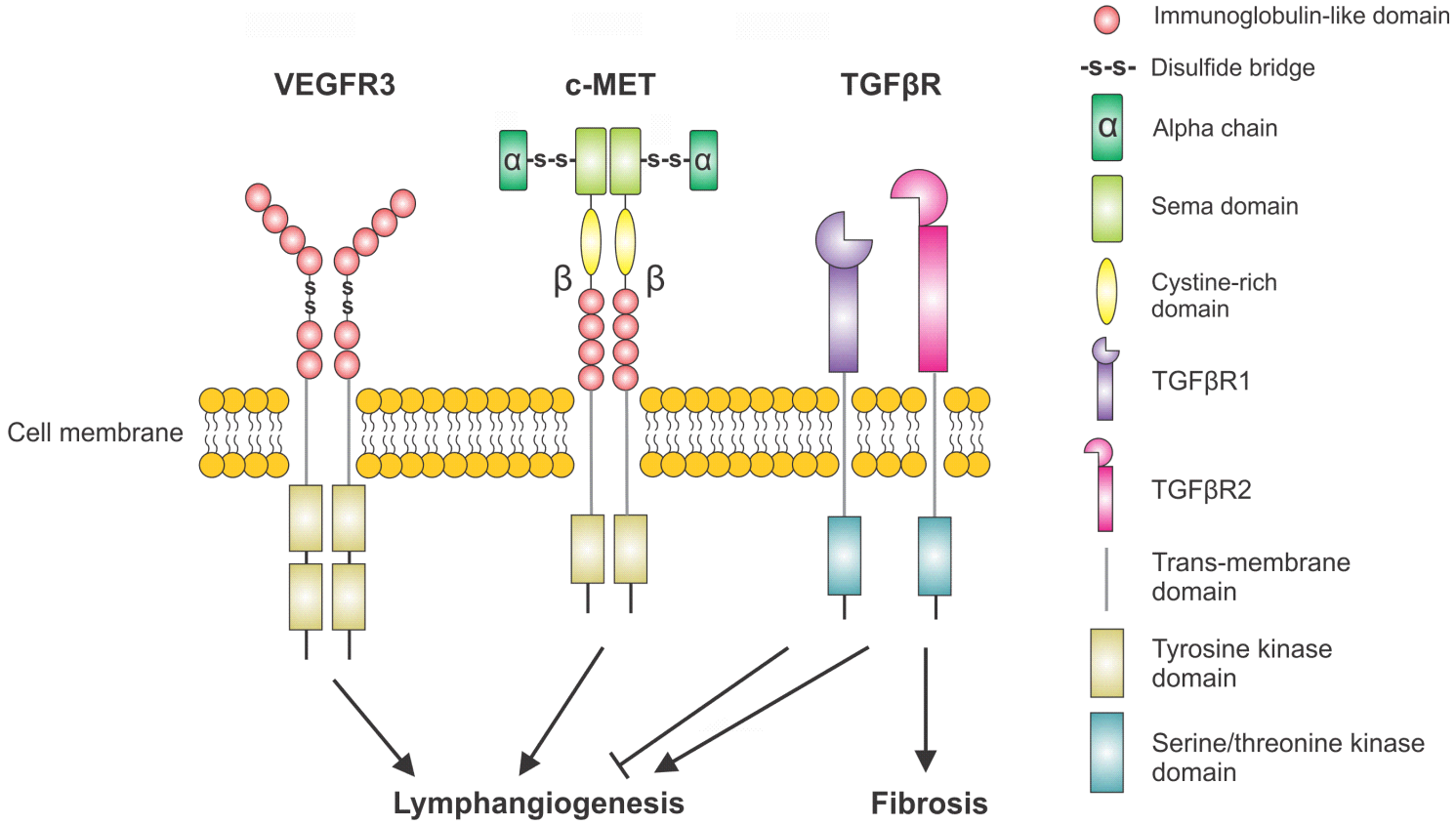

Figure 1.4 Selected molecular signalling pathways regulating lymphangiogenesis and dermal fibrosis in lymphoedema. VEGFR3 (a receptor for VEGFC and VEGFD), c-MET (a receptor for HGF) and TGFβ receptor (TGFβR) are membrane-bound cell surface receptor tyrosine kinases. VEGFR3 and c-MET signalling can promote lymphangiogenesis. TGFβR signalling promotes fibrosis, and can induce or inhibit lymphangiogenesis in a context-dependent manner. The β chain of c-MET spans from its sema domain to its tyrosine kinase domain.

lymphoedema is supported by a number of preclinical studies. For instance, Yoon *et al.* investigated the therapeutic potential of human VEGFC both in the rabbit ear and the mouse tail models of secondary lymphoedema. This study demonstrated that VEGFC significantly reduced ear and tail thickness, and promoted lymphangiogenesis which led to enhanced lymphatic drainage [137]. Likewise, Cheung *et al.* showed that delivery of VEGFC resulted in a significant decrease in mouse tail volume, which was associated with the resolution of inflammation, hypercellularity and microlymphatic dilation [138]. Another study using a rabbit ear model showed that VEGFC not only improved lymphatic function but also restored normal tissue cellularity and tissue architecture that had been perturbed by lymphoedema [139]. Lastly, Tammela *et al.* found that adenoviral delivery of VEGFC in lymph node-excised mice significantly resolved lymphedema [140]. Notably, the VEGFC-treated mice experienced regeneration of lymphatic capillaries which gradually differentiated and developed into functional lymphatic collectors.

A range of studies of VEGFC therapy in secondary lymphoedema suggest that it may be an attractive treatment for patients with this condition; however, there are some potential limitations. Firstly, VEGFC was administered shortly after the surgery for inducing lymphoedema in the animal models, so the therapy was applied before lymphoedema had developed or at a very early stage of lymphoedema. Hence these studies do not provide information about treatment of chronic lymphoedema. It will therefore be important to investigate the effectiveness of VEGFC therapy in the chronic setting. Secondly, not all studies have shown that VEGFC is beneficial, e.g. overexpression of VEGFC in a mouse model of lymphoedema exacerbated the condition by increasing blood vascular leakage and immune cell infiltration [141]. Furthermore, Goldman *et al.* demonstrated that delivery of VEGFC did not induce formation of functional lymphatics, but rather hyperplastic lymphatics with compromised functional characteristics [142]. Thirdly, VEGFC and VEGFR3 have been shown to promote metastasis of breast and colon cancer due to hyperpermeable, functionally compromised lymphatic vessels [143-146]. Thus, there is a concern that VEGFC treatment of patients who developed their lymphoedema consequent to cancer

therapy may promote the spread of residual tumour cells. These considerations illustrate that it will be important to better understand the potential advantages and dangers associated with VEGFC treatment before proceeding to clinical trials involving secondary lymphoedema patients.

1.6.2 Hepatocyte growth factor

In addition to the VEGFC/VEGFD/VEGFR3 signalling pathway, it has become clear that HGF is also involved in the regulation of lymphangiogenesis and lymphatic remodelling. The bioactivities of HGF are mediated by the HGF receptor, also known as c-MET, a membrane-spanning receptor tyrosine kinase expressed in the epithelial cells of various organs, including kidney, prostate, liver and muscle [147, 148]. The c-MET receptor is activated upon binding of HGF to the extracellular portion, which results in receptor homodimerisation and phosphorylation at two specific tyrosine residues (Y1234 and Y1235) in the intracellular catalytic domains [147]. Importantly, Kajiya *et al.* found that c-MET was highly expressed on PROX1-positive lymphatic vessels and that transgenic delivery of HGF in mice induced lymphangiogenesis [149]. Furthermore, Saito *et al.* demonstrated that swelling in rat tails after lymphatic ablation was significantly decreased by administration of plasmid DNA driving expression of human HGF, which enhanced the growth of local lymphatic vessels [150]. Moreover, inactivating mutations in the genes for HGF or c-MET have been detected in some lymphoedema patients suggesting that the HGF/c-MET signalling axis may be important in secondary lymphoedema [151] and may provide a therapeutic target for treating this condition. Interestingly, treatment with HGF was shown to be well tolerated in phase I and IIa clinical trials for patients with critical limb ischemia, with no adverse effects reported [152]. Hence this approach may be well tolerated by secondary lymphoedema patients. Nevertheless, clinical trials will be necessary to determine the risks associated with HGF therapy for patients with lymphoedema. As is the case for VEGFC therapy, HGF therapy to promote lymphangiogenesis in secondary lymphoedema resulting from cancer therapies could have the danger of promoting metastatic spread of residual tumour cells via lymphatics.

1.6.3 Transforming growth factor β

TGFβ exerts its effects by binding to and bringing together TGFβ receptor-type 1 and type 2 (TGFβR1/2) serine/threonine kinases which leads to activation of selected members of the Smad family of signalling proteins, including Smad1, 2, 3, 5, and 8 [153]. TGFβ also activates Smad-independent signalling cascades, including the PI3K/Akt, Ras/MAPK, and JNK/p38 pathways [154]. The role of TGFβ in lymphangiogenesis appears paradoxical and context-dependent. For example, Oka *et al.* showed that TGFβ suppressed lymphangiogenesis during tumorigenesis and inflammation, and that inhibition of TGFβ signalling promoted lymphangiogenesis [155]. In contrast, James *et al.* demonstrated that TGFβ signalling is required for LEC sprouting and proper lymphatic patterning during mouse development [129]. Endothelial cells express two distinct type 1 TGFβ receptors, namely ALK1 and ALK5, which activate Smad 1 and 5, and Smad 2 and 3, respectively[156]. Previous studies have demonstrated that ALK1-mediated TGFβ signalling is required for lymphangiogenesis during early postnatal lymphatic development [157], whereas ALK5 has been reported to inhibit lymphangiogenesis [155, 158]. Therefore, the apparently contradictory findings may reflect the dual-function of TGFβ signalling in lymphangiogenesis in normal and pathological states, which may be regulated by a different combination of Smad proteins in a context dependent fashion.

TGFβ has also been shown to promote dermal fibrosis which occurs as a result of the accumulation of collagen fibres in the dermis; this fibrosis inhibited lymphatic regeneration and impaired lymphatic vessel function in a mouse lymphedema model [159]. Radiation treatment, which can promote development of lymphoedema, has been shown to induce dermal fibrosis that is associated with increased TGFβ expression [160]. Notably, Avraham *et al.* found that TGFβ expression was almost three-fold higher in lymphedematous limbs compared to the normal limbs of patients with post-operative lymphoedema [161]. In addition, long-term treatment of a mouse lymphoedema model with a neutralising TGFβ monoclonal antibody, or a soluble TGFβ receptor, reduced tail volume by 50-60% which was associated with increased lymphangiogenesis, decreased dermal fibrosis and inflammation, and improved overall lymphatic vessel function

[161]. It was also found that short-term inhibition of TGFβ by a small-molecule inhibitor significantly reduced dermal fibrosis and improved lymphatic transport in a mouse lymphoedema model [162]. However, there could be major challenges in clinically translating approaches targeting the TGFβ signalling axis given that prolonged systemic inhibition of TGFβ can lead to immunodeficiency and other pathological conditions, including glomerulosclerosis, cirrhosis and Crohn's disease [163].

1.6.4 Non-steroidal anti-inflammatory drugs

It has been shown that proteins involved in acute inflammation, such as tissue necrosis factor alpha (TNFα), were significantly upregulated in lymphoedematous tissue from a mouse model of lymphoedema [138]. This is consistent with the well-known role of inflammation in the pathogenesis of lymphoedema. The therapeutic effects of NSAIDs have been investigated by Nakamura *et al*, who found that ketoprofen treatment of mice with secondary lymphoedema resulted in restoration of normal dermal-epidermal architecture and marked resolution of inflammatory responses [131]. A more recently study by Tian *et al*. demonstrated that ketoprofen ameliorated lymphoedema processes by inhibiting leukotriene B4, an interleukin involved in inflammation and whose concentration is elevated in a mouse model of secondary lymphoedema as well as in clinical lymphoedema [164]. However, long-term use of ketoprofen would be limited due to various adverse effects reported in patients, including cardiovascular, gastrointestinal, dermatological, renal, respiratory, ophthalmic, and hepatic toxicities [165].

1.6.5 Retinoic acid

Retinoid acid (RA) is a biologically active metabolite of vitamin A, and is involved in regulation of genes implicated in multiple cellular processes, including proliferation, differentiation, apoptosis and metabolism [166-169]. Importantly, 9-cis RA, a form of vitamin A, has already been used in humans for the treatment of Kaposi's sarcoma [170] and chronic hand eczema [171]. Choi *et al*. demonstrated that 9-cis RA promoted proliferation, migration and tube formation of cultured primary human LECs [172]. Moreover, 9-cis RA treatment reduced

swelling of the tail in a mouse lymphoedema model by inducing lymphangiogenesis [172]. To further support these findings, another study investigated the therapeutic effects of 9-cis RA in a mouse hind-limb lymphoedema model, in which combined surgical lymphadenectomy and radiation was performed. It was demonstrated that daily administration of 9-cis RA in the model significantly reduced post-operative limb oedema [132]. Moreover, 9-cis RA-treated mice were shown to exhibit increased lymphatic clearance, associated with less collagen deposition and fewer inflammatory cells, and increased growth of functional lymphatic vessels [132]. The advantage of 9-cis RA is that it has been well characterised for its pharmacological, biochemical and toxicological profiles which may facilitate rapid translation to human clinical trials for lymphoedema. Nevertheless, it is critical to examine long-term effects of 9-cis RA, given that irreversible tissue architectural changes, such as fibrosis and formation of fat tissue, are more likely to appear at a late stage of lymphoedema. Therefore, longer-term studies in animal models will be required to determine the therapeutic potential of 9-cis RA in chronic lymphoedema.

1.6.6 Immune cells and lymphangiogenesis in lymphoedema

A study using animal models of secondary lymphoedema has shown that lymphatic fluid stasis induces significant increases in the population of CD4+ cells, such as macrophages and T cells [173]. This is consistent with clinical secondary lymphoedema in which increased levels of lymphocytes, macrophages, plasma cells, dendritic cells, and neutrophils are observed in the affected skin of lymphoedema patients [174]. LECs can respond to immune mediators produced by macrophages, such as interferon gamma [175], which can impair lymphangiogenesis by inducing apoptosis of endothelial cells [176]. Macrophages also produce iNOS which causes a reduction of lymphatic vessel contraction and thus may lead to accumulation of interstitial fluids [91]. Ogata et al. investigated the roles of macrophages and CD4+ T cell in lymphedema pathogenesis using a mouse model of secondary lymphedema [174]. It was shown that CD4+ T cells interacted with macrophages to promote lymphangiogenesis in this model, and both lymphangiogenesis and oedema were reduced in macrophage-depleted mice, or CD4+ T-cell-

deficient mice [174]. The enhanced lymphangiogenesis was driven by activation of macrophages by type 1 and type 17 T helper cells, which led to production of VEGFC [175]. The role of CD4+ T cells was also studied in a mouse model of secondary lymphoedema employing adaptive transfer techniques in CD4-deficient mice [177]. This study showed that CD4+ T cells that migrated to the lymphoedematous skin inhibited lymphangiogenesis and impaired lymphatic function in the mode l [177]. Further studies using large animal models of lymphoedema may be required to clarify how targeting immune cells may be beneficial for lymphoedema patients, and to establish if modulating the levels or function of these cells could be beneficial for prevention or treatment of this condition.

1.7 Status of current therapeutic strategies for secondary lymphoedema

Although CDT is currently the major therapeutic approach to control and manage secondary lymphoedema, patients are often required to undergo prolonged, often life-long, therapy to achieve durable improvement in symptoms. Likewise, for the surgical approaches used to treat secondary lymphoedema patients are often subjected to prolonged post-operative use of compression garments in order to sustain reduced limb volume. Additionally, degrees of benefit from surgical approaches vary significantly between individuals and among studies, which makes definitive conclusions regarding the benefit of surgery difficult to make. Whilst numerous animal studies have therapeutically stimulated lymphangiogenesis for treatment of secondary lymphoedema, there is no conclusive evidence that lymphangiogenic therapy has long-term efficacy. Further, it may be associated with the risk of malignant recurrence, given the ability of VEGFC to promote cancer metastasis or tumour growth [143]. Overall it is clear that novel therapeutic approaches for treating secondary lymphoedema are required.

1.8 Rationale for targeting fat tissue in secondary lymphoedema

In clinical secondary lymphoedema, an impaired lymphatic vasculature leads to accumulation of interstitial fluid which promotes formation of fat tissue. There is increasing evidence that elevated fat in lymphoedema further compromises lymphatic function, leading to a

vicious cycle in lymphoedema pathophysiology [178] (Figure 1.5). Hence, reducing fat tissue in lymphoedema would not only reduce tissue swelling but may also enhance lymphatic vessel function in the lymphoedematous limb. To this end, a long-term pharmacological approach to restrict adipogenesis in lymphoedema would be attractive, however, the signalling pathways which drive adipogenesis in lymphoedema are unknown. A key step for exploring this approach will be to identify adipogenic signalling pathways that drive the formation of fat in animal models of secondary lymphoedema. Such models should allow study of the early stage of this disease as well as chronic lymphoedema, and testing of pharmacological agents for inhibiting the relevant adipogenic signalling pathways.

1.9 Biology of fat tissue

Humans and animals use fat tissue to store excess calories in the form of triglycerides, and these triglycerides are released as fatty acids into the bloodstream to be used for the maintenance of energy homeostasis during fasting or increasing energy expenditure [179]. Fat tissue has long been known to serve as the major storage site of excess energy. Recently, it has become recognised that fat tissue responds to metabolic signals and that adipocytes in fat tissue can secrete a variety of hormones, such as leptin, IGF1 adiponectin and TNFα [180, 181], thereby acting as an endocrine organ that regulates various biological and metabolic processes [182]. The growth of fat tissue involves both hypertrophy and hyperplasia of adipocytes.

Hypertrophy is a process in which cell size increases due to accumulation of lipid. Adipocytes have limited size potential, meaning that preadipocytes are required to undergo proliferation and differentiation to adipocytes when pre-existing adipocytes encroach on their upper size-limit [183]. This process leads to an increased number of adipocytes (hyperplasia). A variety of cell types are present in fat tissue which can be classified into two distinct cell populations: adipocytes and cells of the stromal vascular fraction (SVF) [184]. Stromal vascular cells include fibroblasts, preadipocytes, endothelial cells, blood cells, pericytes and immune cells, and mesenchymal stem cells (MSCs) which are able to give rise to several cell types [185].

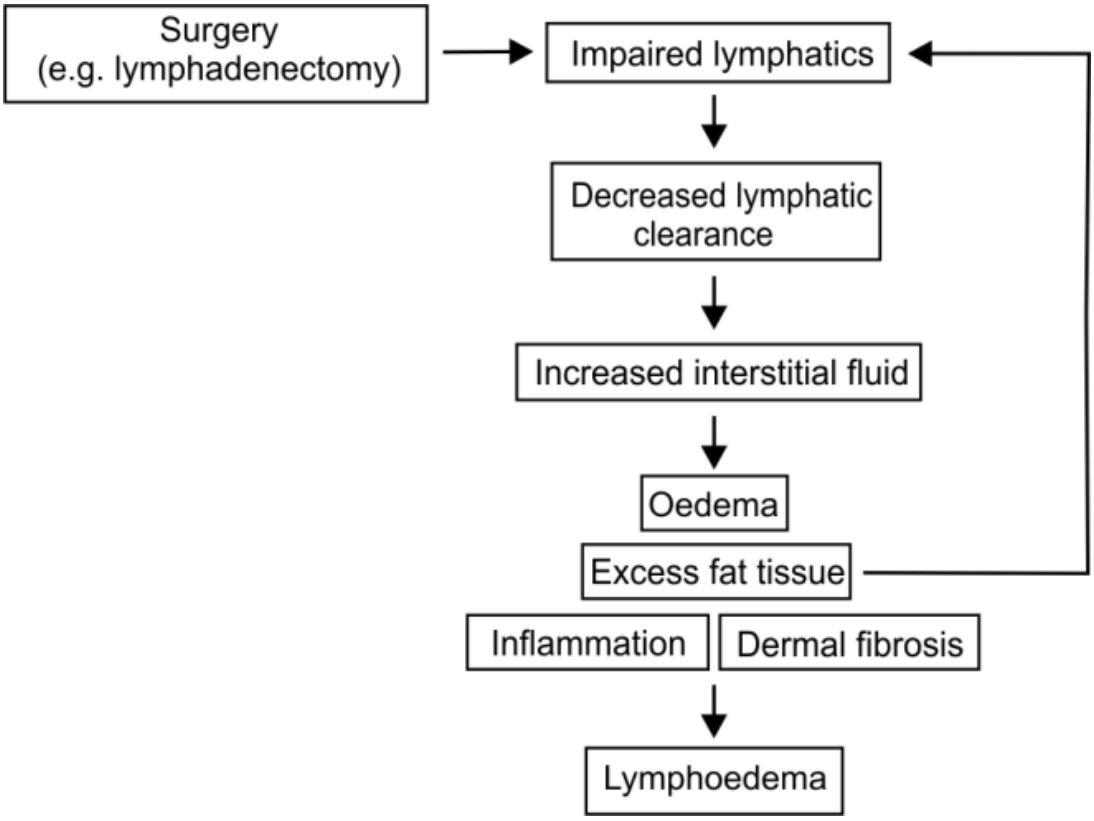

Figure 1.5 Flow diagram summarising the pathological steps that lead to lymphoedema after cancer surgery. A vicious cycle by which excess fat tissue impairs lymphatic function, leading to further development of fat tissue, is illustrated.

Preadipocytes, which morphologically resemble fibroblasts, are capable of differentiating into mature adipocytes which account for one-third of subcutaneous fat tissue by volume (the SVF accounts for the rest) [186]. Mature adipocytes exist in two forms giving rise to brown adipose tissue (BAT) and white adipose tissue (WAT). Although adipocytes in both BAT and WAT accumulate lipid droplets, they are functionally and morphologically distinct. BAT is commonly found in human babies and in most mammalian species, and is critical for energy regulation by non-shivering thermogenesis [187]. In contrast, WAT, which is the main focus of this review, is predominantly found in the subcutaneous and visceral compartments in adult humans and is responsible for energy homeostasis and endocrine actions (Figure 1.6) [188]. Adipocytes in BAT (brown adipocytes) are characterised by many fat droplets, a relatively centralised nucleus and an abundance of mitochondria required for regulation of body temperature [185]. In contrast, adipocytes in WAT (white adipocytes) have one large fat droplet. The cytoplasm is found at the cell periphery and the nucleus is confined between the fat droplet and cytoplasm (Figure 1.6) [185]. The following sections discuss our current knowledge of the molecular signals involved in regulating adipogenesis.

1.9.1 Molecular regulation of adipogenesis

Adipogenesis is a multi-step process by which MSCs give rise to mature adipocytes which is governed by incompletely understood mechanisms involving a cascade of transcription factors and cell-cycle proteins [189]. Although multipotent MSCs also give rise to other types of tissues, including bone, cartilage and muscle, this section will focus on molecular mechanisms by which MSCs give rise to white adipocytes.

The process of adipogenesis begins with the determination phase. In this phase, MSCs differentiate into preadipocytes which are morphologically similar to fibroblasts but can only give rise to adipocytes [190]. Studies have demonstrated that differentiation of MSCs to preadipocytes requires specific molecular signals (Figure 1.7). For example, treatment of MSCs with bone morphogenic protein 4 (BMP4) induces differentiation of these cells to preadipocytes [191].

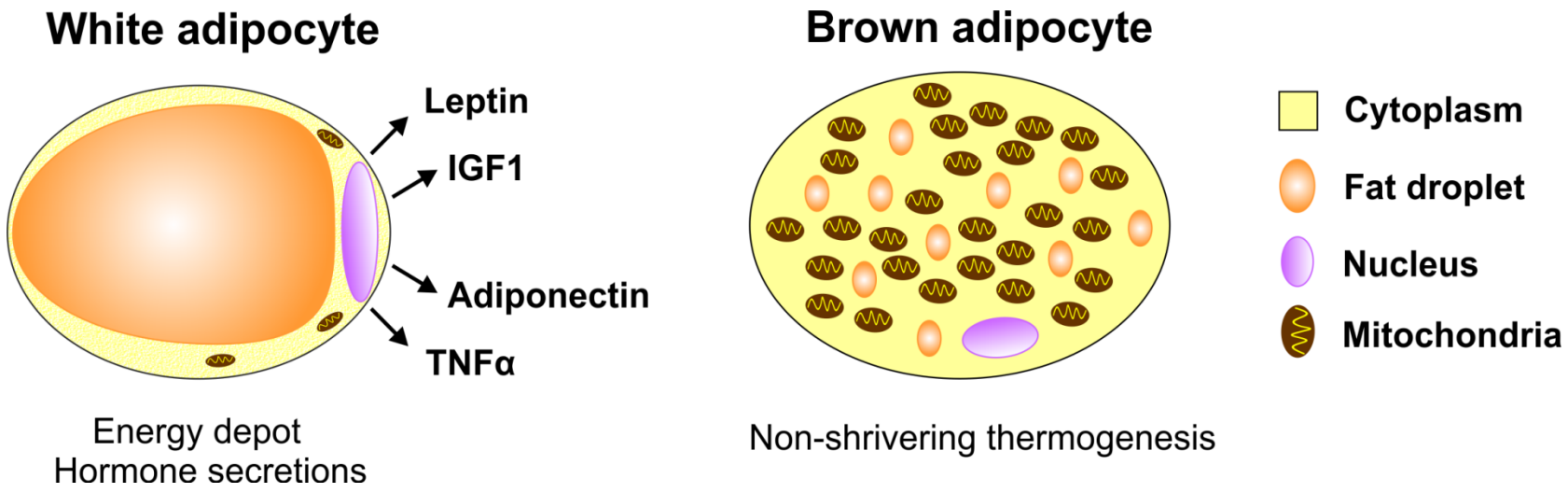

Figure 1.6 Distinct functional and morphological characteristics of white and brown adipocytes. White adipocytes (left) serve as major energy depots and as endocrine cells which secrete hormones called adipokines, including leptin, adiponectin and TNFα. The major role of brown adipocytes (right) is non-shivering thermogenesis. White adipocytes contain one large fat droplet and relatively few mitochondria whereas brown adipocytes have many fat droplets and a high density of mitochondria.

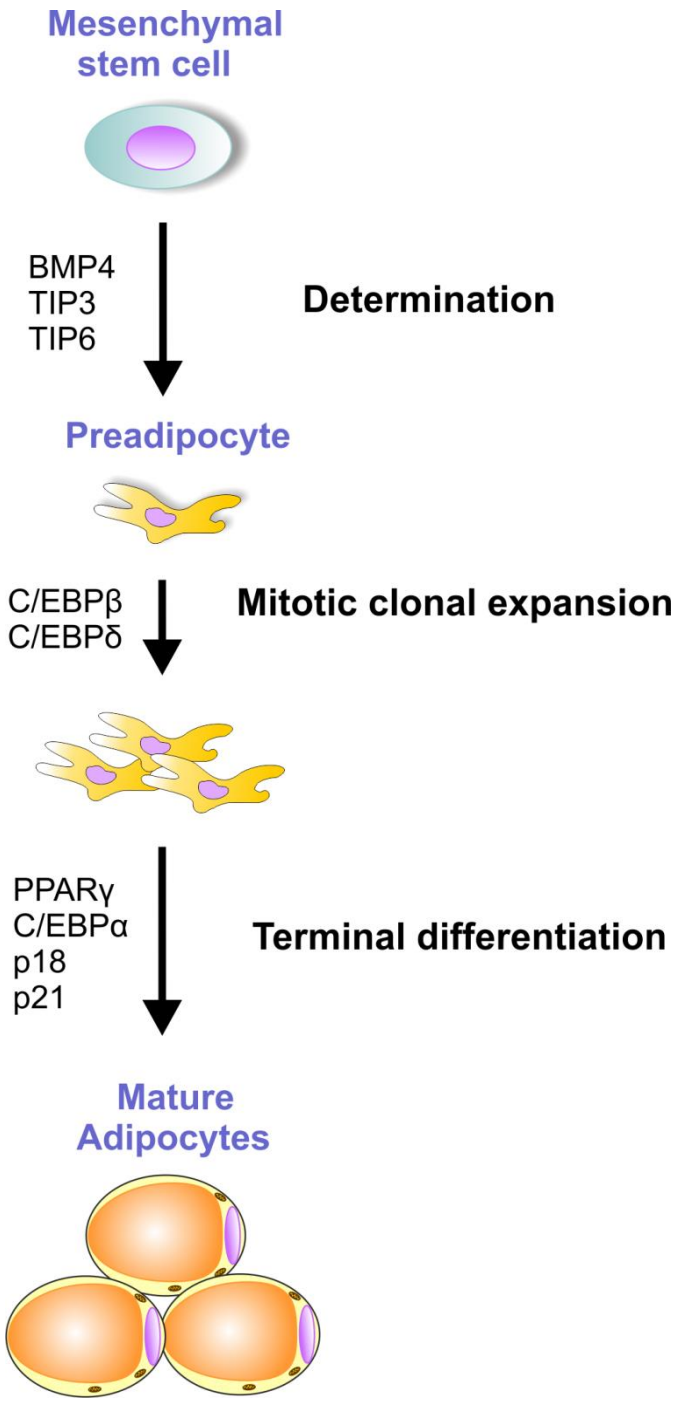

Figure 1.7 Regulatory proteins and transcription factors involved in adipogenesis. Adipogenesis is a multiple-step process by which MSCs give rise to mature adipocytes which is governed by multiple molecular signals. Key regulatory proteins and transcription factors that regulate each major step of adipogenesis are shown.

Moreover, implantation of BMP4-treated MSCs into mice gave rise to WAT [192], implying that this process is also functional *in vivo*.

The commitment of MSCs to the adipogenic lineage is also induced by specific members of the tension-responsive factor family, known as tension-induced/inhibited proteins (TIPs). For example, TIP3 and TIP6 have been shown to induce differentiation of MSCs into preadipocytes, in part by regulating expression of the gene for PPARγ, a transcription factor considered to be a master regulator of adipogenesis [193, 194]. These findings show that commitment of MSCs to the adipocyte lineage during the determination phase of adipogenesis requires coordinate activation of multiple genes.

After the determination phase, preadipocytes re-enter the cell cycle and undergo several rounds of mitosis, known as mitotic clonal expansion (MCE), which is promoted by hormonal adipogenic stimuli [195]. The expressions of the transcription factors C/EBPβ and C/EBPδ are elevated during MCE [196]. These transcription factors directly induce the expression of PPARγ and C/EBPα, the key transcriptional regulators of adipocyte terminal differentiation [197]. C/EBPα is required for development of WAT *in vivo* [198], and PPARγ induces expression of two independent families of cyclin-dependent kinase inhibitors, p18 and p21. These kinase inhibitors allow post-mitotic preadipocytes to acquire all the characteristics of white adipocytes, such as the machinery for storage and biosynthesis of lipid and the secretion of adipocytes-specific hormones [199].

It should be noted that most of our current knowledge about the molecular mechanisms of adipocyte differentiation has been established from *in vitro* studies using 3T3-L1 murine preadipocytes, as these cells are readily differentiated into mature adipocytes upon treatment with hormonal adipogenic stimuli [195, 200]. However, there is currently no evidence that MCE is required for human preadipocytes to differentiate to mature adipocytes *in vitro* or *in vivo* [201].

1.9.2 Other molecular signals that regulate adipogenesis

1.9.2.1 Insulin-like growth factor 1

Other important signalling molecules that influence the process of adipogenesis have also been discovered. It has long been known that differentiation of preadipocytes into adipocytes was triggered by growth hormone and insulin [202, 203]. More recently, studies have shown that insulin-like growth factor 1 (IGF1), a protein with multiple roles in the regulation of development and metabolism, also stimulates proliferation of preadipocytes and their differentiation to adipocytes [204]. IGF1 has been shown to induce adipogenesis through the IGF1 receptor (IGF1R) signalling pathway [205]. Moreover, 3T3-L1 preadipocytes differentiated into lipid-accumulating mature adipocytes upon stimulation with IGF1, and the effect was enhanced by addition of insulin [205, 206]. The presence of both IGF1R and the insulin receptor (IR) has been confirmed in human preadipocytes and adipocytes [207].

1.9.2.2 Fibroblast growth factors

Some members of the fibroblast growth factor (FGF) family have been implicated in the regulation of adipogenesis. Several studies demonstrated that FGF1 promotes differentiation of human preadipocytes into adipocytes [208, 209], and that FGF2 stimulated adipogenesis in human and rat MSCs [210, 211].

1.9.2.3 Carboxypeptidase X 1

The carboxypeptidase superfamily of enzymes is involved in various cellular processes including digestion of food and biosynthesis of neuropeptides [212, 213]. Carboxypeptidase X1 (CPX1) is a secreted collagen-binding glycoprotein, lacking carboxypeptidase activity, which is thought to be involved in osteoclastogenesis [214, 215]. It has recently become clear that CPX1 also serves as a positive regulator of adipogenesis. An *in vitro* study demonstrated that CPX1 promoted differentiation of human preadipocytes into adipocytes. Also, depletion of CPX1 inhibited adipogenesis and reduced lipid droplet accumulation in adipocytes which was associated

with decreased adiponectin secretion and impaired glucose uptake [216]. These findings suggest that CPX1 is required for preadipocytes to acquire the features of mature adipocytes.

1.9.2.4 Preadipocyte factor 1

Preadipocyte factor 1 (PREF1) is an epidermal growth factor-like repeat containing protein present exclusively on the surface of preadipocytes. The expression of PREF1 is completely abolished during the differentiation of 3T3-L1 preadipocytes to adipocytes [217]. Furthermore, experimental approaches that drove constitutive expression of PREF1 in 3T3-L1 preadipocytes inhibited the differentiation of these cells into adipocytes [217]. The evidence that PREF1 is a negative regulator of adipogenesis is further supported by *in vivo* experiments. For example, PREF1-deficient mice exhibited a significantly increased fat tissue mass and body weight which was associated with increased circulating levels of cholesterol, free fatty acids, and triglycerides [218]. In contrast, mice overexpressing PREF1 had a significantly decreased fat tissue mass and a marked reduction in the expression of adipocyte markers such as C/EBPα [219].

1.9.2.5 Growth arrest-specific gene 6

Growth arrest-specific gene 6 (GAS6) is a secreted vitamin K-dependent protein which binds and activates the TYRO3, AXL, and MERTK (collectively known as TAM) receptor tyrosine kinases. The TAM signalling pathways are involved in various biological processes including cell proliferation, survival, differentiation and inflammation [220]. These receptors share GAS6 as their common ligand although they bind GAS6 with different affinities. AXL has the highest affinity for GAS6, followed by TYRO3 and MERTK [221]. Various studies have shown the potential role of the GAS6/AXL signalling pathway in fat tissue development. For example, administration of R428, an inhibitor for AXL, impaired fat tissue development in mice [222]. Similarly, GAS6-deficient mice had significantly less subcutaneous and gonadal fat than wild-type mice [223].

1.9.2.6 Hedgehog signalling pathway

The Hedgehog signalling pathway is known to have a wide variety of regulatory functions during the development of tissues and organs [224], and this pathways has been shown to be a negative regulator of adipogenesis. For instance, a study by Suh *et al.* [225] showed that fat-specific activation of the Hedgehog pathway in *Drosophila* inhibited fat formation, whereas inhibition of this pathway promoted formation of fat. Inhibition of adipogenesis by the Hedgehog signalling pathway was shown to be associated with increased expression of anti-adipogenic transcription factors, such as Gata2 and Gata3, which are known to inhibit *Pparγ* gene expression [225, 226]. These findings provide evidence for a potential inhibitory function of the Hedgehog signalling pathway in adipogenesis.

1.10 Targeting adipogenesis in lymphoedema

The previous sections of this chapter have indicated that the molecular regulation of adipogenesis is complex and involves many signalling pathways. It is currently not clear which of these pathways should be targeted in lymphoedema to restrict the development of, or reduce, fat in this condition. It will be critical to monitor which adipogenic signalling pathways are operative in secondary lymphoedema using an appropriate animal model of this condition. This information would be important for designing pharmacological strategies to target adipogenesis in clinically relevant animal models, potentially leading to clinical trials for testing such an approach.

1.11 Scope of this thesis

The hypothesis to be tested in this thesis is that targeting adipogenesis in secondary lymphoedema would be beneficial for restricting tissue swelling by reducing the volume of fat tissue and enhancing lymphatic function. This approach is designed to break the vicious cycle in lymphoedema pathophysiology by which excess fat tissue impairs lymphatic function leading to further development of fat tissue. This approach could be employed in the settings of prevention or treatment of secondary lymphoedema. The research questions to be addressed in this thesis are:

1. What is an appropriate animal model of secondary lymphoedema in which to study formation of fat tissue?
2. What are the molecular mechanisms driving formation of fat tissue in this animal model? Are these mechanisms operative in clinical secondary lymphoedema?
3. What pharmacological approaches could be used to target formation of fat tissue in this animal model of secondary lymphoedema?

The overall aim of this study is to identify a pharmacological approach to target adipogenesis in secondary lymphoedema. Such an approach might be used for long-term treatment of lymphoedema patients with a view to restricting fat levels and tissue swelling.

Chapter 2
Materials and Methods

2.1 Cell culture

2.1.1 Maintenance of cell lines

The cell lines were obtained from American Type Culture Collection. Cells were cultured in a Falcon® T75 flask (Fisher Scientific, Pittsburgh, PA, USA) containing Roswell Park Memorial Institute (RPMI) 1640 medium (Thermo Fisher Scientific, Waltham, MA, USA) with 10% heat-inactivated fetal bovine serum (FBS), 100 U/ml penicillin, 100 µg/ml streptomycin and 2 mM L-glutamine at 37°C in a 5% CO_2 incubator. This medium including these additives is designated as "complete RPMI 1640 medium" in this thesis. Cells were grown to 80% confluence prior to experimental treatments.

2.1.2 Passaging cells

Cells were passaged into new flasks when they grew to 80-90% confluence. The complete RPMI 1640 medium was removed from a T75 flask and 5 ml of phosphate-buffered saline (PBS) was added to wash away the remaining medium. PBS was removed and 2-4 ml of a pre-warmed commercial solution containing trypsin, ethylenediamine tetraacetic acid (EDTA) and phenol red (TEP) (25200056, Thermo Fisher Scientific) was added and incubated at 37°C for 3-4 min until cells detached. The side of the flask was tapped to enhance detachment of the cells. Ten ml of pre-warmed complete RPMI 1640 medium was added to the flask to inhibit trypsin activity and the cells were resuspended. The resuspended cells were transferred into CELLSTAR® 15 ml Eppendorf tubes (Greiner Bio-One, Kremsmünster, Austria) and centrifuged at 150 × g for 5 min. After centrifugation, the supernatant was carefully discarded without disturbing the cell pellet. The cell pellet was resuspended with 5 ml of complete RMPI 1640 medium, and 1 ml of the resulting cell suspension was added to 10 ml of complete RMPI 1640 medium in a T75 flask. The cells were then incubated at 37°C and 5% CO_2.

2.1.3 Freezing cells

Cells were frozen when they grew to 80-90% confluence. The cells were washed with room temperature PBS, detached from the cell culture flask by treating with pre-warmed commercial solution containing TEP, transferred to a 15 ml centrifuge tube containing 10 ml of pre-warmed complete RPMI 1640 medium and centrifuged at 150 × g for 5 min. After centrifugation, the medium was removed, and cells were resuspended in 5 ml of freezing medium: 45% FBS/45% complete RPMI 1640 medium/10% Dimethyl Sulphoxide (DMSO). One ml of cell suspension was transferred into a cryogenic vial (Greiner Bio-One, Kremsmünster, Austria), and vials were placed into a freezing chamber containing isopropanol and stored at -80°C overnight. The following day, the cells were transferred into liquid nitrogen for long-term storage.

2.1.4 Thawing frozen cells

Vials from frozen storage were thawed in a 37°C water bath by gentle agitation. One ml of thawed cell suspension was transferred to a 15 ml centrifuge tube containing 10 ml of pre-warmed complete RMPI 1640 medium, and centrifuged at 150 × g for 5 min. The supernatant was discarded for complete removal of DMSO which can affect cell viability. The cells were resuspended in 12-15 ml of complete RPMI 1640 medium and transferred to a T75 flask. The medium was changed every 2-3 days to facilitate the growth of the revived cells.

2.2 Western blotting

2.2.1 Preparation of lysates from cell culture

Cells were grown on 8 cm^2 tissue culture dishes (Corning, Inc., NY, USA) until they reached 80-90% confluence and were serum starved overnight. To examine autophosphorylation of IGF1Rβ, cells were treated with 100 ng/ml of recombinant human IGF1 (R&D Systems) in serum free media for 30 min, respectively. Untreated cells were used as negative controls. The tissue culture plates were placed on ice, media were removed, and cells were washed with ice-cold PBS. Culture dishes containing the cells were lysed directly on ice by adding 200 µl of Nonidet P-40 (NP-40) lysis buffer (0.5% NP-40, 10 mM NaCl, 10 mM $MgCl_2$, 10 mM Tris-HCl,

pH 7.4) containing a complete EDTA-free protease inhibitor cocktail and a PhosSTOP™ phosphatase inhibitor cocktail (Roche, Basel, Switzerland). Cells were removed by scraping and collected into 1.5 ml Eppendorf tubes. The collected lysate was incubated with gentle agitation at 4°C for 30 min and cleared by centrifugation at 13,000 × g at 4°C for 5 min. The supernatant was transferred to a new 1.5 ml Eppendorf tube and cell lysates were stored at -80°C until use.

2.2.2 Protein quantification

The total protein concentrations of lysates were determined using the Pierce™ BCA protein assay kit (Thermo Fisher Scientific) according to the manufacturer's protocol. The protein concentration was quantified by measuring absorbance at 560 nm in a 96-well plate with the VersaMax™ ELISA microplate reader (Molecular Devices, Sunnyvale, CA, USA).

2.2.3 Preparation of protein samples for SDS-PAGE

To prepare 100 µl of protein sample for sodium sulfate polyacrylamide gel dodecyl electrophoresis (SDS-PAGE), 65 µl of cell lysate prepared as in Section 2.2.1 was mixed with 25 µl of 4 x Novex® Bolt® LDS sample buffer (Thermo Fisher Scientific) and 10 µl of 10 × Bolt® Sample Reducing Agent containing 500 mM dithiothreitol (Thermo Fisher Scientific). The mixture was heated at 95°C in a heat block for 5 min and briefly centrifuged before loading.

2.2.4 SDS-PAGE

SDS-PAGE was performed with Bolt™ 4-12% Bis-Tris Plus polyacrylamide gels (Thermo Fisher Scientific) and Bolt™ mini gel tank (Thermo Fisher Scientific). Combs were removed gently from precast gels, and the gels were rinsed three times with Bolt™ MES SDS running buffer (Thermo Fisher Scientific). Each cell in the tank was filled with 400 ml of 2-(N-morpholino) ethanesulfonic acid SDS running buffer. Five µl of SeeBlue® Plus2 Pre-stained standard (Thermo Fisher Scientific) was loaded onto a lane, and equal amounts (e.g. 20-30 µg) of protein samples were loaded onto adjacent lanes. The electrodes were attached to a PowerPac™ Basic Power Supply (Bio-Rad, Hercules, CA, USA) and the samples were run for approximately 40 min at 200 V until the dye reached the bottom of the separating gel.

2.2.5 Protein dry-transfer

Separated proteins were transferred to nitrocellulose membranes using iBlot® 2 Transfer Stacks (Thermo Fisher Scientific) and an iBlot® 2 Gel Transfer Device (Thermo Fisher Scientific). The transfer was performed for 10 min at 20 V. Subsequently, membranes were removed from the stack and washed with Milli-Q water with gentle agitation for 2 min to remove polyacrylamide chunks. Odyssey® Blocking Buffer (OBB) (LI-COR, Lincoln, NE, USA) was employed for blocking, and was diluted 2-fold with Tris-buffered saline (TBS) before use. Membranes were rolled into a 50 ml tube and incubated with 10 ml of the diluted OBB for 1 hour at room temperature on a roller bench.

2.2.6 Antibody incubation and protein detection

After blocking, OBB blocking buffer was discarded and membranes were washed with TBS/0.1% Tween 20 (TBST) three times for 5 min. Five ml of antibody incubation buffer was prepared by mixing 2.5 ml of OBB with 2.5 ml of TBST, and was transferred into a 50 ml tube. Primary antibodies and dilutions used are described in Table 2.1. Membranes were transferred into tubes containing primary antibody incubation buffer, and incubated on a roller bench at 4°C overnight. After washing three times with TBST for 5 min at room temperature, membranes were incubated with IRDye 680RD conjugated goat-anti-rabbit secondary antibodies (1:5000 dilution, LI-COR) for 1 hr in 50 ml tubes wrapped with foil to protect from the light. Afterwards, membranes were washed four times (three times with TBST and one last time with TBS). Membranes were left to dry in air for 10-20 min and proteins were detected using an Odyssey® infrared imager (LI-COR) according to the manufacturer's protocol.

Table 2.1 Primary antibodies for Western blotting

Primary antibody	Species	Clonality	Source	Dilution
IGF1Rβ (111A9)	Rabbit	Monoclonal	Cell Signalling Technology (3018)	1:1000
p-IGF1Rβ (Y1161)	Rabbit	Polyclonal	Santa Cruz Biotechnology (sc-101703)	1:500
GAPDH	Rabbit	Polyclonal	Santa Cruz Biotechnology (sc-25788)	1:1000

2.3 Mouse methods

2.3.1 Digital photographic documentation of mouse tail

Photography of mice was performed using a light box, Kaiser RS1 copy stand (L&P Digital Photographic, Artarmon, NSW, Australia) and camera mounted vertically above the mice. A Nikon D3400 digital SLR camera (Nikon Corporation, Tokyo, Japan) with an attached AF-S Micro NIKKOR 60mm f/2.8G ED Macro Lenz (Nikon Corporation, Tokyo, Japan) was attached to the copy stand at 35.5 cm above the light box to face the camera directly downwards onto the light box. The light box was switched on to provide contrast between the white background and the dark mouse tail. A ruler was placed on the light box and a strip of double-sided tape (Scotch Permanent Double-sided Tape 3M, St-Paul, MN, USA) was attached adjacent to the ruler. The mouse was anaesthetised using Isoflurane 100% (Delvet Isoflurane Inhalational Anaesthetic, Isoflurane 100%, Delvet Pty Ltd, Seven Hills, NSW, Australia) administered via an inhalational anaesthetic machine (CIG TM41 Anaesthetic Apparatus, BOC Gases Australia Ltd, North Ryde, NSW, Australia). The tail of the anaesthetised mouse was horizontally placed on the strip of double-sided tape within the camera's field of view and photographed at high resolution. This process was conducted on the day of surgery prior to the surgical procedure and then repeated every day during an experimental period.

2.3.2 Image preparation for tail volume analysis

The digital photographic Nikon Electronic Format images of mouse tails were converted to Tagged Image File Format (TIFF) images using Nikon Capture NX-D software.

2.3.3 Quantification of mouse tail volume

The digital photographic images of each mouse tail were analysed using MetaMorph Microscopy Automation and Image Analysis Software Version 7.8.11.0 (Molecular Devices, Sunnyvale, CA, USA). A custom-made journal was created by Cameron Nowell (Centre for Advanced Microscopy, Ludwig Institute for Cancer Research, Parkville, Victoria, Australia) which measured serial diameters of the mouse tail every 1.2 mm from the distal edge of the wound to the tail tip. These data were inserted into the truncated cone formula [227] using a custom-made Microsoft Excel algorithm designed by Jimmy Zeng (Ludwig Institute for Cancer Research, Parkville, Victoria, Australia) to produce an estimated tail volume. These estimated volumes were then plotted serially to demonstrate the change in tail volume in a mouse over time.

2.3.4 Mouse microsurgical model of lymphoedema

2.3.4.1 Mice

The mouse microsurgical model was conducted with 6-week-old female C57BL/6 mice. All mice were obtained from the Animal Care and Use Program of the Peter MacCallum Cancer Centre located within the Victorian Comprehensive Cancer Centre (Parkville, VIC, Australia).

2.3.4.2 Preparation of mice for surgery

Anaesthetic was prepared by combining 0.5 ml of Ketamine (Ketavet 100, Ketamine HCL, 100 mg/kg, Parnell Laboratories Pty Ltd, Alexandria, NSW, Australia) and 0.5 ml of Xylazine (Ilium Xylazine 20, Xylazine HCL, 20 mg/kg, Ilium, Troy Laboratories Pty Ltd, Smithfield, NSW, Australia) with 9 ml of sterile saline (0.9% NaCl) in a sterile tube. Mice were anaesthetised by intraperitoneal injection of 20 ml/kg of the anaesthetic using a 1 ml syringe and a 26 G needle. Mice were subjected to perioperative hydration by subcutaneous injection of 500

µl of saline into the neck using a 1 ml syringe and a 26 G needle. The surgical region on the tail skin was sterilised with 70% ethanol. The sites of subsequent surgical incisions were clearly marked with a Pilot Fineliner marker and ruler, and the tails were then washed with 70% ethanol. Genteal 0.3% Lubricating Eye Gel (Alcon Laboratories Pty, NSW, Australia) was applied to both eyes of mice. Mice were then photographed prior to operation using the method described in Section 2.3.1.

2.3.4.3 Disruption of small lymphatic network in the dermis

In the microsurgical model used in this thesis, the four lymphatic collectors, all pre-collectors connected to these collectors and the overlying initial lymphatic network in the dermis, were selectively ablated over a 2 mm area near the base of the mouse tail. Mice were placed on foam boards using rubber band restraints held firmly by drawing pins around the base of tails, and were positioned underneath an Olympus SZ-ST Zoom Stereo Microscope (Olympus, Tokyo, Japan). Two circumferential incisions were made at 15 and 17 mm from the mouse anus with Vannas-Tübingen microscissors (Daniels Health Laboratory, Dandenong South, VIC, Australia) and Jeweller's micro-forceps (BD330R, Aesculap, B Braun Australia Pty Ltd, Vella Vista, NSW, Australia). A 2 mm ring of dermis and subcutaneous tissue was excised off underlying connective tissue, using toothed Pierse-Colibri corneal micro-forceps (Kaiser's, Lifehealthcare Pty Ltd, Bibra Lake, WA, Australia), bringing underlying blood and lymphatic vessels into sight. This first excision disrupted the dermal initial lymphatic network, as well as all pre-collectors connecting this network to the deep lymphatic collectors.

2.3.4.4 Identification of lymphatic collectors by microlymphangiography

After disruption of the dermal lymphatic collectors, mice were subcutaneously injected with 10 µl of Patent Blue V dye (198218-25G, Sigma-Aldrich, St. Louis, MO, USA) at the tip tails, using a 30 G insulin syringe. Patent Blue V dye is selectively taken up by lymphatic vessels, thus demonstrating intact lymphatic collectors over the 2 mm surgical field at the base of the tail.

2.3.4.5 Disruption of lymphatic collectors

A window was created between the dorsolateral artery or vein on each side of mouse tails and the adjacent lymphatic collectors highlighted in blue, using a dissecting needle and Jeweller's micro-forceps. Using bipolar Jeweller's micro-forceps connected to an electrosurgical generator (HealForce EB03 High Frequency Surgical Unit, Shanghai Lishen Scientific Equipment Company Ltd. Shanghai, China), all lymphatic collectors and any pre-collectors connected to the lymphatic collectors were cauterised without damaging adjacent blood vessels. Bipolar electrocauterisation is a process involving the passage of a low voltage current between the two tips of the bipolar forceps, which seals and disrupts the lumen of a vessel when selectively grasped by these forceps. Saline was applied to the wound to keep it moist during this process. Subsequently, it was ensured that there were no intact lymphatic collectors over a 2 mm surgical field at the base of tails by performing lymphangiography on each side of tails, confirmed by the absence of Patent Blue V dye. If necessary, these vessels were re-cauterised as described above until no further leak could be detected.

2.3.4.6 Post-operative care and monitoring

Wounds were washed in saline and then gently covered with a sandwich dressing made of two layers of Mefix (Mölnlycke Health Care, Frenchs Forest, NSW, Australia) with the tail in between. Buprenorphine analgesic was prepared by combining 0.5 ml of the 0.3 mg/ml Buprenorphine (Temgesic, Buprenorphine HCl 324 µl/ml, Reckitt Benckiser Healthcare UK Ltd, Hull, United Kingdom) with 9.5 ml of saline in a sterile BD vacutainer (Becton, Dickinson and Company, NJ, USA). Mice were then subcutaneously injected with 100 µl of Buprenorphine solution, using a 26 G needle and 1 ml syringe. Mice were then housed in a static micro-isolator on a heat pad for 24 hours during recovery. Next day, dressings were removed and mice were injected with a further 100 µl of Buprenorphine solution. The mice were photographed thereafter as described in Section 2.3.1.

2.4 Drug treatment

2.4.1 Preparation of linsitinib suspension

Linsitinib was purchased from Ark Pharm, Inc. (AK176016, Arlington Heights, IL, USA) and stored at -20°C. Linsitinib was dissolved in a 25 mM tartaric acid vehicle at a concentration of 5 mg/ml, and the mixture was sonicated to make a suspension and stored at 4°C.

2.4.2 Determination of maximum tolerated dose of linsitinib

Mice were randomly allocated into four treatment groups (10, 25, 40 and 50 mg/kg/day of linsitinib) and one control group (vehicle only) (n=5/group). Mice were administered 10 mg/kg of linsitinib on a daily basis for 14 days by oral gavage. Subsequently, 25 mg/kg of linsitinib was administered to a new group of mice for 14 days, then 40 mg/kg or 50 mg/kg was administered to other groups of mice for 14 days. Mice were sacrificed by CO_2 inhalation when the 14-day dosing was complete. Body weights of mice were recorded on a daily basis throughout the experiment.

2.4.3 Administration of linsitinib in the mouse model of secondary lymphoedema

After the surgery to induce lymphoedema mice were administered a single dose of 40 mg/kg of linsitinib or vehicle per day via oral gavage using 20 ga plastic feeding tubes (FTP-20-30, Walker Scientific, VIC, Australia). The first administration was performed 4 hours post-surgery. To avoid tissue damage to the surgically ablated tails during oral gavage, mice were lightly anaesthetised in an induction chamber (set to ~2.5 – 3% Isoflurane and 2 L/m O_2) until righting reflex was lost. Mice were restrained immediately upon removal from the chamber by being held by the scruff of the neck. Linsitinib was then delivered by oral gavage and mice were readministered light anaesthetic for the purpose of tail measurement.

2.5 Mouse tissue harvesting and processing

2.5.1 Tissue harvesting

Mice were photographed as described in Section 2.3.1 on the day of sacrifice and were culled by CO_2 inhalation. A cylindrical segment of the tail was excised between 2.5 and 5.0 mm distal to the centre of the scar that has formed in response to the surgery. Equivalent sites on the tails of vehicle control mice were also excised.

2.5.2 Tissue processing

All the excised specimens were placed in 5 ml of 4% paraformaldehyde solution (C004-1L, 16% Paraformaldehyde aqueous solution, ProSciTech Pty Ltd, Kirwan, QLD, Australia), and were incubated at 4°C overnight. The next day, tissues were washed with PBS three times and incubated in 12.5% EDTA decalcification solution (Chem-Supply, Gillman, SA, Australia) for 14 days, with the solution being changed every day. The tissues were then removed from EDTA solution, washed with PBS three times and stored in 70% ethanol.

2.5.3 Tissue sectioning

Tissues left in 70% ethanol for at least 24 hours were dehydrated in 95% ethanol for 45 min, followed by incubation in three changes of 100% ethanol (45 min each). The tissues were then incubated in three changes of Xylene (45 min each), and embedded in paraffin wax. Formalin-fixed paraffin-embedded (FFPE) blocks containing the tissue were cut into sections of 4 µm in thickness, which were placed onto glass slides coated with 3-aminopropyltriethoxysilane (Sigma-Aldrich) for immunohistochemistry. Four tissue sections were placed on each slide.

2.6 Immunohistochemistry

Slides with tissue sections generated in Section 2.5.3 were dewaxed in histolene for 11 min and then rehydrated by incubating in 100% ethanol and 70% ethanol for 3 min and 1 min, respectively. For all antigens, slides were incubated in either citrate pH 6.0 Target Retrieval Solution (S1699, DAKO, Productionsvej, Denmark) or pH 9.0 Novocastra™ Epitope Retrieval Solution (RE7119: Leica Microsystems, Wetzlar, Germany). The antigen retrieval methods used for specific antigens in mouse and human tissue sections are described in Table 2.2 and 2.3, respectively. Slides were placed into a chamber filled with the appropriate antigen retrieval

solution, and a heat-induced antigen retrieval method was performed by heating the sections in a DAKO pressure cooker at 125°C for 3 min. Subsequently, slides were washed with Tris-NaCl-Tween (TNT) washing buffer (0.1 M Tris-HCl pH 7.5, 150 mM NaCl and 0.1% v/v Tween 20) three times for 5 min. For mouse IGFBP5 and p-IGF1R, an enzymatic (trypsin-based) antigen retrieval method was also used. To prepare the trypsin solution, 50 mg of trypsin (Difco™ Trypsin 250, Becton Dickinson and Company) and 260 mg of $CaCl_2$ (Molecular Biology Grade, Calbiochem, EMD Bioscience, Inc., La Jolla, CA, USA) were dissolved in 200 ml of 0.05 M Tris-HCl (pH 8.0), and pre-heated to 37 °C. Slides were placed in a chamber filled with pre-heated trypsin solution and incubated for 20 min, followed by washing with TNT buffer three times for 5 min. After antigen retrieval, blocking of endogenous peroxidase activity was performed by incubating slides in 3% hydrogen peroxide (H_2O_2) in methanol at room temperature for 20 min, followed by rinsing with TNT buffer three times for 5 min. To prevent the flow of antibody solution outside each tissue section, the edges of each slide were dried and the tissue boundaries were drawn with a Pap pen (Thermo Fisher Scientific). The sections were blocked by incubating in a humidifying chamber for 30 min with Tris- NaCl blocking buffer (TNB) (0.1 M Tris-HCl pH 7.5, 150 mM NaCl, and 0.5% w/v PerkinElmer blocking reagent). Primary antibodies used for immunohistochemistry are summarised in Table 2.4. Excess TNB was tipped off and slides were incubated with the appropriate primary antibody diluted in TNB in a humidifying chamber at 4°C overnight. The following day, slides were washed with TNT buffer three times for 5 min and then incubated with biotinylated swine anti-rabbit secondary antibody (E0353 Dako, Glostrup, Denmark), or biotinylated rabbit anti-goat secondary antibody (BA-5000, Vector Labs, Burlingame, CA, USA), diluted 1:300 in TNB, at room temperature for 1 hour. Subsequently, slides were washed with TNT buffer three times for 5 min and then incubated with streptavidin-HRP (NEL700001KT, PerkinElmer, Waltham, MA, USA), diluted 1:100 in TNB, at room temperature for 30 min. Slides were washed with TNT buffer three times for 5 min and then incubated in Biotinyl Tyramide Signal Amplification (TSA) solution, diluted1:50 in Amplification Diluent (NEL700001KT, PerkinElmer), at room temperature for 5

min. Slides were washed with TNT buffer three times for 5 min and incubated with streptavidin-HRP, diluted 1:100 in TNB, at room temperature for 30 min, followed by washing with TNT buffer three times for 5 min. Alternatively, slides were incubated for 30 min with VECTASTATIN® ABC Reagent (PK-4000, Vector Labs), prepared as described by the manufacturer. Subsequently, slides were incubated with 3-amino-9-ethylcarbazole working solution (SK-4200, Vector Labs), prepared as described by the manufacturer, for 5 to 10 min to visualise colour change. The colour reaction was stopped by immersing slides in distilled water for 5 min. Subsequently, counterstaining was performed by immersing the sections in Mayer's haematoxylin (Sigma-Aldrich). Concentration-matched negative controls were generated by incubating with affinity purified normal rabbit IgG (sc-2027, Santa Cruz Biotechnology) or affinity purified normal goat IgG (sc-2028, Santa Cruz Biotechnology) at the same concentration as primary antibodies. Finally, the sections were cover slipped with AquaMount (Merck, Darmstadt, Germany) and left to dry. Images were acquired using an Olympus X61microscope and a SPOT Model 25.4 2 Mp Slider digital camera (Diagnostic Instrument Inc. Sterling Heights, MI, USA) using SPOT™ Software Version 5.0. Note that immunohistochemistry was performed mouse tail tissue sections generated previously by Dr. Sidney Levy, which included tissues collected at days 7, 17 and 90 post-surgery from operated mice.

Table 2.2 Primary antibodies and antigen retrieval methods tested for detecting target antigens in mouse model of secondary lymphoedema

Target antigen	Primary antibody	Antigen retrieval method
IGFBP5	IGFBP5: ab4255	Sodium citrate pH 6.0
		Tris/EDTA pH 9.0
		Trypsin
	IGFBP5: AF578	Sodium citrate pH 6.0
		Tris/EDTA pH 9.0
		Trypsin
IGF1	IGF1: ab9572	Sodium citrate pH 6.0
		Tris/EDTA pH 9.0
	IGF1 (H-70): sc-9013	Sodium citrate pH 6.0
		Tris/EDTA pH 9.0
IGF1R	IGF1R: ab131476	Sodium citrate pH 6.0
		Tris/EDTA pH 9.0
IGF1Rα	IGF1Rα (N-20): sc-712	Sodium citrate pH 6.0
		Tris/EDTA pH 9.0
IGF1Rβ	IGF1Rβ (H-60): sc-9038	Sodium citrate pH 6.0
		Tris/EDTA pH 9.0
	IGF1Rβ (C-20): sc-713	Sodium citrate pH 6.0
		Tris/EDTA pH 9.0
p-IGF1R	p-IGF1R (Tyr 1161): sc-101703	Sodium citrate pH 6.0
		Tris/EDTA pH 9.0
		Trypsin
	p-IGF1R (Tyr 1161): ab39398	Sodium citrate pH 6.0
		Tris/EDTA pH 9.0
		Trypsin

Table 2.3 Primary antibodies and antigen retrieval methods tested for detecting target antigens in clinical tissue samples

Target antigen	Primary antibody	Antigen retrieval method
IGF1	IGF1: ab9572	Sodium citrate pH 6.0
		Tris/EDTA pH 9.0
	IGF1 (H-70): sc-9013	Sodium citrate pH 6.0
		Tris/EDTA pH 9.0
IGF1R	IGF1R: ab131476	Sodium citrate pH 6.0
		Tris/EDTA pH 9.0
IGF1Rα	IGF1Rα (N-20): sc-712	Sodium citrate pH 6.0
		Tris/EDTA pH 9.0
IGF1Rβ	IGF1Rβ (H-60): sc-9038	Sodium citrate pH 6.0
		Tris/EDTA pH 9.0
	IGF1Rβ (C-20): sc-713	Sodium citrate pH 6.0
		Tris/EDTA pH 9.0
p-IGF1R	p-IGF1R (Tyr 1161): sc-101703	Sodium citrate pH 6.0
		Tris/EDTA pH 9.0
	p-IGF1R (Tyr 1161): ab39398	Sodium citrate pH 6.0
		Tris/EDTA pH 9.0

Table 2.4 Antibodies for immunohistochemistry

Primary antibody	Species	Clonality	Source	Secondary antibody	Control
Mouse IGFBP5	Goat	Polyclonal	R&D System (AF578)	Rabbit anti-goat biotinylated (BA-5000)	Concentration-matched normal goat IgG (sc-2028)
IGF1	Rabbit	Polyclonal	Abcam (ab9572)	Swine anti-rabbit biotinylated (E0353)	Concentration-matched normal rabbit IgG (sc-2027)
IGF1 (H-70)	Rabbit	Polyclonal	Santa Cruz Biotechnology (sc-9013)	Swine anti-rabbit biotinylated (E0353)	Concentration-matched normal rabbit IgG (sc-2027)
IGF1R	Rabbit	Polyclonal	Abcam (ab131476)	Swine anti-rabbit biotinylated (E0353)	Concentration-matched normal rabbit IgG (sc-2027)
IGF1Rα (N-20)	Rabbit	Polyclonal	Santa Cruz Biotechnology (sc-712)	Swine anti-rabbit biotinylated (E0353)	Concentration-matched normal rabbit IgG (sc-2027)
IGF1Rβ (H-60)	Rabbit	Polyclonal	Stan Cruz Biotechnology (sc-9038)	Swine anti-rabbit biotinylated (E0353)	Concentration-matched normal rabbit IgG (sc-2027)
IGF1Rβ (H-60)	Rabbit	Polyclonal	Santa Cruz Biotechnology (sc-713)	Swine anti-rabbit biotinylated (E0353)	Concentration-matched normal rabbit IgG (sc-2027)
p-IGF1R (Tyr 1161)	Rabbit	Polyclonal	Santa Cruz Biotechnology (sc-101703)	Swine anti-rabbit biotinylated (E0353)	Concentration-matched normal rabbit IgG (sc-2027)
p-IGF1R (Tyr 1161)	Rabbit	Polyclonal	Abcam (ab39398)	Swine anti-rabbit biotinylated (E0353)	Concentration-matched normal rabbit IgG (sc-2027)

2.7 Gene expression study

2.7.1 RNA isolation

Cells at 80-90% confluence in a 10 cm^2 culture plates were detached by treating with 5 ml of pre-warmed TEP, transferred into 1.5 ml Eppendorf tubes and centrifuged at 150 × g for 5 min. Supernatants were removed carefully without disturbing cell pellets. To ensure no solution containing TEP was left, the pellets were further washed with ice-cold PBS by pipetting, and was centrifuged at 13,000 × g at 4°C for 5 min. PBS was carefully removed without disrupting pellets. Total RNA was isolated using the RNeasy Mini Kit (74104, Qiagen, Hilden, Germany) according to the manufacturer's protocol. The concentration and purity of RNA samples were assessed using a NanoDrop™ 2000 Spectrophotometer (Thermo Fisher Scientific). The concentration was determined by measuring absorbance at 260 nm and the purity was assessed based on both 260/280 and 260/230 ratios. Only samples with 280/260 values between 1.8 and 2.0, and 260/230 values between 2.0 and 2.2, were used for subsequent analysis.

2.7.2 DNAse treatment

RNA was treated with Ambion® TURBO DNase Treatment and Removal Reagents (Thermo Fisher Scientific) as described by the manufacturer.

2.7.3 Complementary DNA synthesis

Complementary DNA (cDNA) synthesis was performed on ice using an Applied Biosystems™ High-Capacity cDNA Reverse Transcription Kit (4368814, Thermo Fisher Scientific) according to the manufacturer's protocol. One µg of RNA was used per reaction.

2.7.4 Real-time quantitative PCR

The mRNA for human IGF1R was analysed using TaqMan® Fast Advanced Master Mix (2×) and TaqMan® Gene Expression Assay (product Hs00609566_m1, Thermo Fisher Scientific). Reactions were carried out in a MicroAmp® Fast Optical 96-well reaction plate (Thermo Fisher Scientific) in a StepOnePlus™ Real-Time PCR System (Thermo Fisher Scientific) as described by the manufacturer. Gene expression was normalised to human β-ACTIN expression, assessed

with TaqMan® Gene Expression Assay (Hs99999903_m1, Thermo Fisher Scientific). In all experiments, a negative control reaction was carried out in which DEPC-treated water was added instead of substrate cDNA. After running for 40 cycles, the C_T values were obtained from the amplification plot and standard curve using Microsoft Excel spreadsheet (Microsoft Corporation, Redmond, Washington, USA).

2.8 Histological analysis

2.8.1 Staining of tissue sections for fat tissue quantification

FFPE tissue sections prepared in Section 2.5.3 were stained with haematoxylin and eosin (H&E) as described by Fischer *et al* [228].

2.8.2 Masson Trichrome staining for quantification of dermal fibrosis

Masson Trichrome staining was performed on FFPE tissue sections prepared in Section 2.5.3 according to a standard protocol as described by Goldner [229].

2.8.3 Photography of stained mouse tail sections

All slides containing mouse tail tissue sections stained with either H&E or using Masson Trichrome method were scanned and photographed at 10× magnification with an Olympus VS120 virtual microscopy slide scanner using OlyVIA® Software Version 2.4 (Olympus Corporation, Tokyo, Japan). The scanned Virtual Slide Images were converted as TIFF images.

2.8.4 Quantification of fat tissue in mouse lymphoedema model

To analyse fat tissue in the mouse model of lymphoedema, fat in the dermis and subcutaneous layer was quantified based on the following parameters:

1) Cross-sectional area covered by adipocytes

2) Number of adipocytes

3) Cross-sectional area of individual adipocytes

These parameters were analysed over the entire cross-section of the mouse tail using transverse

sections (two tissue-sections per mouse). The sections were derived from tissues located between 2.5 and 5 mm distal to the centre of the surgical scar, or at an equivalent site in the tails of non-operated control mice. As for the operated mice, these assessments were performed in the tail tissues harvested at multiple time-points (i.e. days 7, 17 and 90 post-surgery) - these time-points were chosen as they represent initial, developing and chronic stages of lymphoedema, respectively, thus allowing quantification of each measurement parameter at different chronological stages of secondary lymphoedema. The tail sections of the non-operated control mice were all collected at 90 days from the start of the experiment. Quantification of tail volume and fat tissue in the tails of mice treated with linsitinib was performed on tail tissue cross-sections harvested at day 17 post-surgery. In addition to the parameters 1) – 3) listed above, the following parameters were quantified:

4) Cross-sectional area of bone combined with muscle

5) Thickness of the subcutaneous layer

6) Thickness of the dermis

7) Cross-sectional area of dermal fibrosis

All histological quantification was carried out blinded.

2.8.4.1 Quantification of the cross-sectional area covered by adipocytes

Adipocytes in the dermis and subcutaneous layer were identified based on their characteristic unilocular appearance. The cross-sectional area covered by adipocytes in each image was traced manually using MetaMorph software and was calculated (in μm^2) using a custom-made MetaMorph journal.

2.8.4.2 Quantification of the number of adipocytes

Adipocytes in the dermis and subcutaneous layer were manually counted in each image.

2.8.4.3 Quantification of cross-sectional area of individual adipocytes

The cross-sectional area of each adipocyte was calculated by dividing the area covered by adipocytes by the number of adipocytes.

2.8.4.4 Quantification of cross-sectional area of bone combined with muscle

The cross-sectional area of bone and muscle in each image was traced manually using MetaMorph software and was calculated (in μm^2) using a custom-made MetaMorph journal.

2.8.4.5 Proportion of tail swelling due to increased area of subcutaneous fat

The cross-sectional area of the mouse tail was traced manually using MetaMorph software and was calculated (in μm^2) using a custom-made MetaMorph journal. The proportion of cross-sectional tail swelling due to increased area of fat tissue was calculated using the formula below and expressed as a percentage.

$$\frac{(\text{Mean area of fat in operated mice}) - (\text{Mean area of fat in non-operated mice})}{(\text{Mean cross sectional area of operated mice}) - (\text{Mean cross sectional area of non-operated mice})} \times 100$$

2.8.4.6 Quantification of the thickness of subcutaneous layer

The thickness of the subcutaneous layer of the mouse tail was quantified by manually drawing four lines (two horizontal and two vertical) between the dermis and the bone/muscle compartment, and the average distance was calculated (in μm) using a custom-made MetaMorph journal.

2.8.4.7 Quantification of the thickness of dermis

The thickness of the dermis was quantified by manually drawing four lines (two horizontal and two vertical) between the epidermal and subcutaneous layer, and the average distance was calculated (in μm) using a custom-made MetaMorph journal.

2.8.4.8 Quantification of dermal fibrosis

Collagen fibres stain green by the Masson Trichrome method (Section 2.8.2). To quantitate fibrosis, the area of green-stained regions in the dermis was automatically calculated (in μm^2) using HALO Image Analysis Software (Indica Labs, Corrales, NM, USA).

2.9 Statistical analysis

In an experiment consisting of only two independent study groups, the two-tailed Student's t-test was used to assess statistical significance with Microsoft Excel spreadsheet (Microsoft Corporation, Redmond, Washington, USA). When an experiment involved more than two study groups, statistical significance was assessed by one-way analysis of variance (ANOVA) followed by Tukey's *post-hoc* test for multiple comparisons using GraphPad Prism 7 (GraphPad Software, Inc., San Diego, CA, USA). The significance level (alpha) for the Tukey's post *hoc* test was set as 0.05 (95% confidence interval).

Chapter 3

Identification of Molecular Signalling Mechanisms Driving Formation of Fat Tissue in a Mouse Model of Secondary Lymphoedema

3.1 Introduction

This chapter is focused on identifying an animal model of secondary lymphoedema in which to study formation of fat tissue (Section 3.2) and using this model to identify signalling mechanisms that drive adipogenesis in secondary lymphoedema (Section 3.3). Ultimately, the work in this chapter is aimed at identifying signalling pathways that could be therapeutically targeted to restrict formation of fat tissue in secondary lymphoedema.

3.2 Identification of a mouse model of secondary lymphoedema in which to study formation of fat tissue

I chose a mouse tail model of secondary lymphoedema as the initial candidate for assessing formation of fat tissue in this disease. The mouse tail was chosen for the following reasons. Firstly, the mouse is a vertebrate and a mammal with a similar lymphatic system structure to humans. Secondly, mice are relatively easy to house and manage in standard biomedical animal facilities, as opposed to larger animal species. Thirdly, mice are readily available as inbred strains which minimises variability between animals, and is advantageous in an experimental setting. Fourthly, mouse genetics is well-understood, thus allowing easy manipulation of genetically modified models of lymphoedema. Fifthly, the mouse has been used successfully in the past as a model of primary and secondary lymphoedema [67, 138, 230]. Sixthly, the mouse tail anatomy is highly reproducible as assessed in histological sections, thus the initial lymphatics and lymphatic collectors are easily identifiable, which facilitates accurate evaluation of each individual lymphatic subtype (Figure 3.1). Although the mouse tail does not contain lymph nodes, it is considered a useful model of secondary lymphoedema given there is no evidence that lymph nodes have a major mechanical role in lymphatic drainage. Lastly, the truncated, cone-shape of

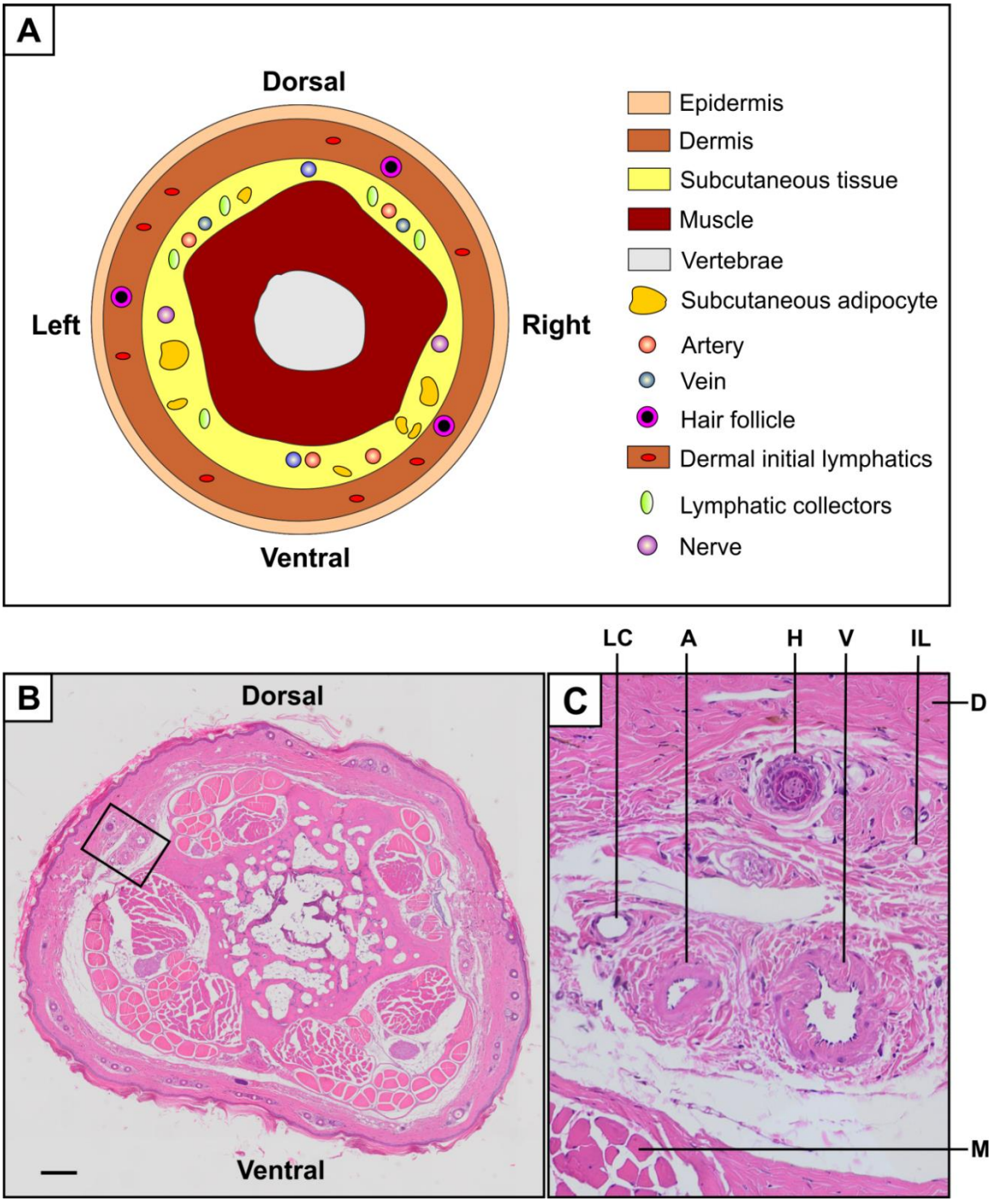

Figure 3.1 Transverse section of the mouse tail. (A) Schematic representation shows major components in the cross-section of mouse tail. (B) Representative H&E stained cross-sectional histological section of the tail for comparison with panel A; scale bar = 400 µm. (C) Magnification from the region within the rectangle in panel B showing dermal initial lymphatic, lymphatic collector, artery and vein. H denotes hair follicle and other abbreviations are defined in panel A

mouse tails, and an elliptical shape on transverse histological section facilitate quantification of measurement parameters using MetaMorph imaging software. All these factors make a mouse tail model of secondary lymphoedema attractive for studying the pathophysiology of the condition.

3.2.1 Mouse tail model of secondary lymphoedema with chronic tissue swelling

Dr. Sidney Levy, a former Ph.D. student in our laboratory, previously developed a novel surgical model of secondary lymphoedema in the mouse tail (Dr. Sidney Levy, Ph.D. Thesis, University of Melbourne, Australia). The four lymphatic collectors in the tail were specifically disrupted using bipolar diathermy, and all pre-collectors and the overlying initial dermal lymphatics were selectively disrupted by shallow circumferential incisions. The model was designed to mimic the extensive lymphatic damage that can occur due to regional lymph node ablation and post-operative radiotherapy performed in the context of treatment for various cancer types, including breast cancer, prostate cancer, melanoma, head and neck cancer and gynaecological cancers [231]. The combination of these two therapeutic approaches is also known to lead to secondary lymphoedema in some patients [232, 233].

In preliminary studies conducted by Dr. Levy, mice were subjected to the surgery ablating all subtypes of lymphatics and were monitored for 3 months post-surgery. Whilst mouse tail lymphoedema models have previously been used in several other studies, most have had drawbacks. For example, Uzarski et al. used a mouse model in which only dermal initial lymphatics were surgically ablated [81], whereas a mouse model employed by Cheung et al. was subjected to the surgery only ligating lymphatic collectors [234]. Given lymphadenectomy results in disruption of all lymphatic subtypes in breast cancer patients, these mouse models do not mimic the condition observed in the clinical setting. Further, most previous studies had short monitoring periods and lack of histological correlation with human lymphoedema [81, 234, 235]. Given clinical lymphoedema is a chronic disease, the model used in this study was designed to allow for assessment of secondary lymphoedema occurrence and histological changes which occur in the human condition, in a chronic setting. Notably, this model exhibits a statistically significant

increase in tail size post-surgery compared with non-operated control mice (Figure 3.2A and B).

The model exhibits a statistically significant increase in tail volume at day 7, which represents an onset stage of secondary lymphoedema during which the tail is swelling rapidly. At day 17 the model represents an intermediate stage of secondary lymphoedema as the rate at which tail volume is increasing begins to moderate. Tail volume continues to increase, albeit slowly, until it reaches a peak of approximately 1.94 ×baseline (baseline is defined as the volume at day 0 pre-operatively) at day 48. Although a partial resolution of the tail swelling occurs thereafter, correlating with detachment of the wound eschar during the process of wound healing, the model exhibits a state of persistent and chronic swelling of approximately 1.7 × baseline at day 90, which hence represents a chronic stage of secondary lymphoedema. Notably, the model also exhibits pathophysiological features of clinical lymphoedema, such as dermal fibrosis, subcutaneous oedema and epidermal hyperkeratosis (Figure 3.2C). In summary, this mouse model of lymphoedema exhibited a rapid onset of profound and chronic tail swelling over a 3-month period. Importantly, the model was monitored post-operatively longer than for any previously reported animal models, which allowed confirmation that the tail swelling was chronic and was associated with pathophysiological features of secondary lymphoedema in the clinical setting.

3.2.2 Evidence of formation of fat tissue in the mouse model of lymphoedema

The mouse tail model of secondary lymphoedema explored above exhibits profound and chronic tissue swelling and demonstrates similar pathophysiological features to human lymphoedema. However, the formation of fat tissue in this model has not previously been studied. Initial inspection of tissue sections from lymphoedematous tails generated in this model indicated that all adipocytes, apart from those in bone marrow, were located in the dermis or subcutaneous layer. To quantitate the formation of fat tissue during the progression of lymphoedema in this model, I analysed fat tissue in the dermis and subcutaneous layer at days 7, 17 and 90 post-surgery using H&E-stained mouse tail sections. The mouse tail sections used for the fat quantification

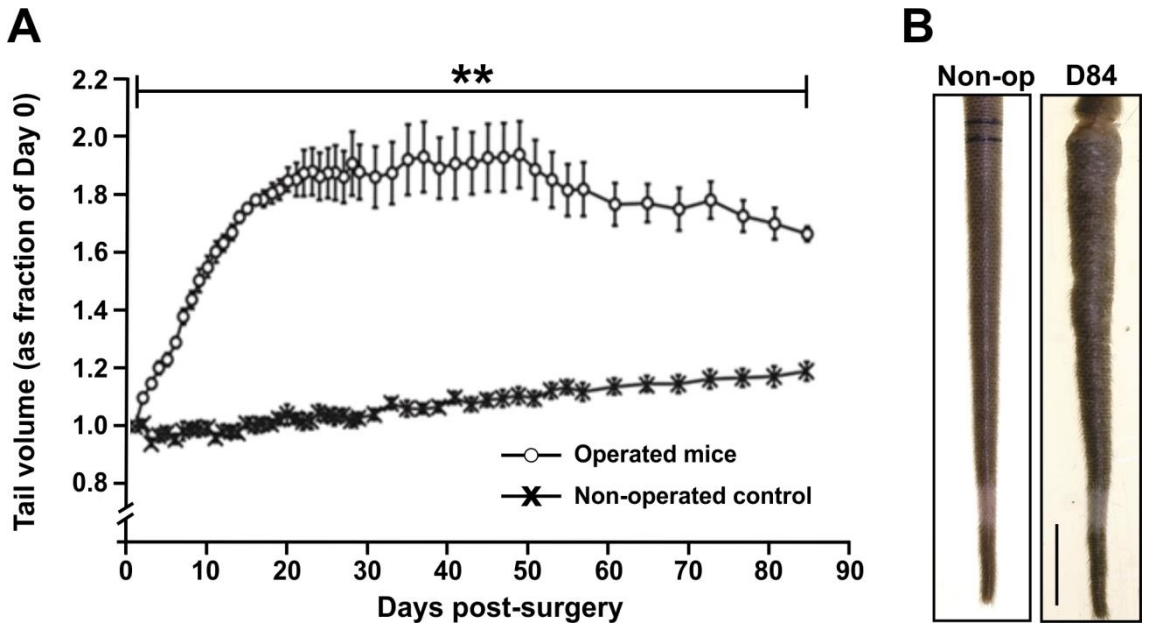

Figure 3.2 Tail swelling and pathophysiological changes in the microsurgical model of secondary lymphoedema. (A) Analysis of tail volume over 3 months post-surgery. Data show mean ± SEM and asterisk denotes $p<0.01$ for comparison with non-operated control (Student's t-test). (B) Representative tails for non-operated ("Non-op") and mice 84 days post-surgery ("D"= days post-surgery); scale bar = 10 mm. Note that the figures for panels A and B were obtained from Dr. Sidney Levy's Ph.D. thesis, and are shown here to introduce the mouse model. (C) Representative H&E-stained cross-sectional histological sections of the tail in the mouse model of lymphoedema. Note the thickness of the subcutaneous layer (S.C.) in the model increases at days 7, 17 and 90 post-surgery, compared to the non-operated control. The model also exhibits dermal fibrosis, subcutaneous oedema and epidermal hyperkeratosis as lymphoedema progresses (these pathophysiological features of secondary lymphoedema were confirmed by Dr. Shona Hendry, a clinical anatomical pathologist at Peter MacCallum Cancer Centre, Melbourne); scale bar = 200 µm.

C

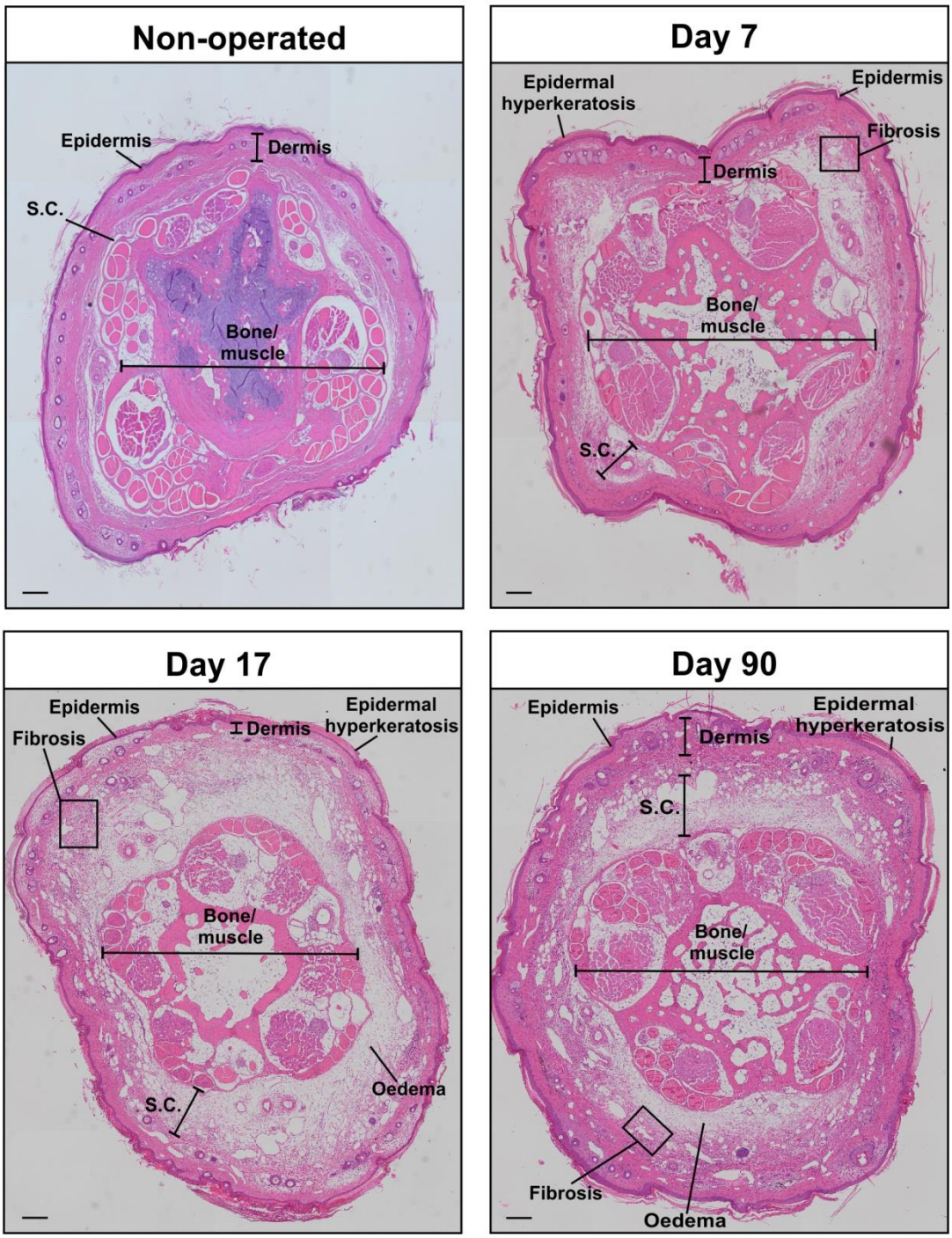
Non-operated
Epidermis
Dermis
S.C.
Bone/
muscle
Day 7
Epidermal
hyperkeratosis
Epidermis
Fibrosis
Dermis
Bone/
muscle
S.C.
Day 17
Epidermis
Fibrosis
Dermis
Epidermal
hyperkeratosis
Bone/
muscle
Oedema
S.C.
Day 90
Epidermis
Dermis
Epidermal
hyperkeratosis
S.C.
Bone/
muscle
Fibrosis
Oedema

were harvested between 2.5 and 5.0 mm distal to the centre of the scar in the tails of the mouse model, or at equivalent sites on the tails of non-operated controls (Figure 3.3A). Quantification of fat tissue at different time- points in the model may provide a better understanding of the timing of formation of fat tissue after surgery and the timing at which a therapeutic intervention, aiming to inhibit formation and expansion of fat tissue in secondary lymphoedema, could be tested.

The mouse model of lymphoedema exhibited an increase in the cross-sectional area of the tail in comparison to the non-operated control at days 7, 17 and 90 post-surgery; however, only the differences at days 17 and 90 post-surgery were statistically significant (Figure 3.3B). To better understand the cause of the increased cross-sectional area of the tails in the model, adipocytes in the dermis and subcutaneous layer were identified based on their characteristic unilocular appearance (Figure 3.3C), and the tails were subsequently quantified for the following parameters: 1) cross-sectional area covered by adipocytes, 2) the number of adipocytes in tissue cross-sections and 3) the cross-sectional area of individual adipocytes. The model exhibited an increase in the cross-sectional area covered by adipocytes at days 7, 17 and 90 post-surgery in comparison to the non-operated control; however, only the differences at days 17 and 90 post-surgery were statistically significant (Figure 3.3D). In addition, the model demonstrated a statistically significant increase in the number of adipocytes at days 7, 17 and 90 post-surgery in comparison to the non-operated control (Figure 3.3E). Similarly, the cross-sectional area of individual adipocytes was also increased at days 7, 17 and 90 post-surgery in the model; however, only the differences at days 17 and 90 post-surgery were statistically significant when compared with the non-operated control (Figure 3.3F). These results indicate that the significantly increased fat observed at days 17 and 90 post-surgery in the model of secondary lymphoedema was due to the increased number of adipocytes and increased cross-sectional area of individual adipocytes.

Given that the mouse model of lymphoedema was found to exhibit significantly increased levels of fat at days 17 and 90 post-surgery, I next sought to determine to what extent the increased fat tissue contributed to the tail swelling. This is important since previous clinical studies have

shown excess amounts of fat tissue in lymphoedematous arms in patients following breast cancer treatment, with a reported range of 68% to 93% greater fat volume compared to normal arms [6, 57, 65]. Of note, it has been reported that approximately 55% of swelling in lymphoedematous arms is due to excess fat tissue [65]. Analysis of the mouse model studied here revealed that approximately 60% of tail swelling was due to the increased area covered by adipocytes at day 17 post-surgery, whereas at day 90 post-surgery, 43% of tail swelling was due to the increased area covered by adipocytes (Figure 3.3G). It is highly likely that tail swelling also results, in part, from other pathological features of secondary lymphoedema in the model, such as dermal fibrosis, subcutaneous oedema and epidermal hyperkeratosis. These factors may make a proportionally bigger contribution to tail swelling at day 90 post-surgery than at day 17 post-surgery, which would explain why formation of fat makes a proportionally larger contribution to tail swelling at day 17 post-surgery than at day 90 post-surgery. In contrast to fat tissue, there was no statistically significant difference in the cross-sectional area of the bone and muscle in mouse tails between the non-operated control and the model at days 7, 17 and 90 post-surgery (Figure 3.3H), suggesting that the bone and muscle compartment in the tail has limited capacity to swell or expand in response to the surgical trauma which occurs in this lymphoedema model.

In summary, these findings indicate that the increased area covered by adipocytes made a major contribution to the swelling in the tail of the mouse lymphoedema model, especially at days 17 and 90 post-surgery. Also, the degree to which the increase in fat tissue contributed to tail swelling was found to be quite similar to what has been reported for secondary lymphoedema in humans. Given these results above, this mouse model of lymphoedema will be employed to study signalling pathways driving formation of fat tissue in secondary lymphoedema.

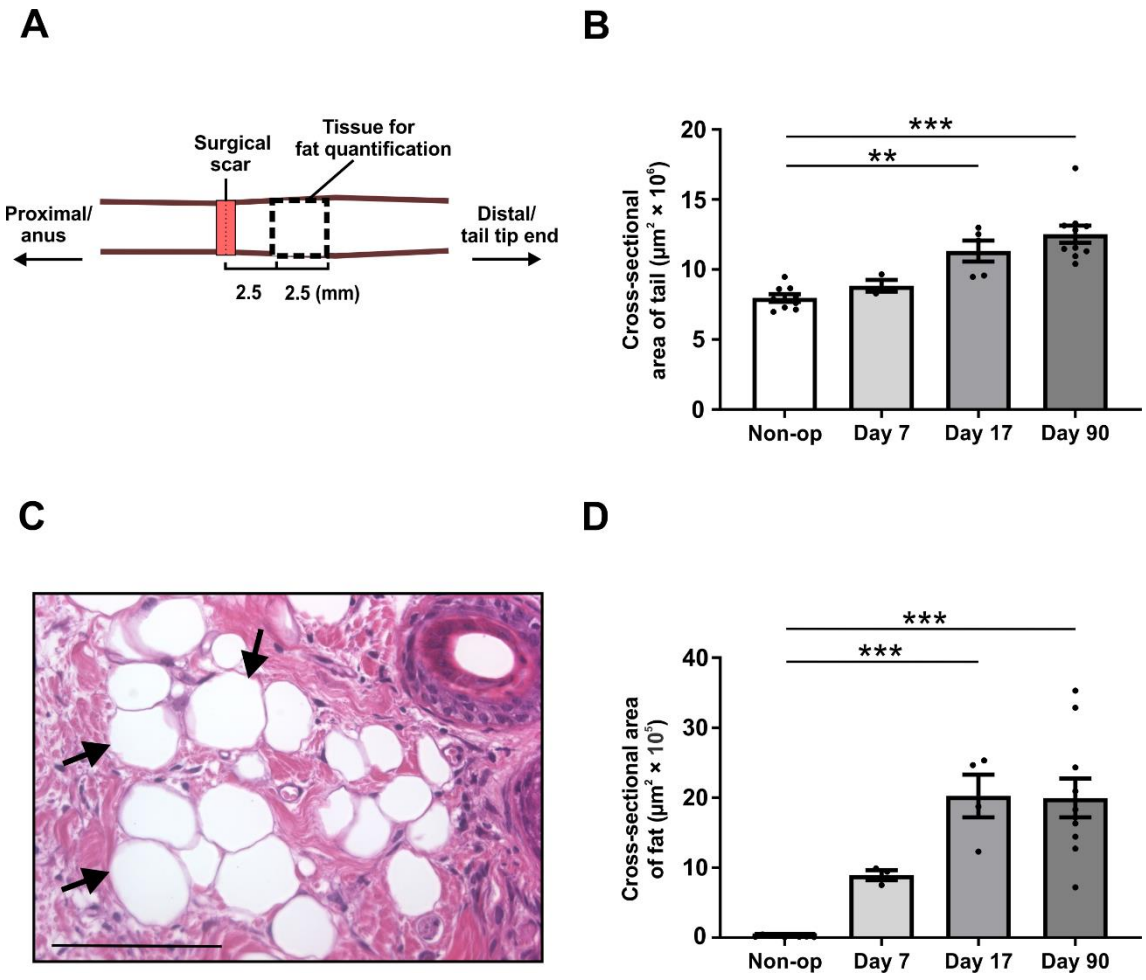

Figure 3.3 Quantification of fat tissue in mouse lymphoedema model. (A) Schematic diagram indicates the location of tail tissue harvested for fat quantification – tissue sections were generated from tissue between 2.5 and 5.0 mm distal to the centre of the scar on the tails of the model or at equivalent sites of non-operated control mice. (B) Mean cross-sectional area of tails. (C) Image showing subcutaneous adipocytes in a mouse tail - adipocytes are easily identified by their characteristic unilocular appearance (indicated by arrows); scale bar = 100 µm. (D) Mean cross-sectional area of tails covered by fat in the dermis and subcutaneous layer. (E) Mean number of adipocytes in tissue cross-sections of mouse tails. (F) Mean cross-sectional area of individual adipocytes in mouse tails. (G) Percentage of tail swelling that is due to increased area of fat at days 17 and 90 post-surgery in mouse model. (H) Mean cross-sectional area of bone and muscle in mouse tails. For panels B, D, E, F, and H: Non-op, n=9; Day 7 post-surgery, n=5; Day 17 post-surgery, n=6; Day 90 post-surgery, n=11. Data show mean ± SEM; statistical significance is indicated as follows: ** $p<0.01$, *** $p<0.001$, **** $p<0.0001$ (one-way ANOVA with Tukey's *post-hoc* multiple comparison test). Black circles depict individual data points.

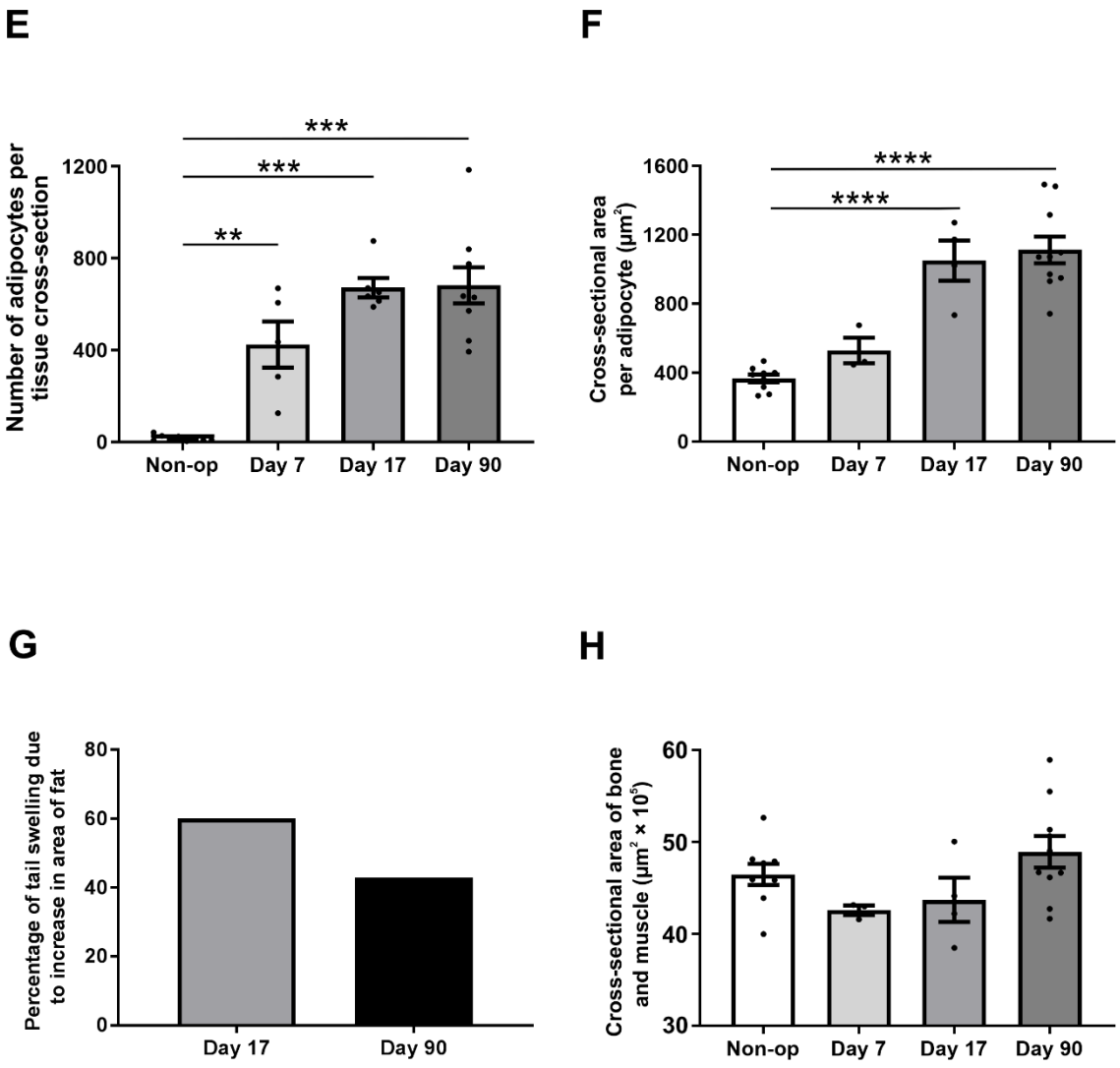
E
Number of adipocytes per tissue cross-section
1200
800
400
0
***
***
**
Non-op
Day 7
Day 17
Day 90
F
Cross-sectional area per adipocyte (μm²)
1600
1200
800
400
0
****
****
Non-op
Day 7
Day 17
Day 90
G
Percentage of tail swelling due to increase in area of fat
80
60
40
20
0
Day 17
Day 90
H
Cross-sectional area of bone and muscle (μm² × 10⁶)
60
50
40
30
Non-op
Day 7
Day 17
Day 90

3.3 Identification of molecular signalling pathways driving formation of fat tissue in lymphoedema

This section presents approaches for identifying signalling pathways that drive formation of fat tissue using the mouse mode of lymphoedema as described in Section 3.2. A range of studies have shown that the development of secondary lymphoedema is driven by molecular signalling pathways leading to various cell biological responses as a result of surgical trauma and/or radiation [137, 150, 155]. Previously, Mr. Yong Qiang Yeo, a former Honours student in our laboratory, performed whole-genome microarray analyses using the mouse lymphoedema model which led to identification of genes that were differentially expressed in the model compared to the non-operated control. A subset of these genes was involved in molecular signalling pathways associated with various biological functions relevant to secondary lymphoedema. However, expression of the proteins encoded by these genes in this model has not previously been studied. In the following sections, I employ immunohistochemical methods to analyse proteins encoded by these genes in the mouse model of lymphoedema, with a specific focus on those that are associated with signalling pathways regulating formation of fat tissue. In addition, immunohistochemical analyses are performed in human lymphoedema tissue samples to gain insight into whether or not these proteins might also be clinically important in driving formation of fat tissue in secondary lymphoedema.

3.3.1 Identification of genes involved in adipogenic pathways in lymphoedema

As demonstrated in the previous section, the mouse model of secondary lymphoedema used in this study exhibits significant adipogenesis (i.e. differentiation of preadipocytes to adipocytes), based on an increased number of adipocytes compared to non-operated controls, as well as increases in the size of adipocytes and of the area of fat tissue. Numerous studies have shown that adipogenesis can be driven by various signalling pathways, such as the insulin-like growth factor (IGF), Tyro3/Axl/Mertk (TAM) and BMP pathways (Table 3.1). However, it is not known if any of these pathways are involved in regulating formation of fat tissue in secondary

Table 3.1 Molecular signalling pathways regulating adipogenesis

Signalling pathway *	Model	Finding from model	Reference
IGF	Murine 3T3-L1 preadipocytes	IGF-1 induced differentiation of 3T3-L1 cells to adipocytes	Smith PJ et al, 1998 (192)
	Cre-lox induced *Igf-1r* gene knockout mouse	*Igf-1r* gene knockout mouse had less adipose tissue	Holzenberger et al, 2001 (264)
TAM	C57BL/6 mouse	Pharmaceutical inhibition of the TAM ligand Gas6 reduced weight gain, and subcutaneous and gonadal fat mass in mouse	Lijnen HR et al, 2011 (215)
	Gas6 gene knockout mouse	*Gas6 gene* knockout mouse had less fat than wild-type	Maquoi E et al. 2005 (216)
BMP	Murine C3H10T1/2 pluriopotent stem cells	Both BMP2 and BMP4 induced differentiation of C3H10T1/2 stem cells to adipocytes	Huang H et al, 2009 (167)
	BALB/c athymic mouse	BMP4 promoted differentiation of C3H10T1/2 stem cells to adipocytes in athymic mouse	Tang QQ et al, 2004 (169)
Wnt/β-catenin	Murine 3T3-L1 cells	Activation of Wnt/β-catenin pathway inhibited differentiation of 3T3-L1 cells to adipocytes	Ross SE et al, 2000 (181)
	C57BL/6 mouse	Activation of Wnt/β-catenin pathway reduced total body adiposity in mouse	Longo KA et al, 2004 (182)
Chemrin/CMKLR1	Murine 3T3-L1 cells	Knockdown of C*hemerin* or *Cmklr1* inhibited differentiation of 3T3-L1 cells to adipocytes	Goralski KB et al, 2007 (223)
	Bone marrow stromal cells	Knockdown of C*hemerin* or *Cmklr1* inhibited differentiation of bone marrow stromal cells to adipocytes	Muruganandan S et al, 2011 (219)
	Cmklr1 gene knockout mouse	*Cmklr1* gene knockout mouse had a reduced total body adiposity	Ernst MC et al, 2012 (222)
Hedgehog	Drosophila	Fat-specific activation of Hedgehog pathway inhibited formation of fly fat	Suh JM et al, 2008 (226)
	Human multipotent adipose-derived stem (hMADS) cells	Activation of Hedhehog pathway impaired adipogenesis	Fontaine et al, 2008 (227)

*** Well-characterised signalling pathways which can regulate adipogenesis are shown**

lymphoedema.

Mr. Yong Qiang Yeo in our laboratory previously performed whole-genome microarray gene expression analyses using RNA extracted from tail skin samples from the mouse model of secondary lymphoedema, at day 90 post-surgery when lymphoedema is chronic, and compared the results to those derived from similar regions of tails from non-operated controls (Figure 3.4). Notably, an analysis by Partek® Genomic Suite® software revealed that, out of all genes known to be involved in adipogenic pathways, only two genes encoding insulin-like growth factor binding protein 5 (IGFBP5) and insulin-like growth factor 1 (IGF1), were identified to be significantly differentially expressed at the mRNA levels in the lymphoedema model compared to the non-op control by microarray. The mRNA levels of IGF1 and IGFBP5 were significantly down-regulated in the model compared to the non-op control. The gene encoding IGFBP5 was selected for further verification by qRT-PCR (Figure 3.5A).

The IGF signalling pathway involved in the regulation of adipogenesis comprises secreted IGF ligands (IGF1 and IGF2), extracellular IGF-binding proteins (IGFBP1 through IGFBP5) and transmembrane IGF receptors (IGF1R and IGF2R) [236-241]. IGF1 binds and activates IGF1R, a cell surface receptor tyrosine kinase which can be expressed on both preadipocytes and adipocytes [242, 243]. Signalling downstream of activated IGF1R drives formation of fat tissue by promoting the clonal expansion of preadipocytes mediated by the Ras/MAPK pathway [244], differentiation of preadipocytes to adipocytes (i.e. adipogenesis) through activation of the PI3K/Akt/mTOR pathway [243, 245] and lipid accumulation in adipocytes [246, 247]. Importantly, IGFBP5 can bind IGF1 thus preventing this ligand from activating IGF1R; hence IGFBP5 can restrict signalling for the development of fat tissue [248, 249]. Consequently, down-regulation of IGFBP5 in the mouse model of lymphoedema may lead to enhanced signalling driven by activated IGF1R, which in turn could promote the formation of fat (Figure 3.5B).

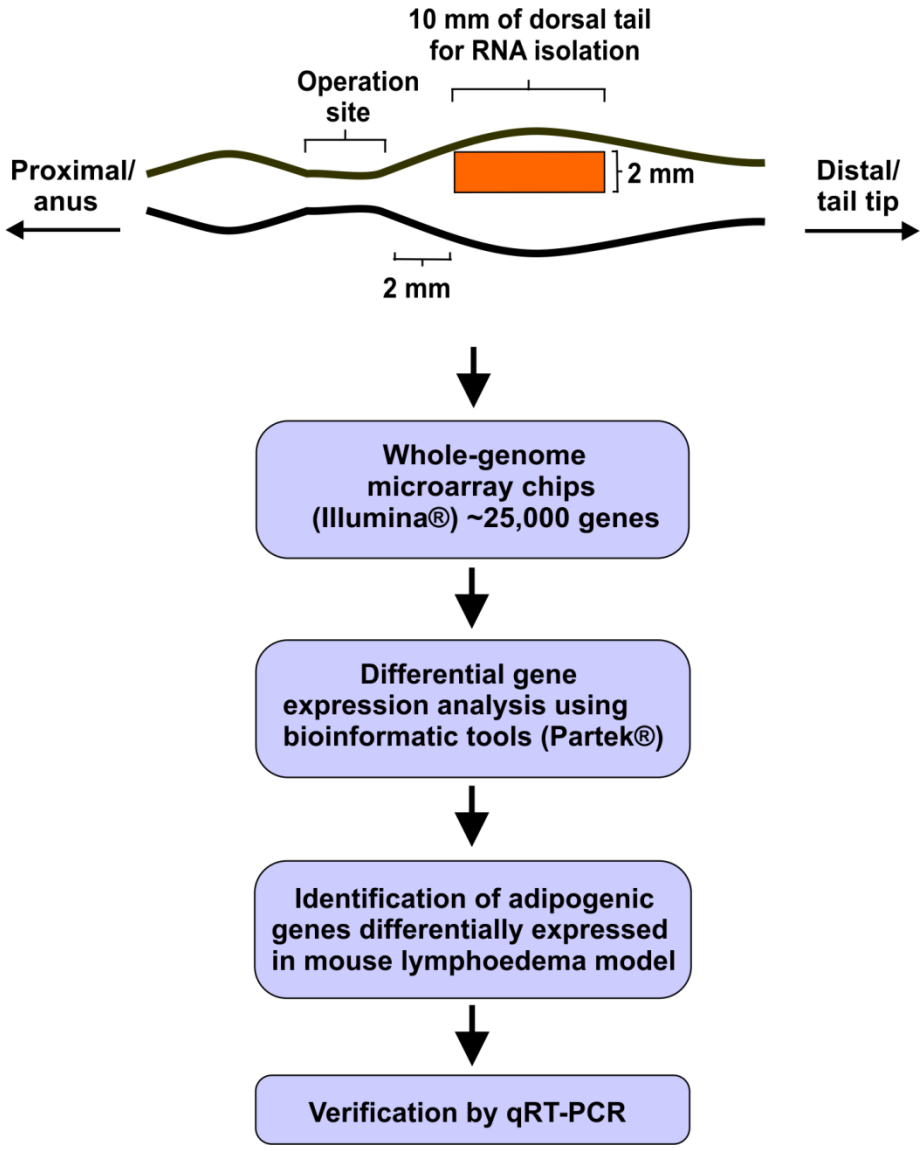

Figure 3.4 Strategy for identifying genes involved in modulating adipogenesis in the mouse model of secondary lymphoedema. A region of tissue encompassing skin and subcutaneous tissue (orange rectangle) was harvested from the mouse model of secondary lymphoedema (top), at day 90 post-surgery when lymphoedema is chronic, and from non-operated control. The microarray data for expression levels of ~25,000 genes were generated by Mr. Yong Qiang Yeo, a former Honours student in our laboratory, and presented in his Honours thesis. The subsequent steps for analysing expression of genes are shown.

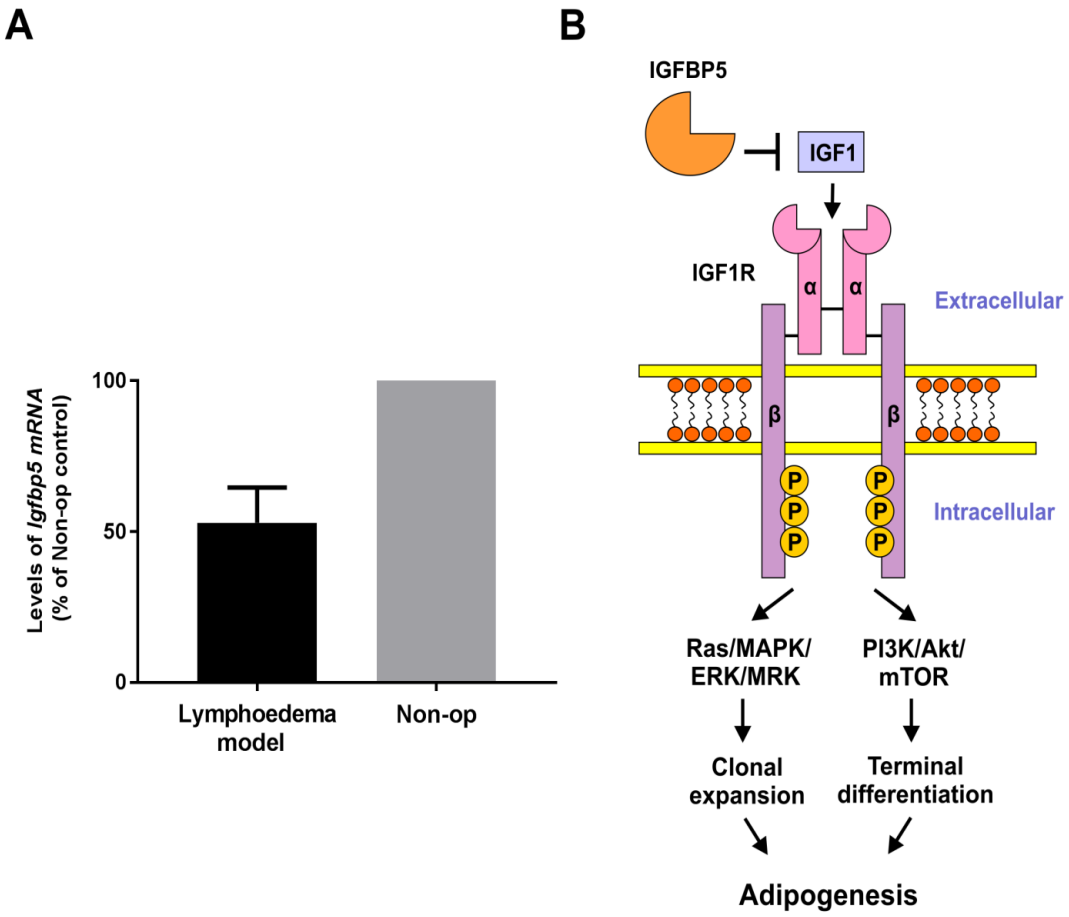

Figure 3.5 *Igfbp5* mRNA in the mouse model of secondary lymphoedema and regulation of adipogenesis levels by IGFBP5. (A) Analysis of *Igfbp5* mRNA levels in mouse lymphoedema model, 90 days post-surgery, by qRT-PCR. The mean level of *Igfbp5* mRNA detected in non-operated control mice (Non-op) is defined as 100%, and *Igfbp5* mRNA level in the mouse lymphoedema model, relative to Non-op, is shown. Data show mean ± SEM; there were four experimental replicates. Expression levels of genes, including *Igfbp5*, were normalised to that of the house-keeping gene, *β-actin*, in the mouse lymphoedema model, which were then averaged and compared to those in the Non-op control. (B) Schematic diagram indicates that IGFBP5 can bind IGF1 and thereby prevent interaction between IGF1 and the extracellular α-subunits of IGF1R (α), thus blocking activation of IGF1R and its downstream cascades such as PI3K/AKT/mTOR and Ras/MAPK/ERK/MRK signalling pathways that lead to adipogenesis. Hence a decrease of IGFBP5 in the lymphoedema model may promote IGF1R signalling and adipogenesis. Black lines between subunits of IGF1R denote disulfide bonds; β denotes β-subunit of IGF1R; "P" in orange circles denotes phosphate group.

3.3.2 Immunohistochemical analysis of IGF system in mouse model of lymphoedema

3.3.2.1 Immunohistochemical detection of IGFBP5 in the mouse model of lymphoedema

As a first step to studying proteins of the IGF system in the mouse lymphoedema model, I planned to analyse IGFBP5 at days 7, 17 and 90 post-surgery, as well as in the non-operated control, by immunohistochemistry. The mouse tail tissue to be studied encompassed a similar region of skin and subcutaneous tissue that was used in the microarray studies (Figure 3.4). The model exhibits a statistically significant increase in tail volume at day 7, which represents an onset stage of secondary lymphoedema during which the tail is swelling rapidly (see Figure 3.2A) and fat is accumulating (see Figure 3.3D). Day 17 represents an intermediate stage of secondary lymphoedema as the rate at which the tail volume is increasing begins to moderate and fat tissue has reached maximum levels. At day 90, the model exhibits a state of persistent and chronic swelling of the tail which represents chronic lymphoedema, and fat levels are comparable to day 17. Immunohistochemical analysis at these time-points may provide an understanding of the timing at which the IGF system could drive formation of fat tissue after surgery as well identifying where components of this system are localised in tail tissue. Other approaches for detecting proteins of the IGF system, such as Western blotting or ELISA, were not as attractive as immunohistochemistry because they would not provide information about the localisation of the proteins in the mouse tail.

When my analysis of IGFBP5 in the lymphoedema model was undertaken, there were no convincing published reports demonstrating detection of IGFBP5 by immunohistochemistry in mouse tissues. Van Kleffens *et al.* claimed to have detected IGFBP5 in adult mouse kidney by immunohistochemistry using anti-IGFBP5 antibodies they generated [250]; however, the negative control they employed, consisting of incubation with pre-immune serum, gave rise to a significant signal which called their conclusions into question. Another study claimed to have detected weak IGFBP5 staining in embryonic and adult mouse heart by immunohistochemistry, however, no negative controls were included in the immunostaining analyses so the data were

also not conclusive [251]. Therefore, it was possible that adult mouse kidney and developing heart could be positive control tissues for detection of IGFBP5 by immunohistochemistry; however, this was not certain given the data from these studies. As I was unable to access the anti-IGFBP5 antibodies used in the two studies referred to above, I tested two commercially available mouse IGFBP5 polyclonal antibodies (ab4255 from Abcam and AF578 from R&D Systems) for their capacity to detect IGFBP5 in the mouse lymphoedema model. These antibodies were tested in parallel on adult mouse kidney and sagittal tissue sections containing developing heart tissue from mouse embryos, at embryonic days 14.5 (E14.5) and 18.5 (E18.5), which were included as potential positive control tissues for IGFBP5 immunostaining.

I tested the ab4255 and AF578 antibodies in mouse tails, adult mouse kidney and mouse embryos using a range of immunohistochemistry protocols developed in my laboratory at the Peter MacCallum Cancer Centre. Non-operated control tails were included in this analysis rather than tails with lymphoedema, based on the results from microarray analysis and qRT-PCR showing higher mRNA levels for IGFBP5 in the non-operated control than in the mouse model of lymphoedema at 90 days post-surgery (see Figure 3.5A), suggesting that there are higher levels of IGFBP5 protein in the non-operated control. Mouse tissue sections were subjected to heat-induced antigen retrieval using sodium citrate or Tris/EDTA buffers of varying pH followed by incubation with the primary antibodies (Figure 3.6). These approaches did not involve signal amplification techniques and resulted in a complete absence of staining in all tissues analysed even when high concentrations of primary antibodies were used (data not shown). Therefore, I tested several signal amplification methods to optimise detection of IGFBP5. These included use of avidin-biotin complex (ABC) or TSA, however, the ABC approach did not give rise to any signal, whereas the TSA approach led to extensive staining which was comparable to results with concentration-matched IgG negative control antibodies (data not shown). Varying the time for signal amplification did not improve these results. Assuming the background staining with the TSA approach was due to endogenous peroxidase activity [252], I increased the time over which

Figure 3.6 Approaches to detect IGFBP5 in mouse tissues by immunohistochemistry. Multiple approaches were assessed for detecting IGFBP5 in mouse tail tissue sections using commercial IGFBP5 antibodies - further details of the protocols are provided in Chapter 2. Results with these approaches are indicated in red boxes. AMP denotes amplification, ABC denotes avidin-biotin complex, and TSA denotes tyramide signal amplification.

endogenous peroxidases were blocked by exposure to 3% H_2O_2. However, this did not resolve the high background staining suggesting that the problem was not due to insufficient quenching of endogenous peroxidases (data not shown). Given some antigens require proteolytic enzyme-mediated retrieval [253, 254], I treated mouse tissue sections with variety of concentrations of trypsin before application of primary antibodies and subsequent signal amplification with ABC or TSA. However, none of these combinations of methods gave rise to IGFBP5 staining in non-operated mouse tail, adult mouse kidney or mouse embryos that was distinct from staining observed with concentration-matched IgG negative control antibodies (data not shown). In summary, despite all efforts, I was not able to develop an immunohistochemical approach for detecting IGFBP5 in mouse tissue using commercially available IGFBP5 antibodies.

3.3.2.2 Immunohistochemical detection of IGF1 and IGF1R in the mouse model of lymphoedema

Given that an immunohistochemical approach for detecting IGFBP5 in mouse tissue could not be established, I next analysed other key components of the IGF system, namely IGF1 and IGF1R, with a view to assessing the activity of this signalling system in lymphoedema.

Other studies previously claimed to have detected IGF1 by immunohistochemistry in various mouse tissues, including cranial sutures from mice exposed to *in utero* thyroxine, and mouse heart after cardiac ischemia and reperfusion [255, 256]. These studies employed commercially available polyclonal anti-IGF1 antibodies (ab9572 from Abcam). However, no negative controls were included in the immunostaining analyses so the data were not conclusive. Since the mice analysed in these studies had been subjected to specialised treatments, I could not readily access comparable tissues as potential positive controls for immunohistochemical analyses. Given the potential of the ab9572 polyclonal antibodies to detect IGF1 in mouse tissues, as claimed by the two studies referred to above, I tested the antibodies for their capacity to detect IGF1 in the mouse tail tissues from the lymphoedema model, at days 7, 17 and 90 post-surgery,

and in non-operated controls using a similar immunohistochemical protocol to that employed by Howie *et al*. [256]. This involved a combination of the ab9572 polyclonal antibodies with heat-induced antigen retrieval in Tris/EDTA buffer and TSA (see Chapter 2, Section 2.6 for further details).

At day 7 post-surgery, strong staining for IGF1 was detected on parts of the plasma membrane of subcutaneous adipocytes and in other regions near adipocytes (Figure 3.7). At day 17, IGF1 was also detected on parts of the plasma membrane of adipocytes, but the staining was less extensive than at day 7, and strong staining was also detected in regions near adipocytes. At day 90, IGF1 staining on the plasma membrane of adipocytes was less extensive than at day 17 but was still pronounced in regions near adipocytes. On the contrary, only extremely weak IGF1 staining was associated with adipocytes in non-operated tails, and no staining was detected in regions near adipocytes. For all samples, immunostaining with concentration-matched IgG negative control antibodies gave no signals, indicating that the immunohistochemical protocol for detecting IGF1 was working well. These results indicate that levels of IGF1 in and around regions of fat in the tail of the mouse lymphoedema model increased profoundly during the first week post-surgery and remained elevated until at least day 90 post-surgery.

The localisation of IGF1 on the plasma membrane of subcutaneous adipocytes may be due to receptor-mediated uptake of this ligand. In order to assess if the high affinity receptor for IGF1, IGF1R, was present on adipocytes and could be signalling for formation of fat tissue, I sought to detect IGF1R by immunohistochemistry. IGF1R is composed of two extracellular α-subunits (IGF1Rα) and two transmembrane β-subunits (IGF1Rβ) held together by disulfide bonds (Fig 3.5B) [257]. The α- and β-subunits of IGF1R are encoded by a single gene transcript which gives rise to a preprotein that is processed to generate the transmembrane receptor by proteolysis and formation of inter-subunit disulfide bonds [258]. The receptor is activated upon binding of IGF1 to IGF1Rα, inducing a conformational change and autophosphorylation of key tyrosine residues in IGF1Rβ, leading to transduction of intracellular signalling kinase cascades [259].

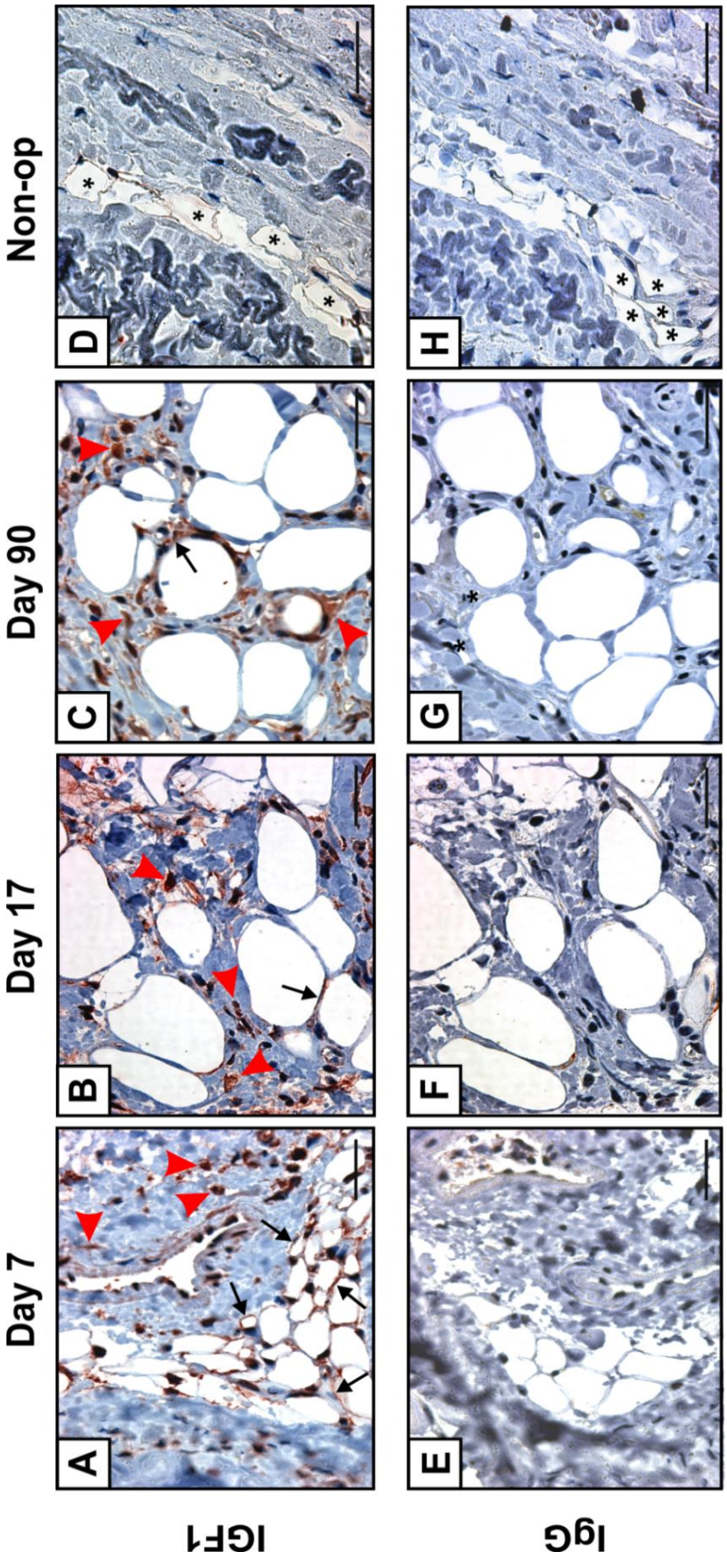

Figure 3.7 Representative images of immunostaining for IGF1 in mouse tails. (A-D) Localisation of IGF1 on the plasma membrane of subcutaneous adipocytes (arrows) in the lymphoedema model at days 7, 17 and 90 post-surgery, and in non-operated control (Non-op). Examples of IGF1 localised nearby adipocytes are indicated by red arrowheads. (E-H) Concentration-matched IgG negative controls. Adipocytes in Non-op are smaller than in the lymphoedema model and are indicated by asterisks. Scale bar = 30 µm.

A previous study claimed to have detected IGF1Rα in chondrocytes of mouse hindlimb using commercially available polyclonal antibodies (sc-712 from Santa Cruz) [260]. Therefore, I employed a similar immunohistochemical protocol to that used in this study, to test the sc-712 polyclonal antibodies for their capacity to detect IGF1Rα in tails the mouse lymphoedema model at days 7, 17 and 90 post-surgery and in non-operated controls. This involved a combination of the sc-712 polyclonal antibodies with heat-induced antigen retrieval in sodium citrate buffer and TSA (see Chapter 2, Section 2.6 for further details).

Staining for IGF1Rα was detected on parts of the plasma membrane of subcutaneous adipocytes at days 7, 17 and 90 post-surgery, as well as in non-operated control tails (Figure 3.8), whereas immunostaining with concentration-matched IgG negative control antibodies resulted in no signals. The intensity of signals for IGF1Rα was similar for all of these samples, suggesting similar levels of IGF1Rα expression on adipocytes throughout lymphoedema development and in non-operated tails.

The presence of IGF1 and IGF1R on the surface of adipocytes in the mouse lymphoedema model is consistent with the hypothesis that IGF1 is associated with these cells due to receptor-mediated uptake of this ligand. The data also indicate that IGF1 levels associated with adipocytes are up-regulated in the mouse lymphoedema model in comparison to non-operated tails, in contrast to IGF1R which is present on adipocytes in both lymphoedematous and non-operated mouse tails.

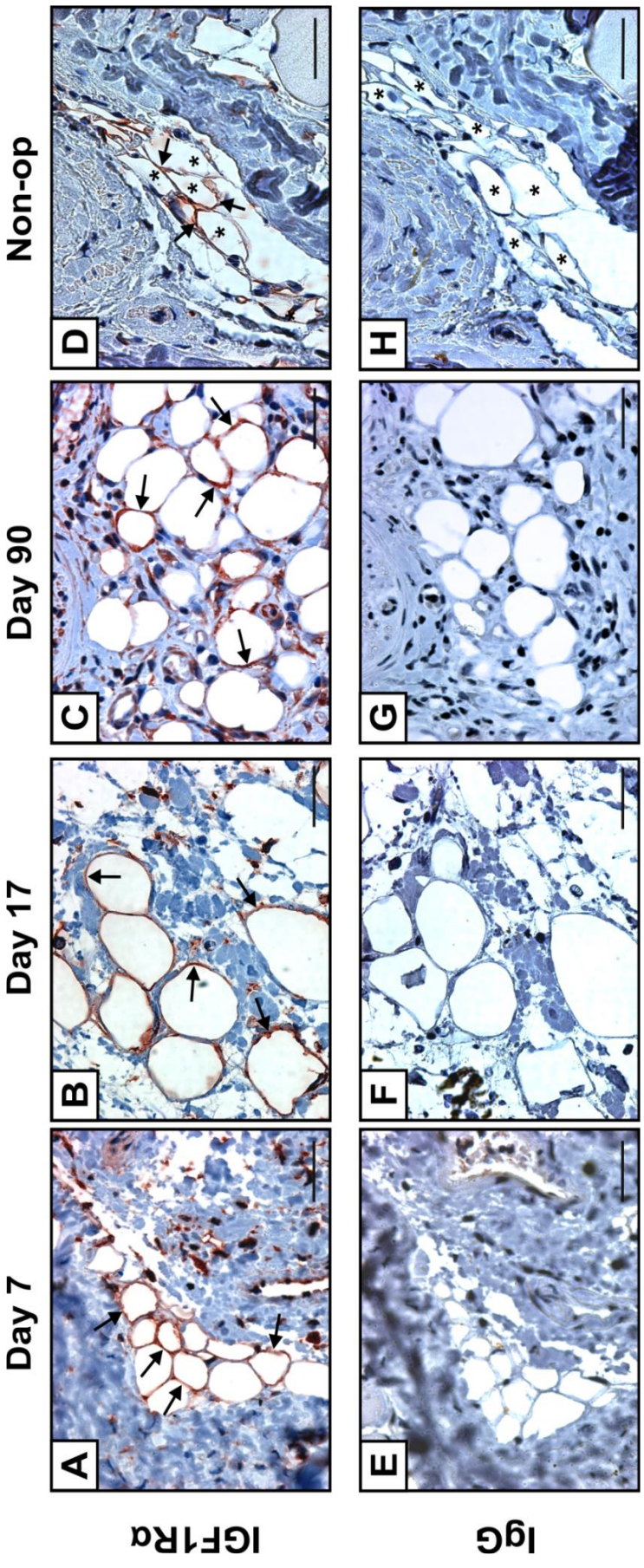

Figure 3.8 Representative images of immunostaining for IGF1R in mouse tails. (A-D) Localisation of the α-subunit of IGF1R (IGF1Rα) on the plasma membrane of subcutaneous adipocytes (arrows) in the lymphoedema model at days 7, 17 and 90 post-surgery, and in non-operated control (Non-op). (E-H) Concentration-matched IgG negative controls. Adipocytes in Non-op are smaller than in the lymphoedema model and are indicated by asterisks. Scale bar = 30 μm.

3.3.2.3 Immunohistochemical detection of phosphorylated IGF1R in the mouse model of lymphoedema

The presence of both IGF1 and IGF1R on adipocytes in the mouse model of lymphoedema is consistent with the hypothesis that the IGF1R signalling pathway could be operative to promote formation of fat tissue in the model. In order to examine whether IGF1R is activated in the model, I sought to detect phosphorylated IGF1R (p-IGF1R) by immunohistochemistry. Upon IGF1 binding, phosphorylation at three tyrosine (Tyr) residues on the activation loop of IGF1Rβ (Tyr-1161, Tyr-1165 and Tyr-1166) occurs and is essential for driving downstream signalling cascades [261, 262]. A previous study claimed to have detected p-IGF1R in lung metastases, arising from the C3 (1)-Tag;*Mmp9*$^{+/+}$ mouse model of mammary carcinoma, by immunohistochemistry using commercially available polyclonal antibodies against Tyr-1161-p-IGF1R (ab39398 from Abcam) [263]. However, no negative controls were presented for this immunostaining so the results were not convincing. Given I was not able to access tissue sections from the C3 (1)-Tag;*Mmp9*$^{+/+}$ model as a potential positive control tissue for p-IGF1R immunostaining, I tested the ab39398 antibodies on sagittal tissue sections from E14.5 and E18.5 mouse embryos as well as on the mouse lymphoedema model. The mouse embryonic tissue sections could be considered as a potential positive control because these sections encompass growing tissues from many developing mouse organs and IGF1R signalling is important in growth and development of mouse embryos [264, 265]. I also tested a second commercially available polyclonal p-IGF1R antibody against Tyr-1161-p-IGF1R (sc-101703 from Santa Cruz) although there were no reports showing that this reagent could detect p-IGF1R in mouse tissues by immunohistochemistry. The testing of these antibodies on the embryo sections, and on the mouse lymphoedema model, was performed using the same range of protocols employed in attempts to detect IGFBP5 (Figure 3.6). However, none of these protocols gave rise to specific signals for p-IGF1R, in comparison to concentration-matched IgG negative control antibodies, in tissue sections from either the mouse embryos or the mouse lymphoedema tail model at days 7, 17 and 90 post-surgery, or in non-operated control tails (data not shown). These results indicate

that I could not develop a protocol for detecting p-IGF1R by immunohistochemistry in mouse tissues using either the ab39398 or sc101703 polyclonal antibodies.

In summary, I showed the presence of both IGF1 and IGF1R on adipocytes in the mouse lymphoedema model by immunohistochemistry, indicating that IGF1R signalling could be operative to promote formation of fat tissue in the lymphoedema model. However, a protocol for detecting p-IGF1R in mouse tissues by immunohistochemistry could not be developed, so it was not possible to confirm if IGF1R was activated on adipocytes in the lymphoedema model by this methodology.

3.3.3 Analysis of IGF system in human lymphoedema

Given the potential role of IGF1R signalling in promoting formation of fat tissue in the mouse lymphoedema model, it was imperative to conduct immunohistochemical analyses on clinical lymphoedema samples with a view to gaining insight into whether or not key protein components of the IGF system (i.e. IGF1 and IGF1R) could be important in driving formation of fat tissue in human lymphoedema. Typically, clinical samples of lymphoedema are difficult to obtain because surgeons are generally unwilling to disrupt lymphoedematous tissue for the purpose of tissue sampling. For this study, a clinical sample of secondary lymphoedema was provided by Mr. David Speakman, a surgeon at Peter MacCallum Cancer Centre. The lymphoedematous tissue used here was obtained from the lower left leg of a 47-year-old female patient and encompassed skin and subcutaneous fat tissue. The tissue was obtained from the lower leg after an above-knee amputation due to angiosarcoma in the left leg that developed post-mastectomy. The lymphoedema in the lower left leg developed after the mastectomy but prior to emergence of the angiosarcoma, and had been pronounced for at least two years before the amputation. There was extensive subcutaneous fat tissue in the lymphoedema tissue sample which was consistent with the occurrence of pronounced adipogenesis. The diagnosis of lymphoedema by a clinical pathologist was based on microscopic analysis of tissue obtained by excision biopsy.

3.3.3.1 Immunohistochemical detection of IGF1, IGF1R and p-IGF1R in human lymphoedema

In order to assess IGF1R signalling in human lymphoedema, I analysed IGF1 and IGF1R in the clinical lymphoedema sample by immunohistochemistry. Previous studies claimed to have detected IGF1 in human breast cancer and colorectal cancer using commercially available polyclonal anti-IGF1 antibodies (ab9572 from Abcam) [266, 267]. Therefore, I tested the ab9572 antibodies using a similar immunostaining protocol to that employed in these studies, involving heat-induced antigen retrieval in sodium citrate buffer and TSA (see Chapter 2, Section 2.6 for further details). The human lymphoedematous tissue exhibited uniform staining for IGF1 on the plasma membrane of subcutaneous adipocytes, whereas immunostaining with concentration-matched IgG negative control antibodies gave no staining (Figure 3.9 A-C). These results indicate that IGF1 can be present on the surface of adipocytes in human lymphoedema, possibly due to uptake of this ligand by IGF1R.

I next sought to detect IGF1R to assess whether or not this receptor was also present on adipocytes. A previous study claimed to have detected IGF1Rα in human classical Hodgkin lymphoma using commercially available polyclonal anti-IGF1Rα antibodies (sc-712 from Santa Cruz) [268]. Since I detected IGF1Rα in mouse tissues using the sc-712 antibodies with heat-induced antigen retrieval in sodium citrate with TSA (see Chapter 2, Section 2.6 for further adipocytes in human lymphoedema. The presence of IGF1 and IGF1R on adipocytes is consistent with the hypothesis that IGF1 is associated with these cells due to receptor-mediated uptake of this ligand, which leads to signalling via IGF1R.

Given the localisation of IGF1 and IGF1R on adipocytes in the human lymphoedema sample, I next sought to detect p-IGF1R by immunohistochemistry with a view to assessing whether or not IGF1R was activated and might thereby drive formation of fat tissue in clinical lymphoedema. Previous studies claimed to have detected p-IGF1R in human triple-negative breast cancer and human hepatocellular carcinoma using commercially available anti-p-IGF1R

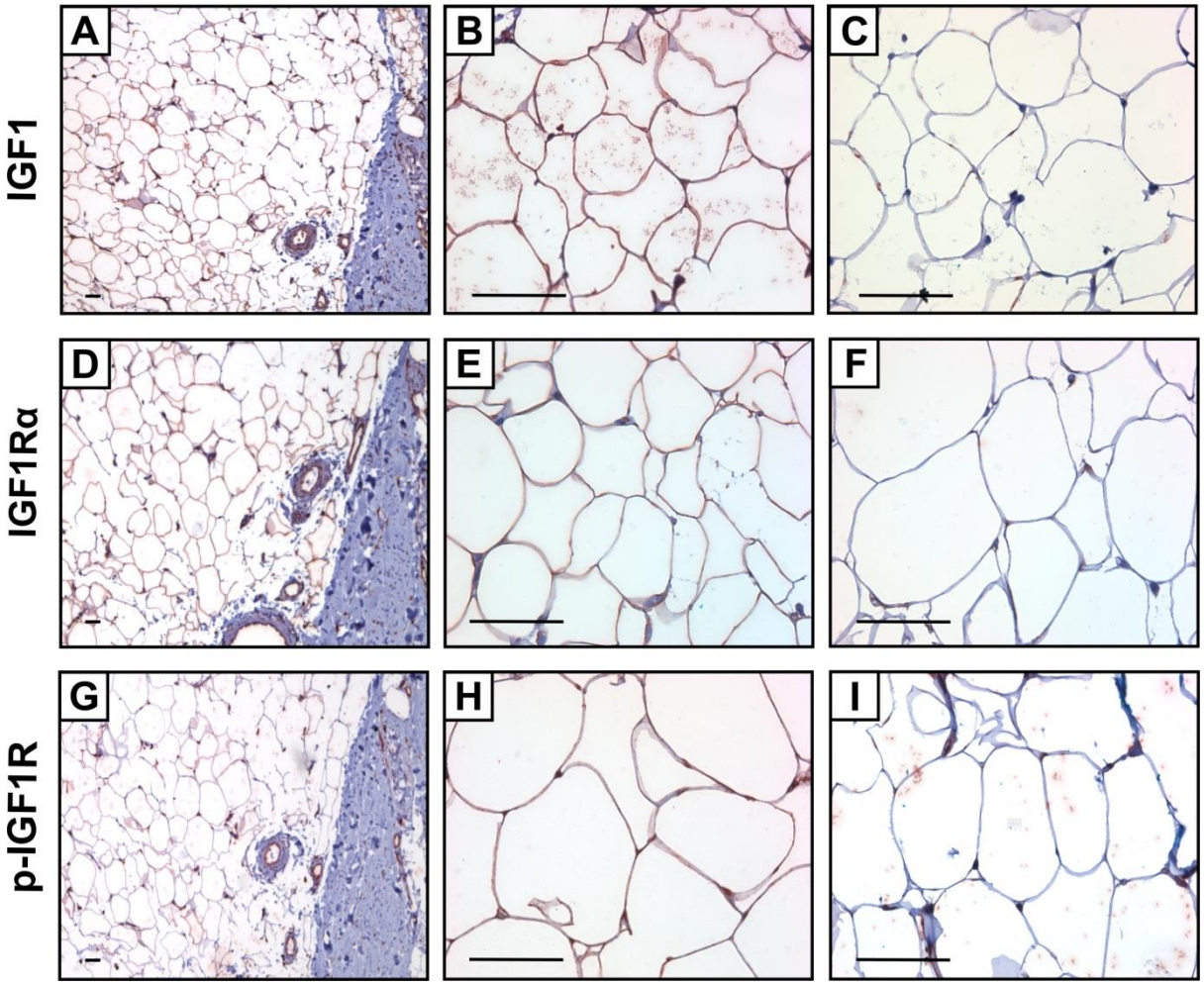

Figure 3.9 Representative images of immunostaining for IGF1, IGF1R and p-IGF1R in clinical sample of lymphoedema. (A, D and G) Localisation of IGF1, IGF1Rα and p-IGF1R in subcutaneous adipose tissue of a sample of human lymphoedema, respectively. (B, E and H) Higher-power images of A, D and G, respectively. (C, F and I) Concentration-matched IgG negative controls for B, E and H, respectively. Scale bar = 50 μm

polyclonal antibodies (ab39398 from Abcam) [269, 270]. However, no negative controls were included in the immunostaining analyses so the results were not conclusive. I tested the ab39398 antibodies in the human lymphoedema sample using a similar immunostaining protocol to that employed by Litzenburger *et al*. [270], which involved heat-induced antigen retrieval in sodium citrate buffer and TSA (see Chapter 2, Section 2.6 for further details). The human lymphoedematous tissue exhibited uniform staining for p-IGF1R on the plasma membrane of subcutaneous adipocytes, whereas no staining for p-IGF1R was detected in concentration-matched IgG negative controls (Figure 3.9 G-I). In summary, these findings demonstrated that both IGF1 and IGF1R are localised on subcutaneous adipocytes in the clinical lymphoedema sample, and importantly, that IGF1R signalling is activated in these cells which may promote formation of subcutaneous fat tissue in lymphoedema.

3.4 Discussion

The novel mouse model of secondary lymphoedema explored in this chapter demonstrated a rapid onset of tail swelling, and the swelling was profound and persistent over 3 months. Importantly, I showed that the tail swelling was correlated with an increase in fat tissue in the dermis and subcutaneous layer. To my knowledge, this is the first example of a mouse lymphoedema model which was assessed with a specific focus on formation of fat tissue across three time-points representing different chronological stages of secondary lymphoedema. The significantly increased area covered by adipocytes in the model was caused by both the increased number and size of adipocytes, and was a major contributor to tail swelling, which correlated well with the published clinical data. Importantly, the increased levels of fat tissue demonstrated in this model allowed analysis of genes and molecular signalling pathways that drive formation of fat in secondary lymphoedema, and led to identification of the IGF signalling pathway as potentially driving development of fat tissue in the mouse model of lymphoedema.

Quantification of fat in the mouse model of lymphoedema was performed following morphological identification of adipocytes in H&E stained paraffin-embedded tail sections. Adipocytes have a distinct morphology characterised by an unilocular lipid droplet, thin circular cytoplasm and pericentral nucleus. These morphological features of adipocytes allow for their unequivocal identification in H&E stained sections. Other common approaches to identify adipocytes include oil red O staining that detects lipid, which is often used in parallel with H&E staining [271]. However, oil red O staining can only be performed on frozen tissue sections, and it was not possible to generate frozen sections in the study described here as the central bone in the mouse tail needed to be processed by decalcification to allow sectioning, which cannot be performed on frozen tissues. An alternative approach to identify adipocytes is to conduct immunostaining for perilipin, a major phosphoprotein abundantly present on the surface layer of intracellular lipid droplets in adipocytes [272], which could be useful for future studies of the mouse lymphoedema model.

The IGF1R signalling pathway has been implicated in regulation of various biological processes, including adipogenesis [273]. The microarray and qRT-PCR analyses reported here demonstrated decreased levels of *Igfbp5* mRNA in the mouse tail lymphoedema model in comparison to the non-operated control. It is known that IGFBP5 can bind IGF1 and thereby prevent this ligand from activating IGF1R [249], a receptor which can signal for adipogenesis [274]. Also, it has been shown that *Igfbp5*-deficient mice have significantly increased body adiposity compared with wild-type mice when they are on a high-fat diet [275]. Therefore, the down-regulation of IGFBP5 in the mouse model of lymphoedema could lead to enhanced formation of fat tissue driven by signalling downstream of activated IGF1R. However, mechanisms by which IGFBP5 regulates IGF1R signalling are rather complex. Although IGFBP5 can bind to IGF1 and thereby inhibit its activity, IGFBP5 may also potentiate the effects of IGF1 through interaction with extracellular matrix (ECM). IGFBP5 has been shown to interact with various ECM components, such as type IV collagen [276], thrombospondin1 (TSP1) and

osteopontin (OPN) [277]. A study demonstrated that when IGFBP5 is bound to ECM or type IV collagen, it exhibits a lower affinity for IGF1 compared to IGFBP5 in solution [276]. Notably, ECM- or type IV collagen-bound IGFBP5 enhanced IGF1-mediated growth on human fibroblasts [276], possibly by allowing an increased amount of IGF1 to be released to IGF1R. Further, TSP1- or OPN-bound IGFBP5 was shown to augment smooth muscle cell responsiveness to IGF1 by interacting with αVβ3 integrin expressed on the cell surface [277], which leads to activation of integrin receptor signalling pathways involved in smooth muscle cell migration and proliferation [278]. These findings suggest that IGFB5 exhibits complex mechanisms regulating IGF1 activities, and further studies are necessary to elucidate the precise roles of IGFBP5 in regulating the IGF1R signalling pathway.

I investigated by immunohistochemistry whether or not key protein components of the IGF system were present in the mouse lymphoedema model, as well as in a clinical sample of lymphoedema, to assess if the IGF system could play a role in promoting formation of fat tissue. The study focused on adipocytes, which are readily identifiable in mouse tissues based on their morphology, as opposed to preadipocytes which cannot be unambiguously identified in mouse tissues. The results presented here demonstrated the presence of IGF1 and IGF1R on the plasma membrane of adipocytes in tails from the mouse lymphoedema model. It is possible that IGF1 was detected on these cells due to receptor-mediated uptake of this ligand, which would be consistent with activation of IGF1R. However, I was unable to develop a successful protocol for detecting p-IGF1R (the activated form of this receptor) by immunohistochemistry in mouse tissues, so I could not assess if this receptor was activated on adipocytes in the lymphoedema model.

Importantly however, both IGF1 and IGF1R were detected on the plasma membrane of adipocytes in the clinical sample of lymphoedema, and p-IGF1R was also localised on the surface of these cells, indicating that the receptor was activated. Taken together, these findings indicate that IGF1R can be activated on adipocytes in lymphoedema by IGF1 and may thereby drive

development of fat tissue. This could occur due to the known capacity of IGF1R signalling to promote accumulation of fat in adipocytes [246, 247], which occurs in the mouse lymphoedema model given that adipocytes are larger in the model than in the non-operated control. In addition, IGF1R signalling may also promote proliferation of preadipocytes and adipogenesis in lymphoedema, given its capacity to drive these biological events [237, 243, 245, 279]. These latter possibilities assume that IGF1R was expressed on preadipocytes in the lymphoedema model; however, these cells were not studied directly here because of the lack of specific markers for detecting them in mouse tissues.

The immunohistochemical analysis suggested that there is more IGF1 associated with the plasma membrane of adipocytes at day 7 post-surgery in the lymphoedema model than at days 17 and 90 post-surgery or in non-operated tails. It is notable that there is a profound increase in the number of adipocytes in the model during the first week post-surgery, whereas the increases between days 7 and 17 post-surgery, and between days 17 and 90 post-surgery, are more modest (see Figure 3.3E). Therefore, the higher levels of IGF1 associated with adipocytes at day 7 post-surgery correlate with the more profound adipogenesis occurring at this stage. This is consistent with the hypothesis that the levels of IGF1 associated with adipocytes are increased by enhanced receptor-mediated uptake of this ligand due to down-regulation of IGFBP5 in secondary lymphoedema.

Although the protein levels for IGF1 appears to be up-regulated in the mouse lymphoedema model as assessed by immunohistochemistry, the mRNA for IGF1 was not identified as up-regulated by the microarray analysis (data not shown). This discrepancy could be because IGF1 was synthesised elsewhere in the lymphoedematous tissue, or IGF1 levels are up-regulated as a result of enhanced translation or protein stability in the mouse lymphoedema model.

The presence of IGF1 and IGF1R, and importantly p-IGF1R, on adipocytes in the clinical lymphoedematous tissue by immunohistochemistry provides evidence for potential molecular

mechanisms associated with formation of fat tissue. Limitations in the immunohistochemical analysis of clinical lymphoedema are that only a single human lymphoedema sample was analysed, and negative control tissues (i.e. normal fat tissue from non-lymphoedematous tissue in the lymphoedema patient) were not included in the analysis due to limited access to such clinical samples. The capacity to further expand the immunohistochemical study of clinical lymphoedema will likely always be hampered by the difficulty in accessing clinical samples of secondary lymphoedema.

In summary, the mouse lymphoedema model employed in this study exhibited chronic tissue swelling associated with formation of fat tissue as in the clinical setting. The immunohistochemical analyses of the IGF signalling system in the mouse lymphoedema model and in human lymphoedema provide evidence that increased formation of fat tissue in lymphoedema could be due to IGF1R signalling. These data hence justify targeting the IGF1R signalling pathway in the mouse model of lymphoedema through pharmacological approaches, and monitoring effects on the development of fat tissue and tissue swelling.

Chapter 4

Pharmacologically Targeting the Formation of Fat Tissue in the Mouse Model of Secondary Lymphoedema

4.1 Introduction

In the previous chapter, I showed that the IGF1R signalling pathway could potentially play an important role in promoting development of fat tissue in the dermis and subcutaneous layer in secondary lymphoedema. This finding warrants further examination with a view to assessing whether or not pharmacologically targeting this signalling pathway could restrict formation of fat tissue, and thereby reduce tissue swelling, in the mouse model of secondary lymphoedema. Ideally this would be done with a drug that has been shown to be well tolerated in humans to facilitate clinical trials. In this chapter, I will test this using a small molecule inhibitor of the enzymatic activity of IGF1R, known as linsitinib.

4.2 Rationale for using linsitinib in vivo

Increased expression of IGF1R and/or its ligands has been shown to be strongly correlated with faster disease progression and poor prognosis in various cancers, including breast cancer [280]. Currently a number of agents targeting this pathway are under clinical development for cancer which can be classified into three classes: 1) monoclonal antibodies (mAbs) against IGF1R ligands (i.e. IGF1 and IGF2), 2) mAbs against IGF1R, and 3) small molecule tyrosine kinase inhibitors of IGF1R. This section will cover our current knowledge of therapeutics targeting the IGF1R signalling axis, and discuss the rationale for selecting linsitinib as a means to inhibit this pathway *in vivo*.

4.2.1 IGF1/IGF2 neutralising mAbs

There are two IGF1/IGF2 co-neutralising mAbs which have been developed for the treatment of cancer, namely dusigitumab [281, 282] and xentuzumab [283]. Dusigitumab binds human IGF2 with a higher affinity than IGF1 [284], whereas xentuzumab exhibits a higher affinity for IGF1 [283]. Preclinical studies using these antibodies have shown promising anti-

proliferative activity against cancer cells *in vitro* and/or solid tumours *in vivo* [283-285]. However, the toxicity of these antibodies in humans has not yet been determined, and they are currently in early-phase clinical trials to assess tolerability.

4.2.2 IGF1R neutralising mAbs

Neutralising mAbs to human IGF1R have been developed to block ligand-receptor interactions, and to induce internalisation and subsequent degradation of IGF1R [286]. Currently at least seven anti-IGF1R mAbs are in clinical trials for cancer, for example, ganitumab [287], istiratumab [288], figitumumab [289], cixutumumab [290], dalotuzumab [291], robatumumab [292] and R-1507 [293]. However, some of these antibodies (e.g. dalotuzumab) do not bind to mouse IGF1R so they are not useful for targeting this receptor in mouse models of disease. Further, these proprietary antibodies are difficult to access from the pharmaceutical companies which are conducting the clinical programs.

4.2.3 Small molecule tyrosine kinase inhibitors of IGF1R

An alternative approach for targeting IGF1R signalling is to use small molecule tyrosine kinase inhibitors that specifically bind to the catalytic domain of the receptor, block autophosphorylation/activation of the receptor and thereby prevent downstream signalling. Several tyrosine kinase inhibitors of IGF1R, such as linsitinib (also known as OSI-906) and BMS-754807, have been developed and entered clinical trials for cancer [294]. Linsitinib is a well-characterised ATP-competitive imidazoparazine-based small molecule inhibitor (Figure 4.1A) which is highly specific for mouse and human IGF1R and has a half maximal inhibitory concentration (IC_{50}) against human IGF1R of 35 nM [295]. Notably, linsitinib exhibits minimal inhibitory effects across a broad range of other protein kinases, although it does exhibit inhibitory activity against the IR (IC_{50} against human IR of 75 nM) [295]. In contrast, BMS-754807 has equipotent activity against human IGF1R and IR (IC_{50} of 1.8 and 1.7 nM, respectively), and exhibits inhibitory effects against other tyrosine kinases such as c-Met, TrkA and TrkB (IC_{50} of 6, 7, and 4 nM, respectively) [296]. Importantly, linsitinib has been used extensively in clinical

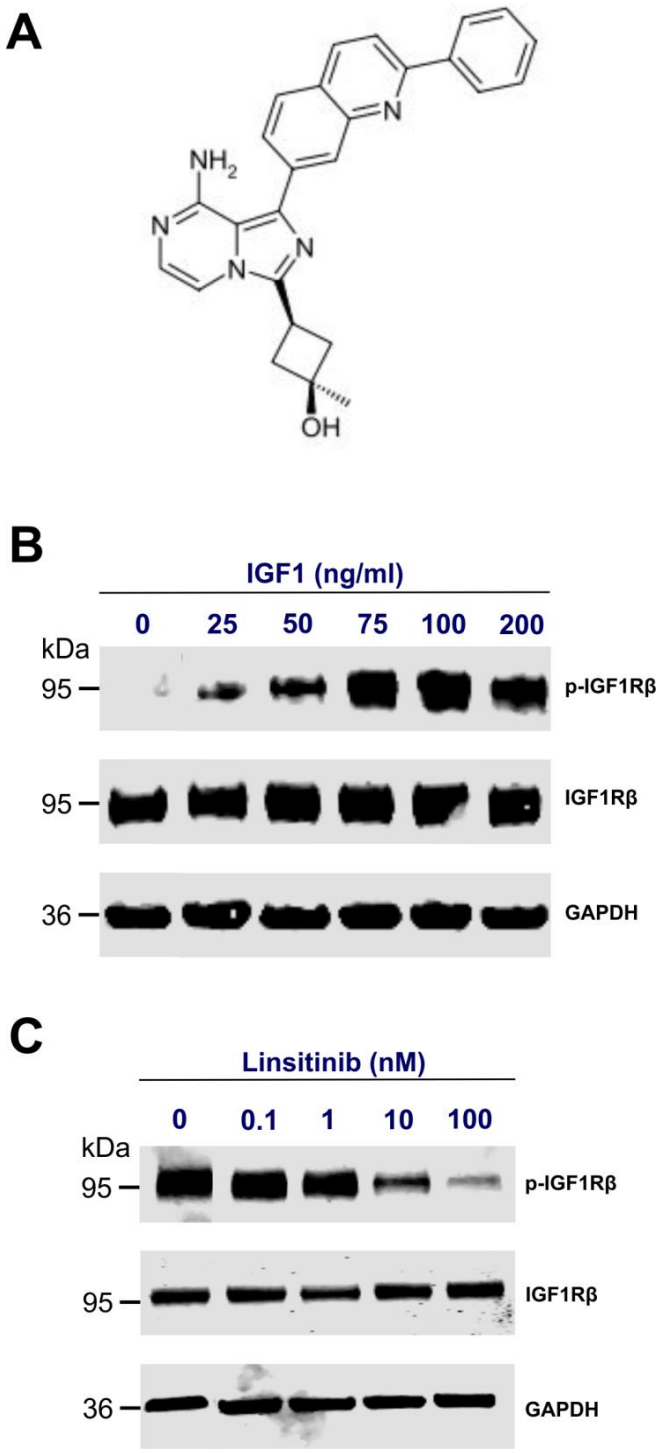

Figure 4.1 Activity of linsitinib *in vitro*. (A) Chemical structure of linsitinib. (B) p-IGF1Rβ (top) and IGF1Rβ (middle) in 3T3-L1 cells following 30 min treatment with IGF1 at the indicated concentrations. (C) Inhibitory effect of linsitinib on IGF1Rβ phosphorylation at the indicated concentrations. Treatment of cells with linsitinib began 1 hour before addition of 100 ng/ml of IGF1. GAPDH was used as loading control.

trials for cancer, e.g. this drug was used to treat 139 patients with adrenocortical cancer in a phase III clinical trial [297]. This trial involved long-term treatment of patients with linsitinib for up to 24 months. Although the drug was not efficacious for treating cancer in this trial, it was shown to be very well tolerated with no adverse events being deemed to be due to linsitinib treatment. Hence, linsitinib may be safe for long-term treatment of patients with secondary lymphoedema.

I chose to use linsitinib for targeting the IGF1R signalling axis in the mouse model of secondary lymphoedema because this drug exhibits high specificity for mouse IGF1R [298], it has been extensively tested in mouse models of disease [298, 299], it is very well tolerated in humans for long periods of time [297] and it is commercially available so it can be accessed for experimental purposes.

4.3 Assessment of linsitinib activity in vitro

The linsitinib used in this study was obtained from Ark Pharm (Arlington Heights, IL, USA) which reported that this compound was greater than 98% pure. The identify and purity of this linsitinib was independently verified by liquid chromatography mass spectrometry in collaboration with Dr. Mark Devlin (Peter MacCallum Cancer Centre, Melbourne) and the Monash Institute of Pharmaceutical Sciences, Melbourne. To confirm the capacity of linsitinib to inhibit IGF1R signalling *in vitro*, I employed the mouse 3T3-L1 fibroblast cell line which has been reported to express IGF1R [300]. Western blotting using an antibody to IGF1Rβ (the catalytic domain of the receptor) demonstrated the presence of a band at 95 kDa which is the expected size for this protein (Figure 4.1B, middle blot). Treatment of these cells with IGF1 for 30 min led to increased levels of phospho-IGF1Rβ (p-IGF1Rβ) in a concentration-dependent manner, as monitored by Western blotting using a monoclonal antibody which detects IGF1Rβ phosphorylated at tyrosine residue 1161 (Figure 4.1B, top blot). Linsitinib, dissolved in 25 mM tartaric acid (a delivery vehicle commonly used for oral administration to mice [295, 301, 302]), was used to treat these cells for testing the inhibitory activity of the drug. Treatment with linsitinib for 1 hour prior to addition of 100 ng/ml of IGF1 led to a dose-dependent decrease in the levels

of IGF1-induced p-IGF1Rβ (Figure 4.1C, top blot). These results are broadly consistent with the reported IC_{50} of 35 nM for the inhibition of phosphorylation of human IGF1Rβ by linsitinib [295].

4.4 Pharmacological testing of linsitinib in the mouse model of secondary lymphoedema

4.4.1 Determination of maximum tolerated dose of linsitinib for use in vivo

Having demonstrated the capacity of linsitinib to inhibit IGF1Rβ phosphorylation *in vitro*, I next sought to identify the maximum tolerated dose of this drug for the female C57BL/6 mice which I use for the mouse model of secondary lymphoedema. This was determined by monitoring loss of body weight over 14 days in response to different doses of linsitinib, with body weight loss of greater than 20% being defined as intolerable. A previous study reported that administration of 50 mg/kg/day of linsitinib to male C57BL/6 mice by oral gavage led to major loss of body weight and a reduction in survival of mice, whereas 40 mg/kg/day was well tolerated [298]. Therefore, C57BL/6 female mice from the animal facility of the Peter MacCallum Cancer Centre were treated with 10, 25, 40 and 50 mg/kg/day of linsitinib by oral gavage. After 3 days, mice treated with 50 mg/kg/day of linsitinib showed signs of ill-health, such as hunching, lack of movement and loss of appetite. Further these mice exhibited a mean loss of body weight of 30% at this time, so this study group was sacrificed. In contrast, while mice treated with the other doses of linsitinib showed statistically significant decreases in body weight compared to the vehicle control, they did not show any signs of illness, nor did they lose more than 10% of body weight at any time over the 14-day monitoring period (Figure 4.2). Thus the results of this analysis of female C57BL/6 mice are similar to those previously reported for male C57BL/6 mice, in that 40 mg/kg/day of linsitinib was well tolerated whereas 50 mg/kg/day was not [298]. Given 40 mg/kg/day was the highest dose that was well tolerated in the female mice, and that this dose previously has been shown to block phosphorylation of IGF1Rβ *in vivo* (as assessed by analysis of this receptor in the liver) [298], this dose was chosen for use in the mouse model of secondary lymphoedema.

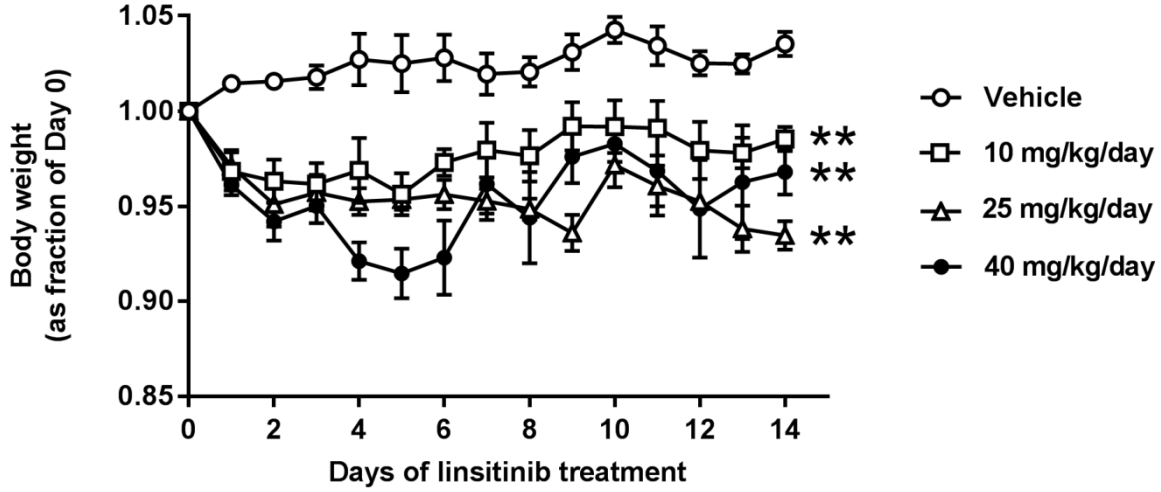

Figure 4.2 Body weight of mice in response to treatment with linsitinib. Analysis of body weight of mice treated with linsitinib (10, 25 or 40 mg/kg/day via oral gavage). Data show mean ± SEM, n=5 for each group, ** denotes $p<0.01$ for comparison with vehicle control at day 14 (One-way ANOVA with Turkey's *post-hoc* multiple comparison test).

4.4.2 Effect of linsitinib on tail swelling in the mouse model of secondary lymphoedema

To study the effect of linsitinib on the development of tail swelling in the mouse model of secondary lymphoedema, female C57BL/6 mice were subjected to the surgery to induce lymphoedema, and administered 40 mg/kg/day of linsitinib by oral gavage from the day of surgery until a pre-defined time-point of 17 days post-surgery (Figure 4.3A). This time-point was chosen because the rapid early increase in tail volume in this mouse model is largely complete by day 17 post-surgery (see Figure 3.2A). Mice were sacrificed, and tails harvested, at this time-point. The vehicle and linsitinib study groups each consisted of 6 mice, and the experiment was conducted twice to monitor reproducibility.

None of the mice in the two experiments exhibited any signs of distress or ill-health, such as hunching, ruffled fur, reduced movement or weight loss of greater than 10%. Importantly, the two experiments demonstrated statistically significant decreases in tail volume in the linsitinib groups compared to the vehicle controls at day 17 post-surgery. The reductions in tail volume in the linsitinib groups for Experiments 1 and 2 were approximately 25% and 35%, respectively, compared to the vehicle controls at day 17 post-surgery (Figure 4.3 B&C, see also Figure 4.3F). These results also show that the degree of swelling of the tails in response to the surgery was reduced by 44% and 58% by linsitinib in Experiments 1 and 2, respectively - this was calculated from the data in Figure 4.3 B&C, based on comparison to the tail volume at day 0. Overall these results demonstrate a consistent effect of linsitinib in restricting tail swelling. The body weight of linsitinib-treated mice at day 17 post-surgery decreased in the two experiments (Figure 4.3 D&E), with a statistically significant reduction of approximately 8% in Experiment 1 and a reduction of 4% in Experiment 2 which was not statistically significant. This finding is consistent with a previous report showing that linsitinib can reduce body weight [298] and another showing that genetically targeting IGF1R can reduce fat levels in mice [303]. In summary, linsitinib significantly restricted the development of tail swelling in this mouse model of secondary lymphoedema, and the relevance of fat tissue to this reduced tail swelling will be explored in the next section.

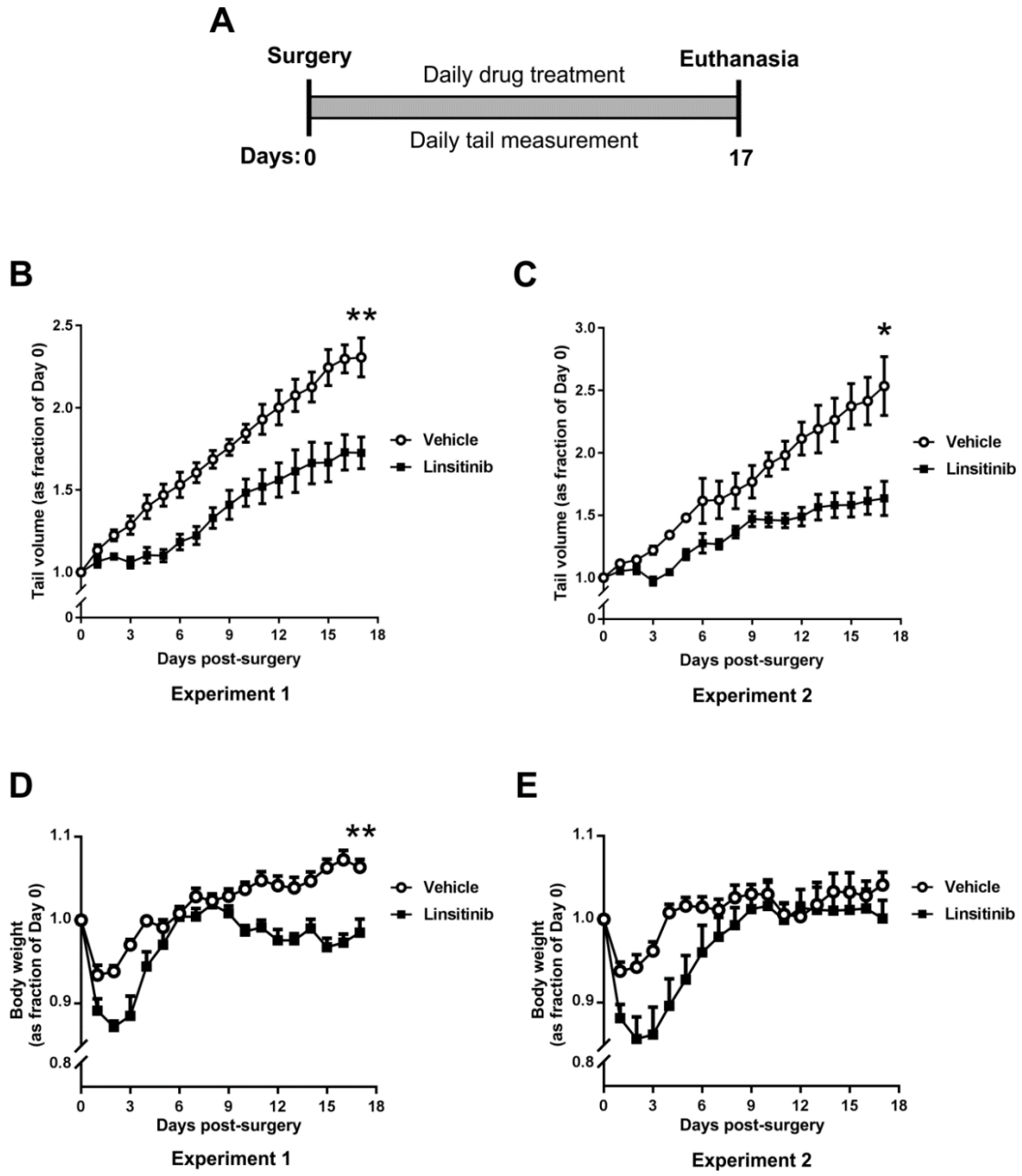

Figure 4.3 Effect of linsitinib on tail swelling in the mouse model of secondary lymphoedema. (A) Schematic representation of study design: female C57BL/6 mice were operated on to induce lymphoedema, and linsitinib was administered (40 mg/kg/day by oral gavage) for 17 days post-surgery. Mice were euthanised and tails were harvested at day 17 post-surgery. The first treatment with linsitinib was conducted 4 hours after surgery. (B)-(E) Two independent experiments showing the effect of linsitinib on mouse tail volume (B&C) and body weight (D&E). For each experiment, data show mean ± SEM, n=6, * denotes $p<0.05$ and ** denotes $p<0.01$ for comparison with vehicle control at day 17 post-surgery (Student's t-test). (F) Representative macroscopic images of changes in mouse tail volume over the 17-day monitoring period. Scale bar = 10 mm.

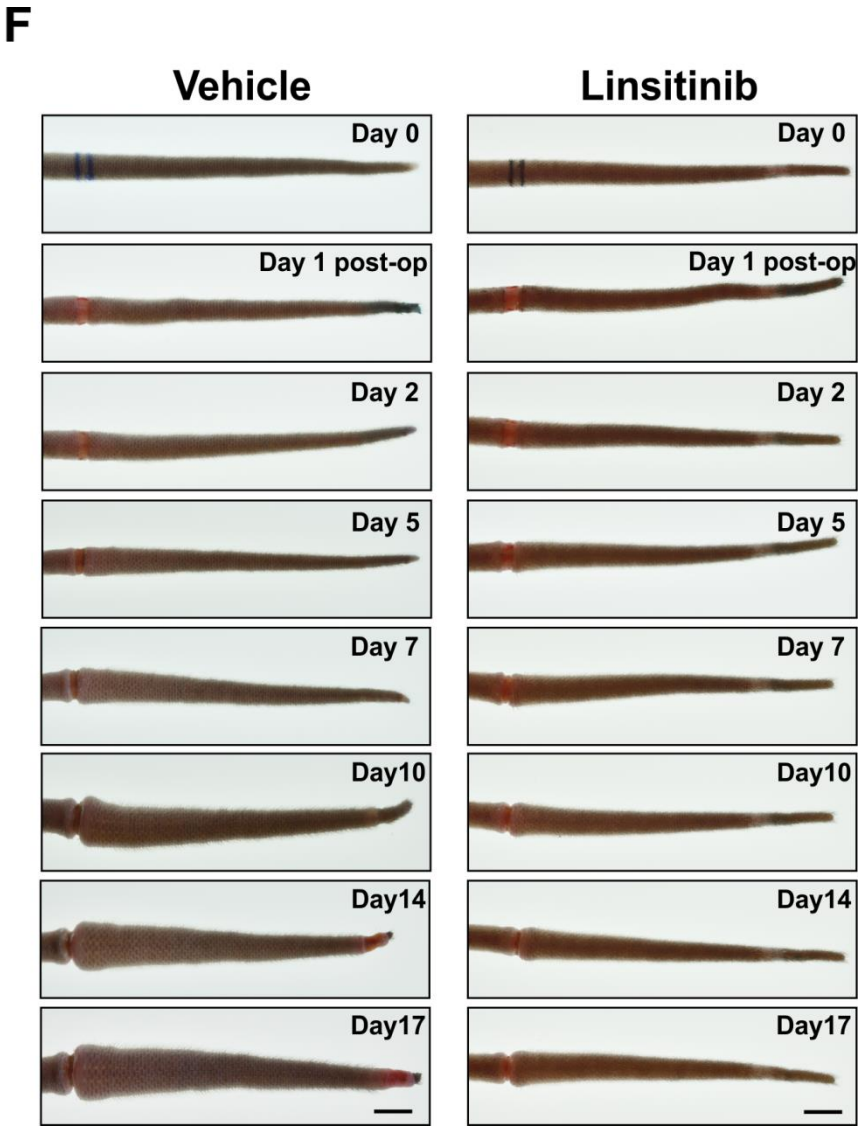
F
Vehicle
Linsitinib
Day 0
Day 0
Day 1 post-op
Day 1 post-op
Day 2
Day 2
Day 5
Day 5
Day 7
Day 7
Day10
Day10
Day14
Day14
Day17
Day17

4.4.3 Effect of linsitinib on fat tissue in the mouse model of secondary lymphoedema

Having confirmed the capacity of linsitinib to significantly restrict tail swelling in the mouse model of lymphoedema, I next sought to investigate the effects of linsitinib on pathological features of this condition. Initial observation of tissue cross-sections indicated that oedema was evident in both the vehicle and linsitinib study groups but there was less pronounced epidermal hyperkeratosis in the linsitinib group (Figure 4.4A). Quantification of the cross-sectional area of tails revealed that the linsitinib group from each of the two experiments exhibited a statistically significant decrease of approximately 21% and 24% compared to the vehicle control at day 17 post-surgery (Experiment 1 and 2, respectively, Figure 4.4B). Importantly, the thickness of the subcutaneous layer was lower in the linsitinib group compared to the vehicle control (Figure 4.4C). The thickness of the dermis was also lower in the linsitinib groups compared to the vehicle controls, although a statistically significant difference was only observed in Experiment 1 (Figure 4.4D). Lastly, there was no difference in the area of bone and muscle between the two study groups (Figure 4.4E).

I hypothesised that there would be less fat in the linsitinib-treated group, given the known role of IGF1R signalling in adipogenesis, so I quantitated various parameters of adipocytes in the dermis and subcutaneous layer in the linsitinib and vehicle control study groups. Linsitinib groups from the two experiments exhibited decreases of approximately 70% and 67% in cross-sectional area covered by fat tissue compared to the vehicle controls at day 17 post-surgery (Experiment 1 and 2, respectively, Figure 4.5A). Moreover, the linsitinib group in each of the two experiments exhibited a statistically significant decrease in the number of adipocytes per tissue cross-section compared to the vehicle control, with a reduction of approximately 54% and 42% at day 17 post-surgery (Experiment 1 and 2, respectively, Figure 4.5B). Lastly, the cross-sectional area of individual adipocytes was statistically significantly decreased in the linsitinib group compared to the vehicle control in each of the two experiments, with reductions of approximately 36% and 42% at day 17 post-surgery (Experiment 1 and 2, respectively, Figure 4.5C). These findings demonstrate that pharmacologically targeting IGF1R with linsitinib led to a significant decrease

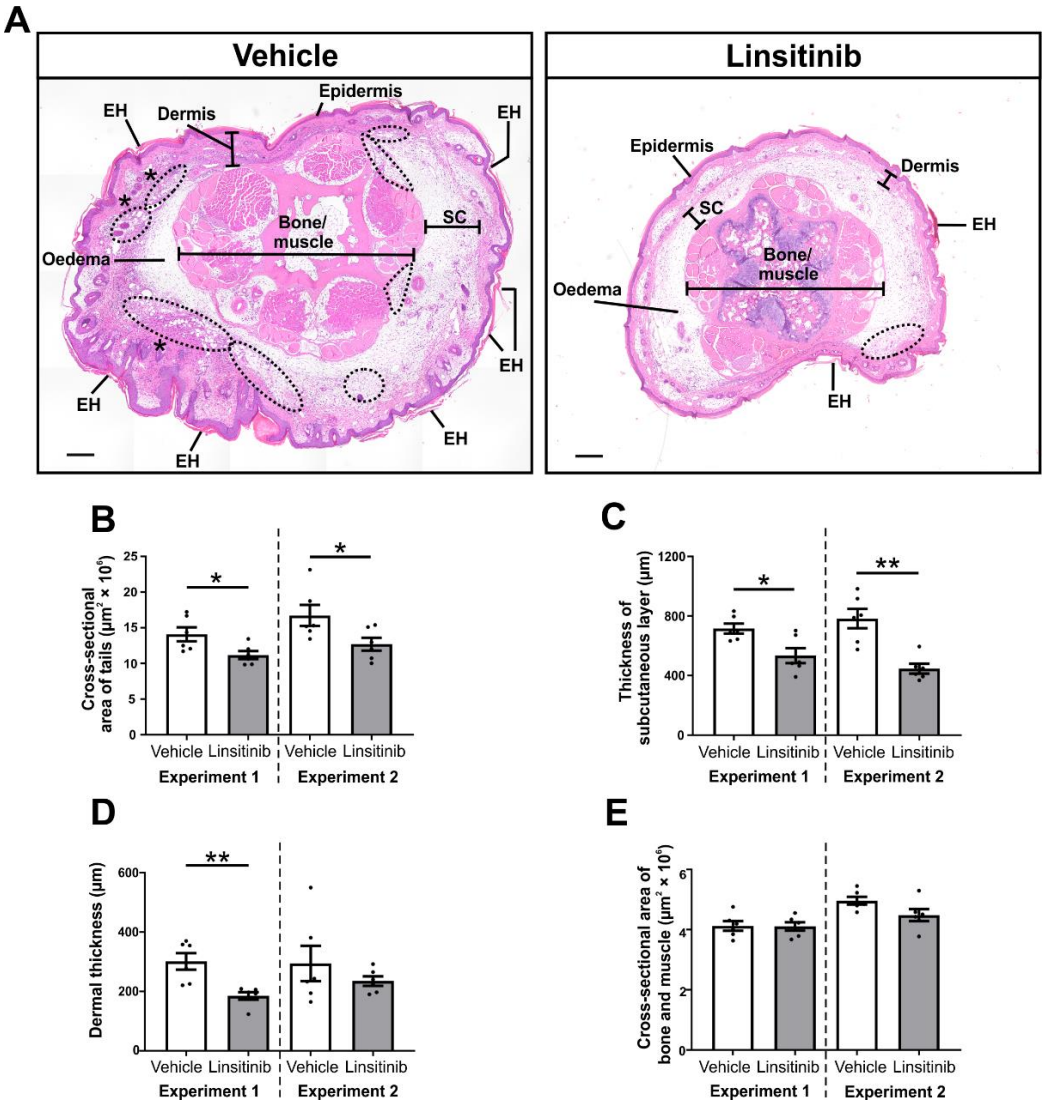

Figure 4.4 Histological changes in the mouse lymphoedema model in response to linsitinib at day 17 post-surgery. (A) Representative H&E-stained cross-sections of mouse tails from the linsitinib and vehicle control groups. Subcutaneous oedema is evident in both the vehicle and linsitinib study groups, whereas epidermal hyperkeratosis (designated EH) appears less pronounced in the linsitinib group compared to the vehicle control. The linsitinib group appears to exhibit a decreased abundance of adipocytes in the dermis and subcutaneous layer (regions rich in adipocytes are indicated by dotted lines; those located in the dermis are marked by asterisks). SC denotes subcutaneous layer and scale bar = 200 μm. The presence of oedema and epidermal hyperkeratosis was confirmed by Professor Stephen Fox, a clinical pathologist at the Peter MacCallum Cancer Centre. (B-E) Two independent experiments (the same as those referred to in Figure 4.3) showing the effect of linsitinib on cross-sectional area of tails (B), thickness of the subcutaneous layer (C), dermal thickness (D), and cross-sectional area of bone and muscle (E). For each experiment, data show mean ± SEM, n=6, * denotes $p<0.05$ and ** denotes $p<0.01$ for comparison with vehicle control at day 17 post-surgery (Student's t-test). Black circles depict individual data points.

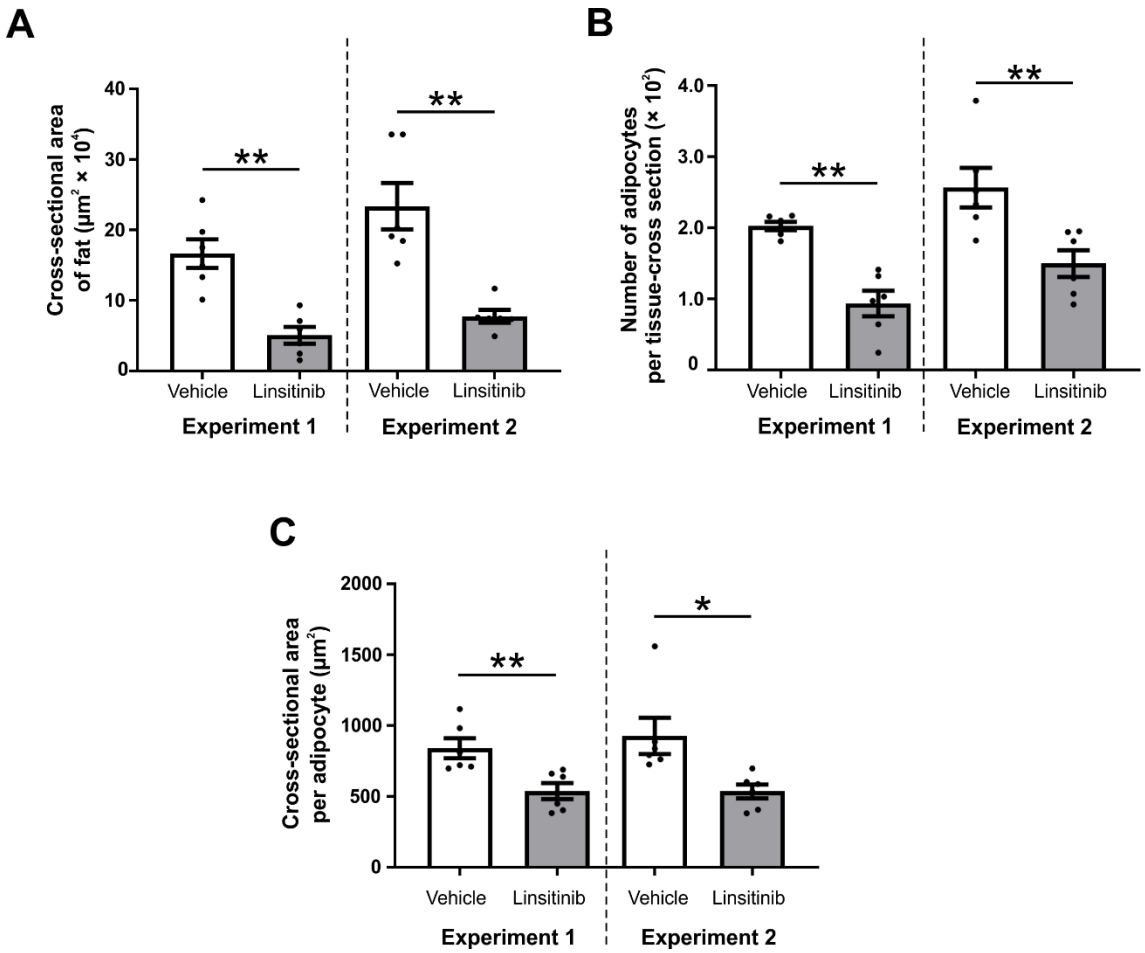

Figure 4.5 Effect of linsitinib on fat tissue in the mouse model of secondary lymphoedema at day 17 post-surgery. Two independent experiments (the same as those referred to in Figures 4.3 and 4.4) showing the effect of linsitinib on cross-sectional area of tails covered by fat in the dermis and subcutaneous layer (A), number of adipocytes in the dermis and subcutaneous layer of tissue sections of mouse tails (B) and cross-sectional area of individual adipocytes in mouse tails (C). For each experiment, data show mean ± SEM, n=6, * denotes $p<0.05$ and ** denotes $p<0.01$ for comparison with vehicle control (Student's t-test). Black circles depict individual data points.

in the levels of fat tissue in the dermis and subcutaneous layer due to decreases in the abundance and size of adipocytes.

4.4.4 Effect of linsitinib on fibrosis in the mouse model of secondary lymphoedema

Fibrosis in the dermis is a hallmark of clinical secondary lymphoedema so I assessed if linsitinib restricted dermal fibrosis in the mouse model. Fibrosis is characterised by excess deposition of extracellular matrix components, especially type I collagen which is secreted by fibroblasts [304, 305]. Fibrosis is known to impair lymphatic vessel function and regeneration [159], and to exacerbate lymphoedema [306]. The type I collagen involved in fibrosis can be readily detected by Masson trichrome staining [307, 308]; the collagen stains green whereas muscle and epithelium stain red or pink. This staining method allows fibrosis to be quantified using image analysis software.

Mouse tails in the lymphoedema model exhibited fibrosis in the dermis as monitored by Masson trichrome staining (Figure 4.6A), which is consistent with published *in vivo* data from animal models of secondary lymphoedema [159, 309] and clinical samples of lymphoedema [310, 311]. Quantitative analysis indicated that the areas of dermal fibrosis in the linsitinib study groups were smaller than for the vehicle controls in the two experiments, with a statistically significant reduction of approximately 18% in Experiment 1 and a reduction of 11% in Experiment 2 which was not statistically significant (Figure 4.6B). The reduction in the area of dermal fibrosis in response to linsitinib correlates well with the decreased thickness of the dermis in the linsitinib study group (Figure 4.4D). These findings suggest that linsitinib restricted dermal fibrosis, in addition to limiting the expansion of fat tissue, in the mouse model of secondary lymphoedema.

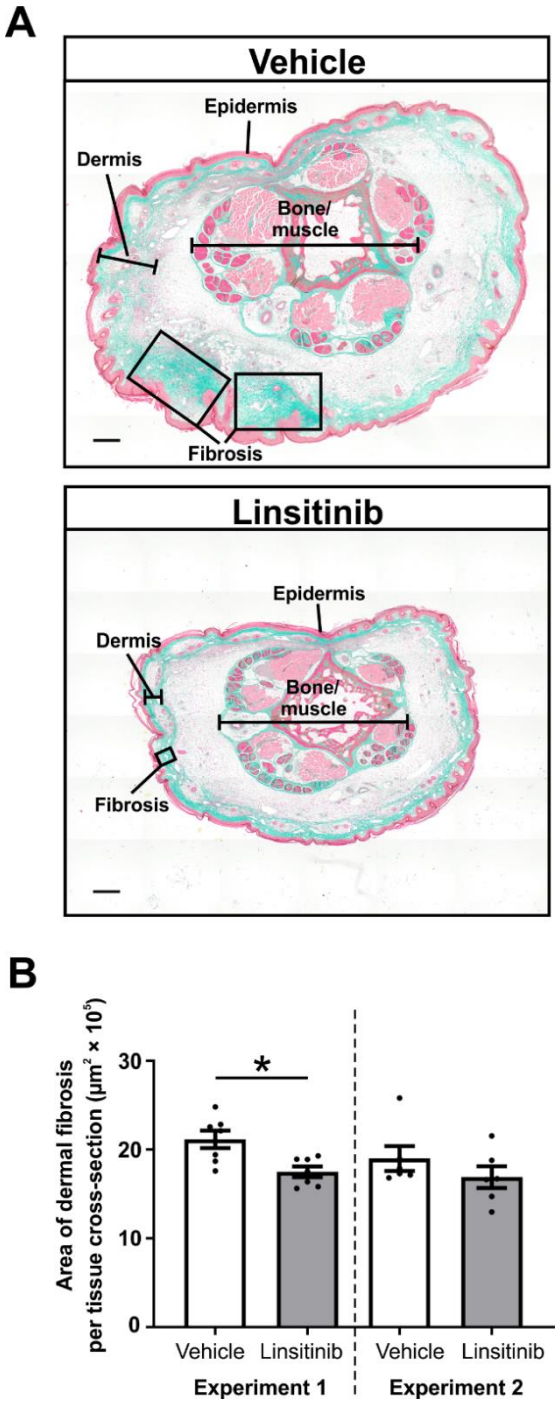

Figure 4.6 Effect of linsitinib on dermal fibrosis in the mouse model of secondary lymphoedema at day 17 post-surgery. (A) Masson Trichrome staining of cross-sections of representative mouse tails from the linsitinib and vehicle control groups. Collagen fibres stain green whereas muscle and epithelium stain red/pink. Regions of pronounced dermal fibrosis are indicated by rectangles. Scale bar = 200 μm. (B) Quantification of area of dermal fibrosis in two independent experiments (the same experiments as shown in Figures 4.3, 4.4 and 4.5). For each experiment, data show mean ± SEM, n=6, * denotes $p<0.05$ for comparison with vehicle control (Student's t-test). Black circles depict individual data points.

4.5 Discussion

The activation of the IGF1R signalling pathway has been implicated in the pathogenesis of various diseases, including cancer [312]. This led to the development of therapeutic agents targeting this signalling pathway, such as linsitinib. The hypothesis underlying the work in this chapter was that targeting the IGF1R signalling pathway may reduce the development of fat and thereby restrict tissue swelling in the mouse model of secondary lymphoedema. Notably, I demonstrated that pharmacological inhibition of IGF1R with linsitinib markedly reduced formation of fat tissue in the dermis and subcutaneous layer, and restricted tissue swelling, in this mouse model. The significantly decreased area of fat in the tail was due to decreases in both the abundance and size of adipocytes. Linsitinib may have also restricted dermal fibrosis, another clinically relevant feature of secondary lymphoedema, in the mouse model. However, the effect of linsitinib on dermal fibrosis was statistically significant in only one of the two experiments and therefore requires further study. Linsitinib also appeared to restrict epidermal hyperkeratosis although this feature of lymphoedema is difficult to rigorously quantify. Oedema was observed in both the linsitinib and vehicle control study groups in the subcutaneous layer, but this parameter is also difficult to reliable quantify and was not analysed here.

The expansion of fat tissue in a range of biological settings, such as embryonic development and obesity, involves two cellular mechanisms: hypertrophy (increase in adipocyte size) and hyperplasia (increase in adipocyte number) [313, 314] both of which can be promoted by IGF1R signalling [243, 246]. Hypertrophy occurs due to accumulation of lipid in adipocytes and triggers hyperplasia once the cell size reaches its upper limit [183]. This induction of hyperplasia involves secretion of growth factors, including IGF1 [315], by fat-laden adipocytes which promote proliferation of preadipocytes and their differentiation to adipocytes [243]. In the mouse lymphoedema model used here, a relatively low number of adipocytes, all of which were small, were detected in non-operated control tails (see Figure 3.3 E&F) which could potentially accumulate fat post-surgery for lymphoedema and then trigger adipocyte hyperplasia. This cycle of hypertrophy and hyperplasia leads to a dramatic increase in the levels of fat in the tails of mice

subjected to the surgery. Linsitinib significantly reduced fat tissue by decreasing both the abundance and size of adipocytes in the mouse lymphoedema model which is consistent with the role of IGF1R signalling in adipocyte hypertrophy and hyperplasia [243, 246]. These findings with linsitinib are also consistent with a previous study demonstrating that treatment with linsitinib led to a significant reduction in adipocyte size and weight of fat pads in epididymal and inguinal regions in mice, although the effect on adipocyte number was not assessed [299]. Therefore, it is possible that linsitinib targeted fat accumulation generally in the mice used in my study, rather than specifically targeting fat in the tail. Future studies with the mouse lymphoedema model should include analysis of the effect of linsitinib on fat in other tissues, such as in epididymal or inguinal regions.

The reduction in fat levels caused by linsitinib treatment in the mouse lymphoedema model could be related to inhibition of the IGF1R and/or IR signalling pathways, given linsitinib is a dual inhibitor for IGF1R and IR, and that the IR signalling pathway also drives fat tissue development in mice[316, 317]. It is hence important to determine the relative contribution of IGF1R and IR to the effects observed in the mouse model in this study, using, for example, monoclonal neutralising antibodies specific for mouse IGF1R or IR. Additionally, lymphoedema may be surgically induced in conditional knockout mice deficient for IGF1R or IR to assess the role of the IGF1R and IR signalling pathways in promoting fat tissue formation in secondary lymphoedema.

Importantly, IGF2, another ligand for IGF1R and IR [318, 319], has been shown to be expressed in embryos, and is required for normal foetal development in both mouse and humans [317]. However, the expression of IGF2 is dramatically down-regulated in mice postnatally [320], whereas it is abundantly present in human adults [321]. This suggests that the increased levels of fat tissue in the mouse lymphoedema model might be more likely mediated by IGF1/IGF1R signalling, rather than IGF2/IGF1R signalling, whereas in human this potentially could be driven by IGF1 or IGF2. Notably, IGF2, like IGF1, can promote adipogenesis and enhance lipid

deposition by binding IR on human preadipocytes[322]. linsitinib could be a useful therapeutic tool to target adipogenesis driven by either IGF1 or IGF2 in human lymphoedema given its capacity to block both signalling by IGF1R and IR.

A previous study has also shown that treatment of mice with linsitinib can lead to a minor reduction in body weight due to reduced levels of fat [299]. The results shown here are consistent with this in that there was a statistically significant reduction in body weight in Experiment 1, however, there was no significant difference in Experiment 2 indicating that this issue requires further study.

The finding that linsitinib may have exerted beneficial effects in restricting dermal fibrosis in the mouse model is clinically relevant because secondary lymphoedema patients commonly present with dermal fibrosis associated with elevated collagen deposition [310, 323]. The question arises as to whether the decreased dermal fibrosis in response to linsitinib in the mouse model is directly due to inhibition of IGF1R in the fibroblasts that secret type I collagen, or is a secondary effect due to the reduced levels of fat consequent to linsitinib treatment. The former possibility is supported by previous studies demonstrating expression of IGF1R in fibroblasts [324, 325], and that these cells can secret type I collagen [326-328] in response to stimulation with IGF1 [329-331]. The latter possibility is supported by previous reports that adipocytes can secrete the pro-fibrotic cytokine TGFβ [332], and that TGFβ stimulates secretion of type I collagen by fibroblasts [333, 334]. Hence the reduced fat levels consequent to linsitinib treatment may lead to lower levels of TGFβ in the extracellular milieu resulting in less dermal fibrosis. The importance of TGFβ in driving dermal fibrosis was previously demonstrated in a mouse lymphoedema model [161] and its relevance in the model of secondary lymphoedema employed here could be explored in future with inhibitors of the TGFβ signalling axis.

In the present study, linsitinib treatment began almost immediately after the surgery to generate lymphoedema. Thus, the study examined the effect of linsitinib on restricting the initial expansion of fat tissue, and tissue swelling, in response to the surgery. As such, the study models an approach for preventing or restricting the development of lymphoedema. Given the encouraging results of this approach in terms of restricting fat expansion, dermal fibrosis and tissue swelling, it will be important to monitor the effect of linsitinib on key disease parameters when treatment begins as soon as lymphoedema is apparent or when it is chronic - two other clinically relevant scenarios. Other issues that need to be explored are the effects of long-term linsitinib treatment, either during or after such treatment, in these lymphoedema scenarios. The mouse model of secondary lymphoedema employed here would be ideal for these studies because lymphoedema becomes chronic and long-standing thus providing sufficient time to monitor the effect of linsitinib during and after treatment.

Chapter 5
Conclusions and Future Directions

5.1 Conclusions

In this study, a surgical mouse tail model of secondary lymphoedema was employed to investigate molecular pathways that drive adipogenesis in this condition. This mouse model involved the ablation of small lymphatic vessels and lymphatic collectors which are typically damaged in the clinical setting of lymphadenectomy combined with radiotherapy for cancer – these cancer therapies are major causes of secondary lymphoedema. The model exhibited key pathophysiological features of secondary lymphoedema such as tissue swelling, oedema in the subcutaneous region, excess fat tissue, dermal fibrosis and epidermal hyperkeratosis. The lymphoedema generated in this model was long-lasting, allowing study of chronic lymphoedema as well as development of the condition. The model was characterised by increased levels of fat in lymphoedematous tissue, as in the clinical setting, with the excess fat being located in the subcutaneous region and dermis. The expansion of fat occurred during the early phase of lymphoedema, and enhanced levels of fat persisted in the chronic phase, so the model can be used to analyse mechanisms driving the initial formation of fat as well as the persistence of excess fat tissue in the chronic setting. Overall, the pathophysiological features and chronic nature of the lymphoedema generated in this model make it well suited for studying adipogenesis in secondary lymphoedema.

A whole-genome microarray analysis of the lymphoedema model identified that mRNA for IGFBP5, an inhibitor of the IGF1R adipogenic signalling axis, was down-regulated in lymphoedematous tissue compared to healthy tissue. This led to immunohistochemical analyses which revealed that IGF1 and IGF1R were present on adipocytes in the model and in a clinical sample of secondary lymphoedema, and that IGF1R was activated in the clinical sample. Furthermore, it appeared that IGF1 levels associated with adipocytes were higher in lymphoedematous tissue compared to healthy tissue. These findings suggest that the IGF1R

signalling axis could be active and promote formation of fat tissue in secondary lymphoedema due to decreased levels of IGFBP5 and increased levels of IGF1 which is an activating ligand for IGF1R.

The results discussed above led to the hypothesis that the IGF1R signalling pathway promotes formation of fat in secondary lymphoedema. This was tested using a pharmacological approach, based on the small molecule IGF1R inhibitor linsitinib, in the mouse model of secondary lymphoedema. In this study, treatment with linsitinib began almost immediately after the surgery for generating lymphoedema, so the experimental approach was designed to monitor the effect of linsitinib on restricting the initial expansion of fat tissue in the mouse lymphoedema model. Importantly, linsitinib significantly reduced both tissue swelling and fat expansion in the model. The effect on fat expansion was due to statistically significant reductions in the size and number of adipocytes in lymphoedematous tissue. In addition, linsitinib caused reductions in the degree of dermal fibrosis, and the thickness of the dermis and subcutaneous layer in the model. In conclusion, this study has demonstrated that targeting IGF1R with linsitinib is a potentially attractive approach for restricting fat levels and tissue swelling in secondary lymphoedema.

5.2 Future directions

5.2.1 Determine the effect of linsitinib on lymphatic function

In secondary lymphodema compromised lymphatic function leads to accumulation of interstitial fluid which is thought to stimulate production of excess fat. The resulting elevated abundance of fat tissue has been proposed to further compromise lymphatic function thus promoting even greater fluid accumulation. This constitutes a vicious cycle in lymphoedema pathophysiology [178]. Given that linsitinib markedly reduced fat levels in the mouse lymphodema model, it will be important to assess if this reduction in fat is associated with improvement in lymphatic function. This may be analysed by injecting liposomal indocyanine green (LP-ICG, a compound specifically taken up and transported by lymphatics [335]) into the dermis of the mouse lymphodema model distal to the surigcal wound, and conducting sequential

near-infrared imaging to monitor transit of LP-ICG across the wound and beyond. This technique allows quantitative imaging to measure lymphatic flow and will indicate if targeting IGF1R in the mouse lymphoedema model breaks the vicious cycle involving the accumulation of interstitial fluid, expansion of fat and impaired lymphatic function.

5.2.2 Investigate the effect of linsitinib on lymphoedema in clinically relevant scenarios

In this thesis, the effects of linsitinib in the mouse model of secondary lymphoedema were studied during the first 17 days post-surgery when lymphoedema was developing. The findings showed that linsitinib restricted tissue swelling and fat expansion in this setting which is relevant to the clinical scenario of preventing or restricting the development of lymphoedema. However, other relevant clinical scenarios would involve beginning treatment when lymphoedema is first detected or chronic. These two extra scenarios could be readily tested in the mouse model of secondary lymphoedema used here because lymphoedema is long-lasting in this model. Lymphoedema is first reliably detectable in this model at day five post-surgery and the model exhibits all the hallmarks of chronic lymphoedema by day 40 post-surgery. Hence these two extra scenarios could be explored by starting linsitinib therapy at these time-points.

The therapeutic strategy of pharmacologically restricting fat tissue in secondary lymphoedema would likely require long-term treatment of patients with an agent targeting IGF1R because the accumulation of interstitial fluid in lymphoedema would likely induce adipogenesis after cessation of this therapy. Nevertheless, this needs to be assessed by monitoring fat levels for prolonged periods after linsitinib treatment in the mouse model of secondary lymphoedema employed here. It is noteworthy that linsitinib was shown to be very well tolerated in humans for up to two years in a clinical trial for cancer with no adverse events being deemed due to linsitinib treatment [297]. Additionally, long-term IGF1R blockade in mouse genetic models was shown to have beneficial effects on aging-relevant metabolism [303]. Therefore, even if long-term linsitinib treatment is required in lymphoedema, it may be sufficiently well tolerated to be a viable therapeutic strategy in the clinic.

5.2.3 Explore molecular mechanisms initiating altered IGF1R signalling in lymphoedema

This study indicated that decreased levels of IGFBP5 may contribute to activation of IGF1R signalling in the mouse model of secondary lymphoedema. However, the mechanisms driving the decrease of *Igfbp5* mRNA levels in lymphoedema are not understood. To address this, *in situ* hybridisation could be employed to identify the cell type(s) expressing *Igfbp5* mRNA in healthy tail tissue, and in which it is down-regulated in lymphoedema. This information could be used to develop an *in vitro* system in which to study this question. For example, a relevant cell type which expresses IGFBP5 could be treated with interstitial fluid derived from lymphoedematous tissue of the mouse model to test if IGFBP5 becomes down-regulated. If so, a range of systems biology approaches could be used to monitor the alteration of signalling pathways in response to this fluid, e.g. reverse-phase protein array which simultaneously monitors multiple signal transduction pathways. The physiological relevance of pathway(s) identified by such an approach could be tested by pharmacologically targeting it in the mouse model of secondary lymphoedema. The identification of the molecular mechanisms by which the accumulation of interstitial fluid in secondary lymphoedema enhances the activity of the IGF1R signalling pathway could provide alternative pharmacological strategies for restricting formation of fat in this disease.

5.2.4 Validation of the role of the IGF1R signalling pathway in promoting fat formation in lymphoedema

In the present study, immunohistochemistry was employed to demonstrate the presence of IGF1 and IGF1R on the plasma membrane of adipocytes in both the mouse lymphoedema model and in a clinical sample. However, the association between IGF1R signalling and lymphoedema should be further confirmed using various approaches. For example, Western blotting using lymphoedematous and normal mouse tails should be performed to assess whether the antibodies used for the immunohistochemistry target a band of the correct size for IGF1Rβ. This approach will also allow monitoring of the relative levels of IGF1Rβ in these mouse tissues.

Further, in situ hybridisation can be conducted to identify the sites of synthesis of IGFBP5, IGF1 and IGF1Rβ in mouse lymphoedematous and normal tails. It will also be important to conduct specificity controls for immunohistochemistry for IGF1 and IGF1Rβ in the presence of the antigens used to generate the primary antibodies. In addition, the use of conditional knockout mice deficient for IGF1 [336] or IGF1R [303], or treatment with highly specific neutralising monoclonal antibodies as inhibitors of mouse IGF1 or IGF1R, could be useful to study the correlation between IGF1R signalling and fat tissue formation in secondary lymphoedema

5.2.5 Investigate the effect of targeting IGF1R in primary lymphoedema

Primary lymphoedema involves oedema, fibrosis, and expansion of subcutaneous fat tissue, and is an unmet need in medicine although it is less common than secondary lymphoedema [67]. Milroy's disease is a form of congenital primary lymphoedema which can be caused by inactivating mutations of the gene for VEGFR3 [337]. The role of IGF1R signalling in the formation of subcutaneous fat in Milroy's disease could be explored using Chy mice which have an inactivating mutation in the *Vegfr3* gene in their germline [67, 337]. Heterozygous Chy mice have thickened adipose tissue and other features of primary lymphoedema. Treatment of these mice with linsitinib, and monitoring of tissue swelling and subcutaneous fat levels, would provide insight as to whether targeting IGF1R is a potential therapeutic strategy in this disease.

Bibliography

1. Rockson, S.G., *Lymphedema.* Am J Med, 2001. **110**(4): p. 288-95.
2. McWayne, J. and S.P. Heiney, *Psychologic and social sequelae of secondary lymphedema: a review.* Cancer, 2005. **104**(3): p. 457-66.
3. Murdaca, G., et al., *Current views on diagnostic approach and treatment of lymphedema.* Am J Med, 2012. **125**(2): p. 134-40.
4. Saito, Y., et al., *Lymphedema and therapeutic lymphangiogenesis.* Biomed Res Int, 2013. **2013**: p. 804675.
5. Zampell, J.C., et al., *Regulation of adipogenesis by lymphatic fluid stasis: part I. Adipogenesis, fibrosis, and inflammation.* Plast Reconstr Surg, 2012. **129**(4): p. 825-34.
6. Brorson, H., et al., *Adipose tissue dominates chronic arm lymphedema following breast cancer: an analysis using volume rendered CT images.* Lymphat Res Biol, 2006. **4**(4): p. 199-210.
7. Greenlee, R., et al., *Developmental disorders of the lymphatic system.* Lymphology, 1993. **26**(4): p. 156-68.
8. Hidden, G., *[Some recent, or claiming to be recent, data on the superficial lymphatic circulation of the limbs].* J Mal Vasc, 1990. **15**(2): p. 149-51.
9. *Lymphatic filariasis: the disease and its control. Fifth report of the WHO Expert Committee on Filariasis.* World Health Organ Tech Rep Ser, 1992. **821**: p. 1-71.
10. Dacre, J.E., D.L. Scott, and E.C. Huskisson, *Lymphoedema of the limbs as an extra-articular feature of rheumatoid arthritis.* Ann Rheum Dis, 1990. **49**(9): p. 722-4.
11. Segerstrom, K., et al., *Factors that influence the incidence of brachial oedema after treatment of breast cancer.* Scand J Plast Reconstr Surg Hand Surg, 1992. **26**(2): p. 223-7.
12. Cormier, J.N., et al., *Lymphedema beyond breast cancer: a systematic review and meta-analysis of cancer-related secondary lymphedema.* Cancer, 2010. **116**(22): p. 5138-49.
13. Centre, N.B.a.O.C., *Review of research evidence on secondary lymphoedema: Incidence, prevention, risk factors and treatmen.* NBOCC, 2008: p. 83.
14. Sierla, R., et al., *Access to treatment for breast cancer-related lymphoedema in Australia.* Aust Fam Physician, 2013. **42**(12): p. 892-5.
15. Gartner, R., et al., *Self-reported arm-lymphedema and functional impairment after breast cancer treatment--a nationwide study of prevalence and associated factors.* Breast, 2010. **19**(6): p. 506-15.
16. Harvey, N.L. and G. Oliver, *Choose your fate: artery, vein or lymphatic vessel?* Curr Opin Genet Dev, 2004. **14**(5): p. 499-505.
17. Oliver, G. and K. Alitalo, *The lymphatic vasculature: recent progress and paradigms.* Annu Rev Cell Dev Biol, 2005. **21**: p. 457-83.
18. Zoltzer, H., *Initial lymphatics--morphology and function of the endothelial cells.* Lymphology, 2003. **36**(1): p. 7-25.
19. Margaris, K.N. and R.A. Black, *Modelling the lymphatic system: challenges and opportunities.* J R Soc Interface, 2012. **9**(69): p. 601-12.
20. Sacchi, G., et al., *The structure of superficial lymphatics in the human thigh: precollectors.* Anat Rec, 1997. **247**(1): p. 53-62.
21. Skandalakis, J.E., L.J. Skandalakis, and P.N. Skandalakis, *Anatomy of the lymphatics.* Surg Oncol Clin N Am, 2007. **16**(1): p. 1-16.
22. Junt, T., E. Scandella, and B. Ludewig, *Form follows function: lymphoid tissue microarchitecture in antimicrobial immune defence.* Nat Rev Immunol, 2008. **8**(10): p. 764-75.
23. Petrova, T.V. and G.Y. Koh, *Organ-specific lymphatic vasculature: From development to pathophysiology.* J Exp Med, 2018. **215**(1): p. 35-49.
24. Randolph, G.J. and N.E. Miller, *Lymphatic transport of high-density lipoproteins and chylomicrons.* J Clin Invest, 2014. **124**(3): p. 929-35.

25. Louveau, A., et al., *Structural and functional features of central nervous system lymphatic vessels.* Nature, 2015. **523**(7560): p. 337-41.
26. Aspelund, A., et al., *A dural lymphatic vascular system that drains brain interstitial fluid and macromolecules.* J Exp Med, 2015. **212**(7): p. 991-9.
27. Patel, T.K., et al., *Dural lymphatics regulate clearance of extracellular tau from the CNS.* Mol Neurodegener, 2019. **14**(1): p. 11.
28. Iliff, J.J., et al., *A paravascular pathway facilitates CSF flow through the brain parenchyma and the clearance of interstitial solutes, including amyloid beta.* Sci Transl Med, 2012. **4**(147): p. 147ra111.
29. Jessen, N.A., et al., *The Glymphatic System: A Beginner's Guide.* Neurochem Res, 2015. **40**(12): p. 2583-99.
30. Park, D.Y., et al., *Lymphatic regulator PROX1 determines Schlemm's canal integrity and identity.* J Clin Invest, 2014. **124**(9): p. 3960-74.
31. Jonas, J.B., et al., *Glaucoma.* Lancet, 2017. **390**(10108): p. 2183-2193.
32. Kizhatil, K., et al., *Schlemm's canal is a unique vessel with a combination of blood vascular and lymphatic phenotypes that forms by a novel developmental process.* PLoS Biol, 2014. **12**(7): p. e1001912.
33. Aspelund, A., et al., *The Schlemm's canal is a VEGF-C/VEGFR-3-responsive lymphatic-like vessel.* J Clin Invest, 2014. **124**(9): p. 3975-86.
34. Weber, E., et al., *Pulmonary lymphatic vessel morphology: a review.* Ann Anat, 2018. **218**: p. 110-117.
35. Pelosi, P., et al., *The extracellular matrix of the lung and its role in edema formation.* An Acad Bras Cienc, 2007. **79**(2): p. 285-97.
36. Jakus, Z., et al., *Lymphatic function is required prenatally for lung inflation at birth.* J Exp Med, 2014. **211**(5): p. 815-26.
37. Schraufnagel, D.E., *Lung lymphatic anatomy and correlates.* Pathophysiology, 2010. **17**(4): p. 337-43.
38. Tanaka, M. and Y. Iwakiri, *The Hepatic Lymphatic Vascular System: Structure, Function, Markers, and Lymphangiogenesis.* Cell Mol Gastroenterol Hepatol, 2016. **2**(6): p. 733-749.
39. Tanaka, M. and Y. Iwakiri, *Lymphatics in the liver.* Curr Opin Immunol, 2018. **53**: p. 137-142.
40. Yazdani, S., et al., *Lymphangiogenesis in renal diseases: passive bystander or active participant?* Expert Rev Mol Med, 2014. **16**: p. e15.
41. Russell, P.S., et al., *Renal Lymphatics: Anatomy, Physiology, and Clinical Implications.* Front Physiol, 2019. **10**: p. 251.
42. Rawson, A.J., *Distribution of the lymphatics of the human kidney as shown in a case of carcinomatous permeation.* Arch Pathol (Chic), 1949. **47**(3): p. 283-92.
43. Ishikawa, Y., et al., *The human renal lymphatics under normal and pathological conditions.* Histopathology, 2006. **49**(3): p. 265-73.
44. Moffat, D.B., *New ideas on the anatomy of the kidney.* J Clin Pathol, 1981. **34**(11): p. 1197-1206.
45. Lever, A.F. and W.S. Peart, *Renin and angiotensin-like activity in renal lymph.* J Physiol, 1962. **160**: p. 548-63.
46. Loukas, M., et al., *The cardiac lymphatic system.* Clin Anat, 2011. **24**(6): p. 684-91.
47. Cui, Y., *The role of lymphatic vessels in the heart.* Pathophysiology, 2010. **17**(4): p. 307-14.
48. Vieira, J.M., et al., *The cardiac lymphatic system stimulates resolution of inflammation following myocardial infarction.* J Clin Invest, 2018. **128**(8): p. 3402-3412.
49. Shimizu, Y., et al., *Impact of Lymphangiogenesis on Cardiac Remodeling After Ischemia and Reperfusion Injury.* J Am Heart Assoc, 2018. **7**(19): p. e009565.
50. Harvey, N.L., *The link between lymphatic function and adipose biology.* Ann N Y Acad Sci, 2008. **1131**: p. 82-8.

51. Pond, C.M. and C.A. Mattacks, *Interactions between adipose tissue around lymph nodes and lymphoid cells in vitro.* J Lipid Res, 1995. **36**(10): p. 2219-31.
52. Pond, C.M. and C.A. Mattacks, *In vivo evidence for the involvement of the adipose tissue surrounding lymph nodes in immune responses.* Immunol Lett, 1998. **63**(3): p. 159-67.
53. Pond, C.M. and C.A. Mattacks, *The source of fatty acids incorporated into proliferating lymphoid cells in immune-stimulated lymph nodes.* Br J Nutr, 2003. **89**(3): p. 375-83.
54. Nougues, J., Y. Reyne, and J.P. Dulor, *Differentiation of rabbit adipocyte precursors in primary culture.* Int J Obes, 1988. **12**(4): p. 321-33.
55. Mattacks, C.A., D. Sadler, and C.M. Pond, *The cellular structure and lipid/protein composition of adipose tissue surrounding chronically stimulated lymph nodes in rats.* J Anat, 2003. **202**(6): p. 551-61.
56. Tavakkolizadeh, A., K.Q. Wolfe, and L. Kangesu, *Cutaneous lymphatic malformation with secondary fat hypertrophy.* Br J Plast Surg, 2001. **54**(4): p. 367-9.
57. Brorson, H. and H. Svensson, *Complete reduction of lymphoedema of the arm by liposuction after breast cancer.* Scand J Plast Reconstr Surg Hand Surg, 1997. **31**(2): p. 137-43.
58. Escobedo, N., et al., *Restoration of lymphatic function rescues obesity in Prox1-haploinsufficient mice.* JCI Insight, 2016. **1**(2).
59. Sedger, L.M., et al., *Lipidomic Profiling of Adipose Tissue Reveals an Inflammatory Signature in Cancer-Related and Primary Lymphedema.* PLoS One, 2016. **11**(5): p. e0154650.
60. Calder, P.C., *n-3 polyunsaturated fatty acids, inflammation, and inflammatory diseases.* Am J Clin Nutr, 2006. **83**(6 Suppl): p. 1505S-1519S.
61. Gomez-Munoz, A., et al., *Control of inflammatory responses by ceramide, sphingosine 1-phosphate and ceramide 1-phosphate.* Prog Lipid Res, 2016. **61**: p. 51-62.
62. Ryan, T.J., *Lymphatics and adipose tissue.* Clin Dermatol, 1995. **13**(5): p. 493-8.
63. Schirger, A., E.G. Harrison, Jr., and J.M. Janes, *Idiopathic lymphedema. Review of 131 cases.* JAMA, 1962. **182**: p. 14-22.
64. Brorson, H., *Adipose tissue in lymphedema: the ignorance of adipose tissue in lymphedema.* Lymphology, 2004. **37**(4): p. 175-7.
65. Brorson, H., et al., *Breast cancer-related chronic arm lymphedema is associated with excess adipose and muscle tissue.* Lymphat Res Biol, 2009. **7**(1): p. 3-10.
66. Aoki, Y. and G. Tosato, *Lymphatic regeneration: new insights from VEGFR-3 blockade.* J Natl Cancer Inst, 2005. **97**(1): p. 2-3.
67. Karkkainen, M.J., et al., *A model for gene therapy of human hereditary lymphedema.* Proc Natl Acad Sci U S A, 2001. **98**(22): p. 12677-82.
68. Rutkowski, J.M., et al., *Dermal collagen and lipid deposition correlate with tissue swelling and hydraulic conductivity in murine primary lymphedema.* Am J Pathol, 2010. **176**(3): p. 1122-9.
69. Harvey, N.L., et al., *Lymphatic vascular defects promoted by Prox1 haploinsufficiency cause adult-onset obesity.* Nat Genet, 2005. **37**(10): p. 1072-81.
70. Savetsky, I.L., et al., *Obesity increases inflammation and impairs lymphatic function in a mouse model of lymphedema.* Am J Physiol Heart Circ Physiol, 2014. **307**(2): p. H165-72.
71. Aschen, S., et al., *Regulation of adipogenesis by lymphatic fluid stasis: part II. Expression of adipose differentiation genes.* Plast Reconstr Surg, 2012. **129**(4): p. 838-47.
72. Levi, B., et al., *Molecular analysis and differentiation capacity of adipose-derived stem cells from lymphedema tissue.* Plast Reconstr Surg, 2013. **132**(3): p. 580-9.
73. McLaughlin, S.A., et al., *Prevalence of lymphedema in women with breast cancer 5 years after sentinel lymph node biopsy or axillary dissection: objective measurements.* J Clin Oncol, 2008. **26**(32): p. 5213-9.
74. Petrek, J.A., et al., *Lymphedema in a cohort of breast carcinoma survivors 20 years after diagnosis.* Cancer, 2001. **92**(6): p. 1368-77.

75. DiSipio, T., et al., *Incidence of unilateral arm lymphoedema after breast cancer: a systematic review and meta-analysis.* Lancet Oncol, 2013. **14**(6): p. 500-15.
76. Treves, N., *An evaluation of the etiological factors of lymphedema following radical mastectomy; an analysis of 1,007 cases.* Cancer, 1957. **10**(3): p. 444-59.
77. Helyer, L.K., et al., *Obesity is a risk factor for developing postoperative lymphedema in breast cancer patients.* Breast J, 2010. **16**(1): p. 48-54.
78. Werner, R.S., et al., *Arm edema in conservatively managed breast cancer: obesity is a major predictive factor.* Radiology, 1991. **180**(1): p. 177-84.
79. Greene, A.K., F.D. Grant, and S.A. Slavin, *Lower-extremity lymphedema and elevated body-mass index.* N Engl J Med, 2012. **366**(22): p. 2136-7.
80. Arngrim, N., et al., *Reduced adipose tissue lymphatic drainage of macromolecules in obese subjects: a possible link between obesity and local tissue inflammation?* Int J Obes (Lond), 2013. **37**(5): p. 748-50.
81. Uzarski, J., et al., *The resolution of lymphedema by interstitial flow in the mouse tail skin.* Am J Physiol Heart Circ Physiol, 2008. **294**(3): p. H1326-34.
82. Mendez, U., et al., *A chronic and latent lymphatic insufficiency follows recovery from acute lymphedema in the rat foreleg.* Am J Physiol Heart Circ Physiol, 2012. **303**(9): p. H1107-13.
83. Garcia Nores, G.D., et al., *Obesity but not high-fat diet impairs lymphatic function.* Int J Obes (Lond), 2016. **40**(10): p. 1582-1590.
84. Gousopoulos, E., et al., *High-Fat Diet in the Absence of Obesity Does Not Aggravate Surgically Induced Lymphoedema in Mice.* Eur Surg Res, 2017. **58**(3-4): p. 180-192.
85. Lim, H.Y., et al., *Hypercholesterolemic mice exhibit lymphatic vessel dysfunction and degeneration.* Am J Pathol, 2009. **175**(3): p. 1328-37.
86. Hespe, G.E., et al., *Exercise training improves obesity-related lymphatic dysfunction.* J Physiol, 2016.
87. Samaan, M.C., et al., *Endurance interval training in obese mice reduces muscle inflammation and macrophage content independently of weight loss.* Physiol Rep, 2014. **2**(5).
88. Nitti, M.D., et al., *Obesity-induced lymphatic dysfunction is reversible with weight loss.* J Physiol, 2016. **594**(23): p. 7073-7087.
89. Torrisi, J.S., et al., *Inhibition of Inflammation and iNOS Improves Lymphatic Function in Obesity.* Sci Rep, 2016. **6**: p. 19817.
90. Cromer, W.E., et al., *The effects of inflammatory cytokines on lymphatic endothelial barrier function.* Angiogenesis, 2014. **17**(2): p. 395-406.
91. Liao, S., et al., *Impaired lymphatic contraction associated with immunosuppression.* Proc Natl Acad Sci U S A, 2011. **108**(46): p. 18784-9.
92. Kligman, L., et al., *The treatment of lymphedema related to breast cancer: a systematic review and evidence summary.* Support Care Cancer, 2004. **12**(6): p. 421-31.
93. Foldi, E., *The treatment of lymphedema.* Cancer, 1998. **83**(12 Suppl American): p. 2833-4.
94. Partsch, H. and B. Lee, *Phlebology and lymphology--a family affair.* Phlebology, 2014. **29**(10): p. 645-7.
95. Bogusz, A.M., et al., *Massive localized lymphedema with unusual presentations: report of 2 cases and review of the literature.* Int J Surg Pathol, 2011. **19**(2): p. 212-6.
96. Badger, C.M., J.L. Peacock, and P.S. Mortimer, *A randomized, controlled, parallel-group clinical trial comparing multilayer bandaging followed by hosiery versus hosiery alone in the treatment of patients with lymphedema of the limb.* Cancer, 2000. **88**(12): p. 2832-7.
97. Stout Gergich, N.L., et al., *Preoperative assessment enables the early diagnosis and successful treatment of lymphedema.* Cancer, 2008. **112**(12): p. 2809-19.
98. Partsch, H. and G. Mosti, *Thigh compression.* Phlebology, 2008. **23**(6): p. 252-8.

99. Williams, A.F., et al., *A randomized controlled crossover study of manual lymphatic drainage therapy in women with breast cancer-related lymphoedema.* Eur J Cancer Care (Engl), 2002. **11**(4): p. 254-61.
100. Torres Lacomba, M., et al., *Effectiveness of early physiotherapy to prevent lymphoedema after surgery for breast cancer: randomised, single blinded, clinical trial.* BMJ, 2010. **340**: p. b5396.
101. Badger, C., et al., *Physical therapies for reducing and controlling lymphoedema of the limbs.* Cochrane Database Syst Rev, 2004(4): p. CD003141.
102. Johansson, K., et al., *Effects of compression bandaging with or without manual lymph drainage treatment in patients with postoperative arm lymphedema.* Lymphology, 1999. **32**(3): p. 103-10.
103. McNeely, M.L., et al., *The addition of manual lymph drainage to compression therapy for breast cancer related lymphedema: a randomized controlled trial.* Breast Cancer Res Treat, 2004. **86**(2): p. 95-106.
104. Vignes, S., et al., *Factors influencing breast cancer-related lymphedema volume after intensive decongestive physiotherapy.* Support Care Cancer, 2011. **19**(7): p. 935-40.
105. Woo, P.C., et al., *Cellulitis complicating lymphoedema.* Eur J Clin Microbiol Infect Dis, 2000. **19**(4): p. 294-7.
106. Garcia Hidalgo, L., *Dermatological complications of obesity.* Am J Clin Dermatol, 2002. **3**(7): p. 497-506.
107. Kwan, M.L., et al., *Exercise in patients with lymphedema: a systematic review of the contemporary literature.* J Cancer Surviv, 2011. **5**(4): p. 320-36.
108. Moseley, A.L., N.B. Piller, and C.J. Carati, *The effect of gentle arm exercise and deep breathing on secondary arm lymphedema.* Lymphology, 2005. **38**(3): p. 136-45.
109. Schmitz, K.H., et al., *Weight lifting for women at risk for breast cancer-related lymphedema: a randomized trial.* JAMA, 2010. **304**(24): p. 2699-705.
110. Ahmed, R.L., et al., *Randomized controlled trial of weight training and lymphedema in breast cancer survivors.* J Clin Oncol, 2006. **24**(18): p. 2765-72.
111. Courneya, K.S., et al., *Effects of aerobic and resistance exercise in breast cancer patients receiving adjuvant chemotherapy: a multicenter randomized controlled trial.* J Clin Oncol, 2007. **25**(28): p. 4396-404.
112. Milne, H.M., et al., *Effects of a combined aerobic and resistance exercise program in breast cancer survivors: a randomized controlled trial.* Breast Cancer Res Treat, 2008. **108**(2): p. 279-88.
113. Brorson, H., *Liposuction in arm lymphedema treatment.* Scand J Surg, 2003. **92**(4): p. 287-95.
114. Brorson, H., *Liposuction gives complete reduction of chronic large arm lymphedema after breast cancer.* Acta Oncol, 2000. **39**(3): p. 407-20.
115. Brorson, H. and H. Svensson, *Liposuction combined with controlled compression therapy reduces arm lymphedema more effectively than controlled compression therapy alone.* Plast Reconstr Surg, 1998. **102**(4): p. 1058-67; discussion 1068.
116. Dixit, V.V. and M.S. Wagh, *Unfavourable outcomes of liposuction and their management.* Indian J Plast Surg, 2013. **46**(2): p. 377-92.
117. Khanna, A. and G. Filobbos, *Avoiding unfavourable outcomes in liposuction.* Indian J Plast Surg, 2013. **46**(2): p. 393-400.
118. Poth, E.J., S.R. Barnes, and G.T. Ross, *A new operative treatment for elephantiasis.* Surg Gynecol Obstet, 1947. **84**(4-A): p. 642-4.
119. Kim, D.I., et al., *Excisional surgery for chronic advanced lymphedema.* Surg Today, 2004. **34**(2): p. 134-7.
120. Salgado, C.J., et al., *Radical reduction of upper extremity lymphedema with preservation of perforators.* Ann Plast Surg, 2009. **63**(3): p. 302-6.
121. Shaitelman, S.F., et al., *Recent progress in the treatment and prevention of cancer-related lymphedema.* CA Cancer J Clin, 2015. **65**(1): p. 55-81.

122. O'Brien, B.M., et al., *Long-term results after microlymphaticovenous anastomoses for the treatment of obstructive lymphedema.* Plast Reconstr Surg, 1990. **85**(4): p. 562-72.
123. Olszewski, W.L., *The treatment of lymphedema of the extremities with microsurgical lympho-venous anastomoses.* Int Angiol, 1988. **7**(4): p. 312-21.
124. Baumeister, R.G. and S. Siuda, *Treatment of lymphedemas by microsurgical lymphatic grafting: what is proved?* Plast Reconstr Surg, 1990. **85**(1): p. 64-74; discussion 75-6.
125. Chang, D.W., H. Suami, and R. Skoracki, *A prospective analysis of 100 consecutive lymphovenous bypass cases for treatment of extremity lymphedema.* Plast Reconstr Surg, 2013. **132**(5): p. 1305-14.
126. Ito, R., et al., *Successful treatment of early-stage lower extremity lymphedema with side-to-end lymphovenous anastomosis with indocyanine green lymphography assisted.* Microsurgery, 2015.
127. Saharinen, P. and T.V. Petrova, *Molecular regulation of lymphangiogenesis.* Ann N Y Acad Sci, 2004. **1014**: p. 76-87.
128. Cao, R., et al., *Hepatocyte growth factor is a lymphangiogenic factor with an indirect mechanism of action.* Blood, 2006. **107**(9): p. 3531-6.
129. James, J.M., A. Nalbandian, and Y.S. Mukouyama, *TGFbeta signaling is required for sprouting lymphangiogenesis during lymphatic network development in the skin.* Development, 2013. **140**(18): p. 3903-14.
130. Branton, M.H. and J.B. Kopp, *TGF-beta and fibrosis.* Microbes Infect, 1999. **1**(15): p. 1349-65.
131. Nakamura, K., et al., *Anti-inflammatory pharmacotherapy with ketoprofen ameliorates experimental lymphatic vascular insufficiency in mice.* PLoS One, 2009. **4**(12): p. e8380.
132. Bramos, A., et al., *Prevention of Postsurgical Lymphedema by 9-cis Retinoic Acid.* Ann Surg, 2015.
133. Jussila, L. and K. Alitalo, *Vascular growth factors and lymphangiogenesis.* Physiol Rev, 2002. **82**(3): p. 673-700.
134. Stacker, S.A., et al., *Lymphangiogenesis and lymphatic vessel remodelling in cancer.* Nat Rev Cancer, 2014. **14**(3): p. 159-72.
135. Koch, S. and L. Claesson-Welsh, *Signal transduction by vascular endothelial growth factor receptors.* Cold Spring Harb Perspect Med, 2012. **2**(7): p. a006502.
136. Karkkainen, M.J., et al., *Vascular endothelial growth factor C is required for sprouting of the first lymphatic vessels from embryonic veins.* Nat Immunol, 2004. **5**(1): p. 74-80.
137. Yoon, Y.S., et al., *VEGF-C gene therapy augments postnatal lymphangiogenesis and ameliorates secondary lymphedema.* J Clin Invest, 2003. **111**(5): p. 717-25.
138. Tabibiazar, R., et al., *Inflammatory manifestations of experimental lymphatic insufficiency.* PLoS Med, 2006. **3**(7): p. e254.
139. Szuba, A., et al., *Therapeutic lymphangiogenesis with human recombinant VEGF-C.* FASEB J, 2002. **16**(14): p. 1985-7.
140. Tammela, T., et al., *Therapeutic differentiation and maturation of lymphatic vessels after lymph node dissection and transplantation.* Nat Med, 2007. **13**(12): p. 1458-66.
141. Gousopoulos, E., et al., *An Important Role of VEGF-C in Promoting Lymphedema Development.* J Invest Dermatol, 2017. **137**(9): p. 1995-2004.
142. Goldman, J., et al., *Overexpression of VEGF-C causes transient lymphatic hyperplasia but not increased lymphangiogenesis in regenerating skin.* Circ Res, 2005. **96**(11): p. 1193-9.
143. Skobe, M., et al., *Induction of tumor lymphangiogenesis by VEGF-C promotes breast cancer metastasis.* Nat Med, 2001. **7**(2): p. 192-8.
144. Ito, Y., et al., *Lymphangiogenesis and Axillary Lymph Node Metastases Correlated with VEGF-C Expression in Two Immunocompetent Mouse Mammary Carcinoma Models.* Int J Breast Cancer, 2011. **2011**: p. 867152.
145. Hirakawa, S., et al., *VEGF-C-induced lymphangiogenesis in sentinel lymph nodes promotes tumor metastasis to distant sites.* Blood, 2007. **109**(3): p. 1010-7.

146. Tacconi, C., et al., *Vascular endothelial growth factor C disrupts the endothelial lymphatic barrier to promote colorectal cancer invasion.* Gastroenterology, 2015. **148**(7): p. 1438-51 e8.
147. Organ, S.L. and M.S. Tsao, *An overview of the c-MET signaling pathway.* Ther Adv Med Oncol, 2011. **3**(1 Suppl): p. S7-S19.
148. Comoglio, P.M., S. Giordano, and L. Trusolino, *Drug development of MET inhibitors: targeting oncogene addiction and expedience.* Nat Rev Drug Discov, 2008. **7**(6): p. 504-16.
149. Kajiya, K., et al., *Hepatocyte growth factor promotes lymphatic vessel formation and function.* EMBO J, 2005. **24**(16): p. 2885-95.
150. Saito, Y., et al., *Transfection of human hepatocyte growth factor gene ameliorates secondary lymphedema via promotion of lymphangiogenesis.* Circulation, 2006. **114**(11): p. 1177-84.
151. Finegold, D.N., et al., *HGF and MET mutations in primary and secondary lymphedema.* Lymphat Res Biol, 2008. **6**(2): p. 65-8.
152. Morishita, R., et al., *Safety evaluation of clinical gene therapy using hepatocyte growth factor to treat peripheral arterial disease.* Hypertension, 2004. **44**(2): p. 203-9.
153. Wu, J.W., et al., *Crystal structure of a phosphorylated Smad2. Recognition of phosphoserine by the MH2 domain and insights on Smad function in TGF-beta signaling.* Mol Cell, 2001. **8**(6): p. 1277-89.
154. Zhang, Y.E., *Non-Smad pathways in TGF-beta signaling.* Cell Res, 2009. **19**(1): p. 128-39.
155. Oka, M., et al., *Inhibition of endogenous TGF-beta signaling enhances lymphangiogenesis.* Blood, 2008. **111**(9): p. 4571-9.
156. ten Dijke, P. and H.M. Arthur, *Extracellular control of TGFbeta signalling in vascular development and disease.* Nat Rev Mol Cell Biol, 2007. **8**(11): p. 857-69.
157. Niessen, K., et al., *ALK1 signaling regulates early postnatal lymphatic vessel development.* Blood, 2010. **115**(8): p. 1654-61.
158. Goumans, M.J., et al., *Activin receptor-like kinase (ALK)1 is an antagonistic mediator of lateral TGFbeta/ALK5 signaling.* Mol Cell, 2003. **12**(4): p. 817-28.
159. Avraham, T., et al., *Fibrosis is a key inhibitor of lymphatic regeneration.* Plast Reconstr Surg, 2009. **124**(2): p. 438-50.
160. Martin, M., J. Lefaix, and S. Delanian, *TGF-beta1 and radiation fibrosis: a master switch and a specific therapeutic target?* Int J Radiat Oncol Biol Phys, 2000. **47**(2): p. 277-90.
161. Avraham, T., et al., *Blockade of transforming growth factor-beta1 accelerates lymphatic regeneration during wound repair.* Am J Pathol, 2010. **177**(6): p. 3202-14.
162. Avraham, T., et al., *Radiation therapy causes loss of dermal lymphatic vessels and interferes with lymphatic function by TGF-beta1-mediated tissue fibrosis.* Am J Physiol Cell Physiol, 2010. **299**(3): p. C589-605.
163. Prud'homme, G.J., *Pathobiology of transforming growth factor beta in cancer, fibrosis and immunologic disease, and therapeutic considerations.* Lab Invest, 2007. **87**(11): p. 1077-91.
164. Tian, W., et al., *Leukotriene B4 antagonism ameliorates experimental lymphedema.* Sci Transl Med, 2017. **9**(389).
165. Carbone, C., et al., *The safety of ketoprofen in different ages.* J Pharmacol Pharmacother, 2013. **4**(Suppl 1): p. S99-S103.
166. Wolf, G., *Retinoic acid as cause of cell proliferation or cell growth inhibition depending on activation of one of two different nuclear receptors.* Nutr Rev, 2008. **66**(1): p. 55-9.
167. Tonge, P.D. and P.W. Andrews, *Retinoic acid directs neuronal differentiation of human pluripotent stem cell lines in a non-cell-autonomous manner.* Differentiation, 2010. **80**(1): p. 20-30.
168. Zhang, H., et al., *All-trans retinoic acid (atRA) differentially induces apoptosis in matched primary and metastatic melanoma cells -- a speculation on damage effect of*

atRA via mitochondrial dysfunction and cell cycle redistribution. Carcinogenesis, 2003. **24**(2): p. 185-91.
169. Napoli, J.L., *Retinoic acid: its biosynthesis and metabolism.* Prog Nucleic Acid Res Mol Biol, 1999. **63**: p. 139-88.
170. Johnson, J.R., G. Williams, and R. Pazdur, *End points and United States Food and Drug Administration approval of oncology drugs.* J Clin Oncol, 2003. **21**(7): p. 1404-11.
171. Schmith, G.D., et al., *Use of Longitudinal Dose-Response Modeling to Support the Efficacy and Tolerability of Alitretinoin in Severe Refractory Chronic Hand Eczema (CHE).* CPT Pharmacometrics Syst Pharmacol, 2015. **4**(4): p. 255-62.
172. Choi, I., et al., *9-cis retinoic acid promotes lymphangiogenesis and enhances lymphatic vessel regeneration: therapeutic implications of 9-cis retinoic acid for secondary lymphedema.* Circulation, 2012. **125**(7): p. 872-82.
173. Zampell, J.C., et al., *CD4(+) cells regulate fibrosis and lymphangiogenesis in response to lymphatic fluid stasis.* PLoS One, 2012. **7**(11): p. e49940.
174. Ogata, F., et al., *Excess Lymphangiogenesis Cooperatively Induced by Macrophages and CD4(+) T Cells Drives the Pathogenesis of Lymphedema.* J Invest Dermatol, 2016. **136**(3): p. 706-14.
175. Chaitanya, G.V., et al., *Differential cytokine responses in human and mouse lymphatic endothelial cells to cytokines in vitro.* Lymphat Res Biol, 2010. **8**(3): p. 155-64.
176. Shao, X. and C. Liu, *Influence of IFN- alpha and IFN- gamma on lymphangiogenesis.* J Interferon Cytokine Res, 2006. **26**(8): p. 568-74.
177. Garcia Nores, G.D., et al., *CD4(+) T cells are activated in regional lymph nodes and migrate to skin to initiate lymphedema.* Nat Commun, 2018. **9**(1): p. 1970.
178. Cucchi, F., et al., *A vicious circle in chronic lymphoedema pathophysiology? An adipocentric view.* Obes Rev, 2017. **18**(10): p. 1159-1169.
179. Ahmadian, M., et al., *Triacylglycerol metabolism in adipose tissue.* Future Lipidol, 2007. **2**(2): p. 229-237.
180. Gormez, S., et al., *Adipose tissue gene expression of adiponectin, tumor necrosis factor-alpha and leptin in metabolic syndrome patients with coronary artery disease.* Intern Med, 2011. **50**(8): p. 805-10.
181. Kloting, N., et al., *Autocrine IGF-1 action in adipocytes controls systemic IGF-1 concentrations and growth.* Diabetes, 2008. **57**(8): p. 2074-82.
182. Saltiel, A.R., *You are what you secrete.* Nat Med, 2001. **7**(8): p. 887-8.
183. Faust, I.M., et al., *Diet-induced adipocyte number increase in adult rats: a new model of obesity.* Am J Physiol, 1978. **235**(3): p. E279-86.
184. Hausman, D.B., et al., *The biology of white adipocyte proliferation.* Obes Rev, 2001. **2**(4): p. 239-54.
185. Sarjeant, K. and J.M. Stephens, *Adipogenesis.* Cold Spring Harb Perspect Biol, 2012. **4**(9): p. a008417.
186. José María Moreno-Navarrete, J.M.F.-R., *Adipose Differentiation*. Adipose Tissue Biology. 2011: Springer New York.
187. Cannon, B. and J. Nedergaard, *Brown adipose tissue: function and physiological significance.* Physiol Rev, 2004. **84**(1): p. 277-359.
188. Trayhurn, P. and J.H. Beattie, *Physiological role of adipose tissue: white adipose tissue as an endocrine and secretory organ.* Proc Nutr Soc, 2001. **60**(3): p. 329-39.
189. Fink, T. and V. Zachar, *Adipogenic differentiation of human mesenchymal stem cells.* Methods Mol Biol, 2011. **698**: p. 243-51.
190. Musri, M.M., R. Gomis, and M. Parrizas, *A chromatin perspective of adipogenesis.* Organogenesis, 2010. **6**(1): p. 15-23.
191. Huang, H., et al., *BMP signaling pathway is required for commitment of C3H10T1/2 pluripotent stem cells to the adipocyte lineage.* Proc Natl Acad Sci U S A, 2009. **106**(31): p. 12670-5.
192. Tang, Q.Q., T.C. Otto, and M.D. Lane, *Commitment of C3H10T1/2 pluripotent stem cells to the adipocyte lineage.* Proc Natl Acad Sci U S A, 2004. **101**(26): p. 9607-11.

193. Jakkaraju, S., et al., *TIPs are tension-responsive proteins involved in myogenic versus adipogenic differentiation.* Dev Cell, 2005. **9**(1): p. 39-49.
194. Badri, K.R., et al., *Effects of the SANT domain of tension-induced/inhibited proteins (TIPs), novel partners of the histone acetyltransferase p300, on p300 activity and TIP-6-induced adipogenesis.* Mol Cell Biol, 2008. **28**(20): p. 6358-72.
195. Ntambi, J.M. and K. Young-Cheul, *Adipocyte differentiation and gene expression.* J Nutr, 2000. **130**(12): p. 3122S-3126S.
196. Cornelius, P., O.A. MacDougald, and M.D. Lane, *Regulation of adipocyte development.* Annu Rev Nutr, 1994. **14**: p. 99-129.
197. Darlington, G.J., S.E. Ross, and O.A. MacDougald, *The role of C/EBP genes in adipocyte differentiation.* J Biol Chem, 1998. **273**(46): p. 30057-60.
198. Linhart, H.G., et al., *C/EBPalpha is required for differentiation of white, but not brown, adipose tissue.* Proc Natl Acad Sci U S A, 2001. **98**(22): p. 12532-7.
199. Morrison, R.F. and S.R. Farmer, *Role of PPARgamma in regulating a cascade expression of cyclin-dependent kinase inhibitors, p18(INK4c) and p21(Waf1/Cip1), during adipogenesis.* J Biol Chem, 1999. **274**(24): p. 17088-97.
200. Farmer, S.R., *Transcriptional control of adipocyte formation.* Cell Metab, 2006. **4**(4): p. 263-73.
201. Aouadi, M., et al., *p38MAP Kinase activity is required for human primary adipocyte differentiation.* FEBS Lett, 2007. **581**(29): p. 5591-6.
202. Zezulak, K.M. and H. Green, *The generation of insulin-like growth factor-1--sensitive cells by growth hormone action.* Science, 1986. **233**(4763): p. 551-3.
203. Nixon, T. and H. Green, *Contribution of growth hormone to the adipogenic activity of serum.* Endocrinology, 1984. **114**(2): p. 527-32.
204. Holly, J., et al., *Adipogenesis and IGF-1.* Metab Syndr Relat Disord, 2006. **4**(1): p. 43-50.
205. Smith, P.J., et al., *Insulin-like growth factor-I is an essential regulator of the differentiation of 3T3-L1 adipocytes.* J Biol Chem, 1988. **263**(19): p. 9402-8.
206. Steinberg, M.M. and B.L. Brownstein, *A clonal analysis of the differentiation of 3T3-L1 preadipose cells: role of insulin.* J Cell Physiol, 1982. **113**(3): p. 359-64.
207. Back, K., et al., *Differential effects of IGF-I, IGF-II and insulin in human preadipocytes and adipocytes--role of insulin and IGF-I receptors.* Mol Cell Endocrinol, 2011. **339**(1-2): p. 130-5.
208. Hutley, L., et al., *Fibroblast growth factor 1: a key regulator of human adipogenesis.* Diabetes, 2004. **53**(12): p. 3097-106.
209. Newell, F.S., et al., *Characterization of the transcriptional and functional effects of fibroblast growth factor-1 on human preadipocyte differentiation.* FASEB J, 2006. **20**(14): p. 2615-7.
210. Song, X., et al., *bFGF promotes adipocyte differentiation in human mesenchymal stem cells derived from embryonic stem cells.* Genet Mol Biol, 2014. **37**(1): p. 127-34.
211. Neubauer, M., et al., *Basic fibroblast growth factor enhances PPARgamma ligand-induced adipogenesis of mesenchymal stem cells.* FEBS Lett, 2004. **577**(1-2): p. 277-83.
212. Fricker, L.D., *Carboxypeptidase E.* Annu Rev Physiol, 1988. **50**: p. 309-21.
213. Fricker, L.D. and L. Devi, *Posttranslational processing of carboxypeptidase E, a neuropeptide-processing enzyme, in AtT-20 cells and bovine pituitary secretory granules.* J Neurochem, 1993. **61**(4): p. 1404-15.
214. Chang, E.J., et al., *Elucidation of CPX-1 involvement in RANKL-induced osteoclastogenesis by a proteomics approach.* FEBS Lett, 2004. **564**(1-2): p. 166-70.
215. Kim, Y.H., H.M. O'Neill, and J.P. Whitehead, *Carboxypeptidase X-1 (CPX-1) is a secreted collagen-binding glycoprotein.* Biochem Biophys Res Commun, 2015. **468**(4): p. 894-9.
216. Kim, Y.H., et al., *Identification of carboxypeptidase X (CPX)-1 as a positive regulator of adipogenesis.* FASEB J, 2016.

217. Smas, C.M. and H.S. Sul, *Pref-1, a protein containing EGF-like repeats, inhibits adipocyte differentiation.* Cell, 1993. **73**(4): p. 725-34.
218. Moon, Y.S., et al., *Mice lacking paternally expressed Pref-1/Dlk1 display growth retardation and accelerated adiposity.* Mol Cell Biol, 2002. **22**(15): p. 5585-92.
219. Lee, K., et al., *Inhibition of adipogenesis and development of glucose intolerance by soluble preadipocyte factor-1 (Pref-1).* J Clin Invest, 2003. **111**(4): p. 453-61.
220. Linger, R.M., et al., *TAM receptor tyrosine kinases: biologic functions, signaling, and potential therapeutic targeting in human cancer.* Adv Cancer Res, 2008. **100**: p. 35-83.
221. Nagata, K., et al., *Identification of the product of growth arrest-specific gene 6 as a common ligand for Axl, Sky, and Mer receptor tyrosine kinases.* J Biol Chem, 1996. **271**(47): p. 30022-7.
222. Lijnen, H.R., V. Christiaens, and L. Scroyen, *Growth arrest-specific protein 6 receptor antagonism impairs adipocyte differentiation and adipose tissue development in mice.* J Pharmacol Exp Ther, 2011. **337**(2): p. 457-64.
223. Maquoi, E., et al., *Role of Gas-6 in adipogenesis and nutritionally induced adipose tissue development in mice.* Arterioscler Thromb Vasc Biol, 2005. **25**(5): p. 1002-7.
224. McMahon, A.P., P.W. Ingham, and C.J. Tabin, *Developmental roles and clinical significance of hedgehog signaling.* Curr Top Dev Biol, 2003. **53**: p. 1-114.
225. Suh, J.M., et al., *Hedgehog signaling plays a conserved role in inhibiting fat formation.* Cell Metab, 2006. **3**(1): p. 25-34.
226. Tong, Q., et al., *Function of GATA transcription factors in preadipocyte-adipocyte transition.* Science, 2000. **290**(5489): p. 134-8.
227. Sitzia, J., *Volume measurement in lymphoedema treatment: examination of formulae.* Eur J Cancer Care (Engl), 1995. **4**(1): p. 11-6.
228. Fischer, A.H., et al., *Hematoxylin and eosin staining of tissue and cell sections.* CSH Protoc, 2008. **2008**: p. pdb prot4986.
229. Goldner, J., *A modification of the masson trichrome technique for routine laboratory purposes.* Am J Pathol, 1938. **14**(2): p. 237-43.
230. Rutkowski, J.M., et al., *Secondary lymphedema in the mouse tail: Lymphatic hyperplasia, VEGF-C upregulation, and the protective role of MMP-9.* Microvasc Res, 2006. **72**(3): p. 161-71.
231. Mohler, E.R. and B. Mehrara, *Clinical features and diagnosis of peripheral lymphedema*, in *UpToDate*. 2016.
232. Mitra, D., et al., *The risk of lymphedema after postoperative radiation therapy in endometrial cancer.* J Gynecol Oncol, 2016. **27**(1): p. e4.
233. Beesley, V., et al., *Lymphedema after gynecological cancer treatment : prevalence, correlates, and supportive care needs.* Cancer, 2007. **109**(12): p. 2607-14.
234. Cheung, L., et al., *An experimental model for the study of lymphedema and its response to therapeutic lymphangiogenesis.* BioDrugs, 2006. **20**(6): p. 363-70.
235. Ongstad, E.L., et al., *Lymphangiogenesis-independent resolution of experimental edema.* Am J Physiol Heart Circ Physiol, 2010. **299**(1): p. H46-54.
236. Laviola, L., A. Natalicchio, and F. Giorgino, *The IGF-I signaling pathway.* Curr Pharm Des, 2007. **13**(7): p. 663-9.
237. Siddals, K.W., et al., *IGF-binding protein-1 inhibits IGF effects on adipocyte function: implications for insulin-like actions at the adipocyte.* J Endocrinol, 2002. **174**(2): p. 289-97.
238. Yau, S.W., et al., *IGFBP-2 inhibits adipogenesis and lipogenesis in human visceral, but not subcutaneous, adipocytes.* Int J Obes (Lond), 2015. **39**(5): p. 770-81.
239. Chan, S.S., et al., *Inhibition of adipocyte differentiation by insulin-like growth factor-binding protein-3.* Am J Physiol Endocrinol Metab, 2009. **296**(4): p. E654-63.
240. Maridas, D.E., et al., *IGFBP4 Is Required for Adipogenesis and Influences the Distribution of Adipose Depots.* Endocrinology, 2017. **158**(10): p. 3488-3500.
241. Baxter, R.C. and S.M. Twigg, *Actions of IGF binding proteins and related proteins in adipose tissue.* Trends Endocrinol Metab, 2009. **20**(10): p. 499-505.

242. Back, K. and H.J. Arnqvist, *Changes in insulin and IGF-I receptor expression during differentiation of human preadipocytes.* Growth Horm IGF Res, 2009. **19**(2): p. 101-11.
243. Christoffersen, C.T., et al., *Insulin and insulin-like growth factor-I receptor mediated differentiation of 3T3-F442A cells into adipocytes: effect of PI 3-kinase inhibition.* Biochem Biophys Res Commun, 1998. **246**(2): p. 426-30.
244. Tang, Q.Q., T.C. Otto, and M.D. Lane, *Mitotic clonal expansion: a synchronous process required for adipogenesis.* Proc Natl Acad Sci U S A, 2003. **100**(1): p. 44-9.
245. Tomiyama, K., et al., *Wortmannin, a specific phosphatidylinositol 3-kinase inhibitor, inhibits adipocytic differentiation of 3T3-L1 cells.* Biochem Biophys Res Commun, 1995. **212**(1): p. 263-9.
246. Scavo, L.M., et al., *Insulin-like growth factor-I stimulates both cell growth and lipogenesis during differentiation of human mesenchymal stem cells into adipocytes.* J Clin Endocrinol Metab, 2004. **89**(7): p. 3543-53.
247. Miki, H., et al., *Essential role of insulin receptor substrate 1 (IRS-1) and IRS-2 in adipocyte differentiation.* Mol Cell Biol, 2001. **21**(7): p. 2521-32.
248. Twigg, S.M. and R.C. Baxter, *Insulin-like growth factor (IGF)-binding protein 5 forms an alternative ternary complex with IGFs and the acid-labile subunit.* J Biol Chem, 1998. **273**(11): p. 6074-9.
249. Kalus, W., et al., *Structure of the IGF-binding domain of the insulin-like growth factor-binding protein-5 (IGFBP-5): implications for IGF and IGF-I receptor interactions.* EMBO J, 1998. **17**(22): p. 6558-72.
250. van Kleffens, M., et al., *Generation of antisera to mouse insulin-like growth factor binding proteins (IGFBP)-1 to -6: comparison of IGFBP protein and messenger ribonucleic acid localization in the mouse embryo.* Endocrinology, 1999. **140**(12): p. 5944-52.
251. Dina, C., et al., *Genetic association analyses highlight biological pathways underlying mitral valve prolapse.* Nat Genet, 2015. **47**(10): p. 1206-11.
252. Bussolati, G. and R.T. Radulescu, *Blocking endogenous peroxidases in immunohistochemistry: a mandatory, yet also subtle measure.* Appl Immunohistochem Mol Morphol, 2011. **19**(5): p. 484.
253. Ordonez, N.G., J.T. Manning, Jr., and T.E. Brooks, *Effect of trypsinization on the immunostaining of formalin-fixed, paraffin-embedded tissues.* Am J Surg Pathol, 1988. **12**(2): p. 121-9.
254. Wilson, C., et al., *The differential anti-tumour effects of zoledronic acid in breast cancer - evidence for a role of the activin signaling pathway.* BMC Cancer, 2015. **15**: p. 55.
255. Tejada, T., et al., *IGF-1 degradation by mouse mast cell protease 4 promotes cell death and adverse cardiac remodeling days after a myocardial infarction.* Proc Natl Acad Sci U S A, 2016. **113**(25): p. 6949-54.
256. Howie, R.N., et al., *Effects of In Utero Thyroxine Exposure on Murine Cranial Suture Growth.* PLoS One, 2016. **11**(12): p. e0167805.
257. Adams, T.E., et al., *Structure and function of the type 1 insulin-like growth factor receptor.* Cell Mol Life Sci, 2000. **57**(7): p. 1050-93.
258. Sepp-Lorenzino, L., *Structure and function of the insulin-like growth factor I receptor.* Breast Cancer Res Treat, 1998. **47**(3): p. 235-53.
259. Li, R., A. Pourpak, and S.W. Morris, *Inhibition of the insulin-like growth factor-1 receptor (IGF1R) tyrosine kinase as a novel cancer therapy approach.* J Med Chem, 2009. **52**(16): p. 4981-5004.
260. Serrat, M.A., C.O. Lovejoy, and D. King, *Age- and site-specific decline in insulin-like growth factor-I receptor expression is correlated with differential growth plate activity in the mouse hindlimb.* Anat Rec (Hoboken), 2007. **290**(4): p. 375-81.
261. Hernandez-Sanchez, C., et al., *The role of the tyrosine kinase domain of the insulin-like growth factor-I receptor in intracellular signaling, cellular proliferation, and tumorigenesis.* J Biol Chem, 1995. **270**(49): p. 29176-81.

262. Kato, H., et al., *Essential role of tyrosine residues 1131, 1135, and 1136 of the insulin-like growth factor-I (IGF-I) receptor in IGF-I action.* Mol Endocrinol, 1994. **8**(1): p. 40-50.
263. Park, J.H., et al., *Presence of insulin-like growth factor binding proteins correlates with tumor-promoting effects of matrix metalloproteinase 9 in breast cancer.* Neoplasia, 2015. **17**(5): p. 421-33.
264. Dupont, J. and M. Holzenberger, *Biology of insulin-like growth factors in development.* Birth Defects Res C Embryo Today, 2003. **69**(4): p. 257-71.
265. Inzunza, J., et al., *Selective insulin-like growth factor-I antagonist inhibits mouse embryo development in a dose-dependent manner.* Fertil Steril, 2010. **93**(8): p. 2621-6.
266. Liu, H., et al., *Correlation between microvascular characteristics and the expression of MVD, IGF-1 and STAT3 in the development of colonic polyps carcinogenesis.* Exp Ther Med, 2017. **13**(1): p. 49-54.
267. Xin, C., et al., *The expression difference of insulin-like growth factor 1 receptor in breast cancers with or without diabetes.* J Cancer Res Ther, 2015. **11**(2): p. 295-9.
268. Ahlen, J., et al., *Insulin-like growth factor type 1 receptor expression correlates to good prognosis in highly malignant soft tissue sarcoma.* Clin Cancer Res, 2005. **11**(1): p. 206-16.
269. Ding, W.Z., et al., *MicroRNA-497 regulates cell proliferation in hepatocellular carcinoma.* Oncol Lett, 2016. **11**(2): p. 1081-1088.
270. Litzenburger, B.C., et al., *High IGF-IR activity in triple-negative breast cancer cell lines and tumorgrafts correlates with sensitivity to anti-IGF-IR therapy.* Clin Cancer Res, 2011. **17**(8): p. 2314-27.
271. Imrie, D. and K.C. Sadler, *White adipose tissue development in zebrafish is regulated by both developmental time and fish size.* Dev Dyn, 2010. **239**(11): p. 3013-23.
272. Blanchette-Mackie, E.J., et al., *Perilipin is located on the surface layer of intracellular lipid droplets in adipocytes.* J Lipid Res, 1995. **36**(6): p. 1211-26.
273. Garten, A., S. Schuster, and W. Kiess, *The insulin-like growth factors in adipogenesis and obesity.* Endocrinol Metab Clin North Am, 2012. **41**(2): p. 283-95, v-vi.
274. Hong, S., et al., *Insulin-like growth factor-1 receptor signaling in 3T3-L1 adipocyte differentiation requires lipid rafts but not caveolae.* Cell Death Differ, 2004. **11**(7): p. 714-23.
275. Gleason, C.E., et al., *Role of insulin-like growth factor-binding protein 5 (IGFBP5) in organismal and pancreatic beta-cell growth.* Mol Endocrinol, 2010. **24**(1): p. 178-92.
276. Jones, J.I., et al., *Extracellular matrix contains insulin-like growth factor binding protein-5: potentiation of the effects of IGF-I.* J Cell Biol, 1993. **121**(3): p. 679-87.
277. Nam, T.J., et al., *Thrombospondin and osteopontin bind to insulin-like growth factor (IGF)-binding protein-5 leading to an alteration in IGF-I-stimulated cell growth.* Endocrinology, 2000. **141**(3): p. 1100-6.
278. Clemmons, D.R., et al., *Role of the integrin alphaVbeta3 in mediating increased smooth muscle cell responsiveness to IGF-I in response to hyperglycemic stress.* Growth Horm IGF Res, 2007. **17**(4): p. 265-70.
279. Sakaue, H., et al., *Role of MAPK phosphatase-1 (MKP-1) in adipocyte differentiation.* J Biol Chem, 2004. **279**(38): p. 39951-7.
280. Christopoulos, P.F., P. Msaouel, and M. Koutsilieris, *The role of the insulin-like growth factor-1 system in breast cancer.* Mol Cancer, 2015. **14**: p. 43.
281. Haluska, P., et al., *Phase I dose-escalation study of MEDI-573, a bispecific, antiligand monoclonal antibody against IGFI and IGFII, in patients with advanced solid tumors.* Clin Cancer Res, 2014. **20**(18): p. 4747-57.
282. Iguchi, H., et al., *Phase I dose-escalation study evaluating safety, tolerability and pharmacokinetics of MEDI-573, a dual IGF-I/II neutralizing antibody, in Japanese patients with advanced solid tumours.* Invest New Drugs, 2015. **33**(1): p. 194-200.

283. Friedbichler, K., et al., *Pharmacodynamic and antineoplastic activity of BI 836845, a fully human IGF ligand-neutralizing antibody, and mechanistic rationale for combination with rapamycin.* Mol Cancer Ther, 2014. **13**(2): p. 399-409.
284. Gao, J., et al., *Dual IGF-I/II-neutralizing antibody MEDI-573 potently inhibits IGF signaling and tumor growth.* Cancer Res, 2011. **71**(3): p. 1029-40.
285. Zhong, H., et al., *MEDI-573, alone or in combination with mammalian target of rapamycin inhibitors, targets the insulin-like growth factor pathway in sarcomas.* Mol Cancer Ther, 2014. **13**(11): p. 2662-73.
286. Burtrum, D., et al., *A fully human monoclonal antibody to the insulin-like growth factor I receptor blocks ligand-dependent signaling and inhibits human tumor growth in vivo.* Cancer Res, 2003. **63**(24): p. 8912-21.
287. Tolcher, A.W., et al., *Phase I, pharmacokinetic, and pharmacodynamic study of AMG 479, a fully human monoclonal antibody to insulin-like growth factor receptor 1.* J Clin Oncol, 2009. **27**(34): p. 5800-7.
288. Fitzgerald, J.B., et al., *MM-141, an IGF-IR- and ErbB3-directed bispecific antibody, overcomes network adaptations that limit activity of IGF-IR inhibitors.* Mol Cancer Ther, 2014. **13**(2): p. 410-25.
289. Scagliotti, G.V., et al., *Randomized, phase III trial of figitumumab in combination with erlotinib versus erlotinib alone in patients with nonadenocarcinoma nonsmall-cell lung cancer.* Ann Oncol, 2015. **26**(3): p. 497-504.
290. Gradishar, W.J., et al., *Clinical and Translational Results of a Phase II, Randomized Trial of an Anti-IGF-1R (Cixutumumab) in Women with Breast Cancer That Progressed on Endocrine Therapy.* Clin Cancer Res, 2016. **22**(2): p. 301-9.
291. Sclafani, F., et al., *A Randomized Phase II/III Study of Dalotuzumab in Combination With Cetuximab and Irinotecan in Chemorefractory, KRAS Wild-Type, Metastatic Colorectal Cancer*. J Natl Cancer Inst, 2015. **107**(12): p. djv258.
292. Anderson, P.M., et al., *A phase II study of clinical activity of SCH 717454 (robatumumab) in patients with relapsed osteosarcoma and Ewing sarcoma.* Pediatr Blood Cancer, 2016. **63**(10): p. 1761-70.
293. Kurzrock, R., et al., *A phase I study of weekly R1507, a human monoclonal antibody insulin-like growth factor-I receptor antagonist, in patients with advanced solid tumors.* Clin Cancer Res, 2010. **16**(8): p. 2458-65.
294. Simpson, A., et al., *Insulin-Like Growth Factor (IGF) Pathway Targeting in Cancer: Role of the IGF Axis and Opportunities for Future Combination Studies.* Target Oncol, 2017. **12**(5): p. 571-597.
295. Mulvihill, M.J., et al., *Discovery of OSI-906: a selective and orally efficacious dual inhibitor of the IGF-1 receptor and insulin receptor.* Future Med Chem, 2009. **1**(6): p. 1153-71.
296. Carboni, J.M., et al., *BMS-754807, a small molecule inhibitor of insulin-like growth factor-1R/IR.* Mol Cancer Ther, 2009. **8**(12): p. 3341-9.
297. Fassnacht, M., et al., *Linsitinib (OSI-906) versus placebo for patients with locally advanced or metastatic adrenocortical carcinoma: a double-blind, randomised, phase 3 study*. Lancet Oncol, 2015. **16**(4): p. 426-35.
298. Shirakawa, J., et al., *Effects of the antitumor drug OSI-906, a dual inhibitor of IGF-1 receptor and insulin receptor, on the glycemic control, beta-cell functions, and beta-cell proliferation in male mice.* Endocrinology, 2014. **155**(6): p. 2102-11.
299. Tajima, K., et al., *Metabolic recovery of lipodystrophy, liver steatosis, and pancreatic beta cell proliferation after the withdrawal of OSI-906.* Sci Rep, 2017. **7**(1): p. 4119.
300. Groeneveld, M.P., et al., *Acute knockdown of the insulin receptor or its substrates Irs1 and 2 in 3T3-L1 adipocytes suppresses adiponectin production.* Sci Rep, 2016. **6**: p. 21105.
301. Buck, E., et al., *Compensatory insulin receptor (IR) activation on inhibition of insulin-like growth factor-1 receptor (IGF-1R): rationale for cotargeting IGF-1R and IR in cancer.* Mol Cancer Ther, 2010. **9**(10): p. 2652-64.

302. Zinn, R.L., et al., *ERK phosphorylation is predictive of resistance to IGF-1R inhibition in small cell lung cancer.* Mol Cancer Ther, 2013. **12**(6): p. 1131-9.
303. Francois, J.C., et al., *Disrupting IGF Signaling in Adult Mice Conditions Leanness, Resilient Energy Metabolism, and High Growth Hormone Pulses.* Endocrinology, 2017. **158**(7): p. 2269-2283.
304. Baiocchini, A., et al., *Extracellular Matrix Molecular Remodeling in Human Liver Fibrosis Evolution.* PLoS One, 2016. **11**(3): p. e0151736.
305. Schwarz, R.I., *Collagen I and the fibroblast: high protein expression requires a new paradigm of post-transcriptional, feedback regulation.* Biochem Biophys Rep, 2015. **3**: p. 38-44.
306. Lynch, L.L., et al., *Fibrosis worsens chronic lymphedema in rodent tissues.* Am J Physiol Heart Circ Physiol, 2015. **308**(10): p. H1229-36.
307. Clarke, M.C., et al., *Apoptosis of vascular smooth muscle cells induces features of plaque vulnerability in atherosclerosis.* Nat Med, 2006. **12**(9): p. 1075-80.
308. Shinohara, M., et al., *Atherosclerotic plaque imaging using phase-contrast X-ray computed tomography.* Am J Physiol Heart Circ Physiol, 2008. **294**(2): p. H1094-100.
309. Zampell, J.C., et al., *Toll-like receptor deficiency worsens inflammation and lymphedema after lymphatic injury.* Am J Physiol Cell Physiol, 2012. **302**(4): p. C709-19.
310. Fife, C.E., et al., *Skin and Wound Care in Lymphedema Patients: A Taxonomy, Primer, and Literature Review.* Adv Skin Wound Care, 2017. **30**(7): p. 305-318.
311. Sopracordevole, F., et al., *Laser CO2 treatment for vulvar lymphedema secondary to gynecological cancer therapy: A report of two cases and review of the literature.* Oncol Lett, 2015. **9**(4): p. 1889-1892.
312. Chen, H.X. and E. Sharon, *IGF-1R as an anti-cancer target--trials and tribulations.* Chin J Cancer, 2013. **32**(5): p. 242-52.
313. Chen, P., et al., *Developmental regulation of adipose tissue growth through hyperplasia and hypertrophy in the embryonic Leghorn and broiler.* Poult Sci, 2014. **93**(7): p. 1809-17.
314. Jo, J., et al., *Hypertrophy and/or Hyperplasia: Dynamics of Adipose Tissue Growth.* PLoS Comput Biol, 2009. **5**(3): p. e1000324.
315. Cao, Y., *Angiogenesis modulates adipogenesis and obesity.* J Clin Invest, 2007. **117**(9): p. 2362-8.
316. Boucher, J., et al., *Differential Roles of Insulin and IGF-1 Receptors in Adipose Tissue Development and Function.* Diabetes, 2016. **65**(8): p. 2201-13.
317. Qiang, G., et al., *Lipodystrophy and severe metabolic dysfunction in mice with adipose tissue-specific insulin receptor ablation.* Mol Metab, 2016. **5**(7): p. 480-490.
318. Sciacca, L., R. Le Moli, and R. Vigneri, *Insulin analogs and cancer.* Front Endocrinol (Lausanne), 2012. **3**: p. 21.
319. Andersson, M.K., P. Aman, and G. Stenman, *IGF2/IGF1R Signaling as a Therapeutic Target in MYB-Positive Adenoid Cystic Carcinomas and Other Fusion Gene-Driven Tumors.* Cells, 2019. **8**(8).
320. Lui, J.C., et al., *An imprinted gene network that controls mammalian somatic growth is down-regulated during postnatal growth deceleration in multiple organs.* Am J Physiol Regul Integr Comp Physiol, 2008. **295**(1): p. R189-96.
321. Livingstone, C., *IGF2 and cancer.* Endocr Relat Cancer, 2013. **20**(6): p. R321-39.
322. Alfares, M.N., et al., *Insulin-like growth factor-II in adipocyte regulation: depot-specific actions suggest a potential role limiting excess visceral adiposity.* Am J Physiol Endocrinol Metab, 2018. **315**(6): p. E1098-E1107.
323. Wilson, S.F., et al., *Histopathologic improvement with lymphedema management, Leogane, Haiti.* Emerg Infect Dis, 2004. **10**(11): p. 1938-46.
324. Douglas, R.S., et al., *Aberrant expression of the insulin-like growth factor-1 receptor by T cells from patients with Graves' disease may carry functional consequences for disease pathogenesis.* J Immunol, 2007. **178**(5): p. 3281-7.

325. Smith, T.J., *Rationale for therapeutic targeting insulin-like growth factor-1 receptor and bone marrow-derived fibrocytes in thyroid-associated ophthalmopathy.* Expert Rev Ophthalmol, 2016. **11**(2): p. 77-79.
326. Jimenez, S.A., et al., *Increased collagen biosynthesis and increased expression of type I and type III procollagen genes in tight skin (TSK) mouse fibroblasts.* J Biol Chem, 1986. **261**(2): p. 657-62.
327. Ivarsson, M., et al., *Type I collagen synthesis in cultured human fibroblasts: regulation by cell spreading, platelet-derived growth factor and interactions with collagen fibers.* Matrix Biol, 1998. **16**(7): p. 409-25.
328. Kim, B., et al., *Ascorbic acid enhances adipogenesis of 3T3-L1 murine preadipocyte through differential expression of collagens.* Lipids Health Dis, 2013. **12**: p. 182.
329. Li, P., et al., *Resveratrol inhibits collagen I synthesis by suppressing IGF-1R activation in intestinal fibroblasts.* World J Gastroenterol, 2014. **20**(16): p. 4648-61.
330. Goldstein, R.H., et al., *Stimulation of collagen formation by insulin and insulin-like growth factor I in cultures of human lung fibroblasts.* Endocrinology, 1989. **124**(2): p. 964-70.
331. Chetty, A., G.J. Cao, and H.C. Nielsen, *Insulin-like Growth Factor-I signaling mechanisms, type I collagen and alpha smooth muscle actin in human fetal lung fibroblasts.* Pediatr Res, 2006. **60**(4): p. 389-94.
332. Fain, J.N., D.S. Tichansky, and A.K. Madan, *Transforming growth factor beta1 release by human adipose tissue is enhanced in obesity.* Metabolism, 2005. **54**(11): p. 1546-51.
333. Pan, X., et al., *Transforming growth factor beta1 induces the expression of collagen type I by DNA methylation in cardiac fibroblasts.* PLoS One, 2013. **8**(4): p. e60335.
334. Fine, A. and R.H. Goldstein, *The effect of transforming growth factor-beta on cell proliferation and collagen formation by lung fibroblasts.* J Biol Chem, 1987. **262**(8): p. 3897-902.
335. Proulx, S.T., et al., *Quantitative imaging of lymphatic function with liposomal indocyanine green.* Cancer Res, 2010. **70**(18): p. 7053-62.
336. Liu, J.L., S. Yakar, and D. LeRoith, *Conditional knockout of mouse insulin-like growth factor-1 gene using the Cre/loxP system.* Proc Soc Exp Biol Med, 2000. **223**(4): p. 344-51.
337. Brice, G., et al., *Milroy disease and the VEGFR-3 mutation phenotype.* J Med Genet, 2005. **42**(2): p. 98-102.